

Dark matter from mediator decay in early matter domination

Rouzbeh Allahverdi ^{*1}, Ngo Phuc Duc Loc ^{†1}, and Jacek K. Osiński ^{‡2}

¹Department of Physics and Astronomy, University of New Mexico, Albuquerque, NM 87131, USA

²AstroCeNT, Nicolaus Copernicus Astronomical Center of the Polish Academy of Sciences, ul. Rektorska 4, 00-614 Warsaw, Poland

Abstract

We study dark matter production from mediator decays in scenarios with an epoch of early matter domination. Particles that mediate interactions between dark matter and the standard model particles are kinematically accessible to the thermal bath as long as their mass is below the reheating temperature of the Universe after inflation. Decay of on-shell mediators can then lead to copious production of dark matter during early matter domination or a preceding radiation-dominated phase. In particular, for mediators that are charged under the standard model, it can exceed the standard freeze-in channel due to inverse annihilations at much lower temperatures (often by many orders of magnitude). The requirement to obtain the correct relic abundance severely constrains the parameter space for dark matter masses above a few TeV.

1 Introduction

While there are many lines of evidence for the existence of dark matter (DM) in the Universe [1], the identity of DM is an outstanding problem at the interface of particle physics and cosmology. Explaining the observed DM abundance is another challenge that in addition depends on the details of the thermal history of the early Universe. Thermal freeze-out in a radiation-dominated (RD) Universe is a simple and attractive mechanism that can yield the correct relic abundance if the (thermally averaged) DM annihilation rate takes the specific value $\langle\sigma_{\text{ann}}v\rangle = 3 \times 10^{-26} \text{cm}^3 \text{s}^{-1}$. However, in nonstandard cosmological histories, the correct DM abundance can be obtained for much larger or smaller values of $\langle\sigma_{\text{ann}}v\rangle$ [2, 3].

It is known that well-motivated classes of models arising from string theory generically lead to nonstandard histories that involve one or more epochs of early matter domination (EMD) [4]. In general, an EMD phase arises when a matter-like component dominates the energy density of the Universe and eventually decays to establish a RD Universe prior to big bang nucleosynthesis (BBN). The matter equation of state can be due to coherent oscillations

*rouzbeh@unm.edu

†locngo148@gmail.com

‡jaksaosinski@gmail.com

Dark matter bound-state formation in the Sun

Xiaoyong Chu,^{1,*} Raghuv eer Garani,^{2,†} Camilo García-Cely,^{3,‡} and Thomas Hambye^{4,5,§}

¹*Institute of High Energy Physics, Austrian Academy of Sciences,*

Nikolsdorfer Gasse 18, 1050 Vienna, Austria

²*INFN Sezione di Firenze, Via G. Sansone 1, I-50019 Sesto Fiorentino, Italy*

³*Instituto de Física Corpuscular (IFIC), Universitat de València-CSIC,*

Parc Científic UV, C/ Catedrático José Beltrán 2, E-46980 Paterna, Spain

⁴*Service de Physique Théorique Université Libre de Bruxelles,*

Boulevard du Triomphe, CP225, 1050 Brussels, Belgium

⁵*CERN, Theoretical Physics Department, Geneva, Switzerland*

The Sun may capture asymmetric dark matter (DM), which can subsequently form bound-states through the radiative emission of a sub-GeV scalar. This process enables generation of scalars without requiring DM annihilation. In addition to DM capture on nucleons, the DM-scalar coupling responsible for bound-state formation also induces capture from self-scatterings of ambient DM particles with DM particles already captured, as well as with DM bound-states formed in-situ within the Sun. This scenario is studied in detail by solving Boltzmann equations numerically and analytically. In particular, we take into consideration that the DM self-capture rates require a treatment beyond the conventional Born approximation. We show that, thanks to DM scatterings on bound-states, the number of DM particles captured increases exponentially, leading to enhanced emission of relativistic scalars through bound-state formation, whose final decay products could be observable. We explore phenomenological signatures with the example that the scalar mediator decays to neutrinos. We find that the neutrino flux emitted can be comparable to atmospheric neutrino fluxes within the range of energies below one hundred MeV. Future facilities like Hyper-K, and direct DM detection experiments can further test such scenario.

* xiaoyong.chu@oeaw.ac.at

† garani@fi.infn.it

‡ camilo.garcia@ific.uv.es

§ thomas.hambye@ulb.be

Towards a precision calculation of N_{eff} in the Standard Model III: Improved estimate of NLO corrections to the collision integral

Marco Drewes,^a Yannis Georis,^a Michael Klasen,^b
Luca Paolo Wiggering^b and Yvonne Y. Y. Wong^c

^aCentre for Cosmology, Particle Physics and Phenomenology, Université catholique de Louvain, Louvain-la-Neuve B-1348, Belgium

^bInstitut für Theoretische Physik, Universität Münster, Wilhelm-Klemm-Straße 9, D-48149 Münster, Germany

^cSydney Consortium for Particle Physics and Cosmology, School of Physics, The University of New South Wales, Sydney NSW 2052, Australia

E-mail: marco.drewes@uclouvain.be, yannis.georis@uclouvain.be,
michael.klasen@uni-muenster.de, luca.wiggering@uni-muenster.de,
yvonne.y.wong@unsw.edu.au

Abstract. We compute the dominant QED correction to the neutrino-electron interaction rate in the vicinity of neutrino decoupling in the early universe, and estimate its impact on the effective number of neutrino species N_{eff} in cosmic microwave background anisotropy observations. We find that the correction to the interaction rate is at the sub-percent level, consistent with a recent estimate by Jackson and Laine. Relative to that work we include the electron mass in our computations, but restrict our analysis to the enhanced t -channel contributions. The fractional change in $N_{\text{eff}}^{\text{SM}}$ due to the rate correction is of order 10^{-5} or below, i.e., about a factor of 30 smaller than that recently claimed by Cielo *et al.*, and below the nominal computational uncertainties of the current benchmark value of $N_{\text{eff}}^{\text{SM}} = 3.0440 \pm 0.0002$. We therefore conclude that aforementioned number remains to be the state-of-the-art benchmark for $N_{\text{eff}}^{\text{SM}}$ in the standard model of particle physics.

Prospects for measuring time variation of astrophysical neutrino sources at dark matter detectors

Yi Zhuang,¹ Louis E. Strigari,¹ Lei Jin,² and Samiran Sinha³

¹*Department of Physics and Astronomy, Mitchell Institute for Fundamental Physics and Astronomy, Texas A&M University, College Station, Texas 77843, USA*

²*Department of Mathematics and Statistics, Texas A&M University-Corpus Christi, Corpus Christi, TX 78412, USA*

³*Department of Statistics, Texas A&M University, College Station, Texas 77843, USA*

(Dated: February 29, 2024)

We study the prospects for measuring the time variation of solar and atmospheric neutrino fluxes at future large-scale Xenon and Argon dark matter detectors. For solar neutrinos, a yearly time variation arises from the eccentricity of the Earth's orbit, and, for charged current interactions, from a smaller energy-dependent day-night variation due to flavor regeneration as neutrinos travel through the Earth. For a 100-ton Xenon detector running for 10 years with a Xenon-136 fraction of $\lesssim 0.1\%$, in the electron recoil channel a time-variation amplitude of about 0.8% is detectable with a power of 90% and the level of significance of 10%. This is sufficient to detect time variation due to eccentricity, which has amplitude of $\sim 3\%$. In the nuclear recoil channel, the detectable amplitude is about 10% under current detector resolution and efficiency conditions, and this generally reduces to about 1% for improved detector resolution and efficiency, the latter of which is sufficient to detect time variation due to eccentricity. Our analysis assumes both known and unknown periods. We provide scalings to determine the sensitivity to an arbitrary time-varying amplitude as a function of detector parameters. Identifying the time variation of the neutrino fluxes will be important for distinguishing neutrinos from dark matter signals and other detector-related backgrounds, and extracting properties of neutrinos that can be uniquely studied in dark matter experiments.

arXiv:2402.18454v1 [hep-ph] 28 Feb 2024

2

I. INTRODUCTION

Over the past several decades, direct dark matter detection experiments have made tremendous progress in constraining weak-scale particle dark matter [1, 2]. Future larger-scale detectors will be sensitive to not only particle dark matter, but also astrophysical neutrinos and various other rare-event phenomenology [3]. The most prominent of the neutrino signals are from the Sun, the atmosphere, and the diffuse supernova neutrino background (DSNB) [4]. Understanding these signals has important implications for the future of particle dark matter searches, but also for understanding the nature of the sources and the properties of neutrinos [5].

Various methods have been proposed to distinguish neutrinos and a possible dark matter signal. These include exploiting the energy distribution of nuclear recoils between neutrinos and dark matter [6, 7], the differences in arrival directions [8], and the differences in the periodicities of the signal [9, 10]. New physics in the neutrino sector may also change the nature of the predicted neutrino signal [11–13], and provide a method to discriminate from dark matter.

Here we examine the time variations of the neutrino signals in more detail and study the prospects for measuring these time variations. For solar neutrinos, the time variation of the flux is due to the eccentricity of the Earth's orbit and the day-night effect. The former is independent of the neutrino flavor, while the latter, which results from neutrino interactions with the matter as they pass through the Earth, is flavor dependent. Both effects are present in a dark matter experiment through the nuclear recoil and electron recoil channels. Beyond solar neutrinos, there may be detectable time variation of other components of the astrophysical neutrino flux. Due to the solar cycle, there is a time variation of the atmospheric neutrino flux which is $\sim 10 - 30\%$ [14] depending on the detector location. We present the first estimates of the detectability of the time variation of the atmospheric neutrino flux given realistic future detector configurations.

Identifying the time variation for the different neutrino sources is important for properly extracting the signal and distinguishing it from dark matter [4, 15]. In addition, it is important to characterize these signals to constrain neutrino properties. Previous studies of neutrinos in dark matter experiments have only considered the time variation of solar neutrinos as being due to the eccentricity of the Earth's orbit, and for idealistic values of the nuclear recoil threshold [9]. In addition to examining more realistic and updated detector configurations, we consider the prospects for measuring time variation of solar neutrinos using the neutrino-electron elastic scattering channel for the first time.

Solar neutrino experiments have previously searched for time variations in their signals, including experiments that have successfully established time variation due to the eccentricity of the Earth's orbit [16, 17] and the day-night effect [18]. These experiments each used a range of statistical techniques to identify the time variable signal. As part of our analysis, we rigorously compare the different statistical methodologies for extracting the time-varying signal. We present results for the sensitivity of given experiments to time-varying amplitudes, and quantify the prospects for signal extraction as a function of experimental sensitivity and background levels.

This paper is organized as follows. In Section II, we briefly describe the signals and the models for the detector efficiency. In Section III we describe the periodic signals used in this work, and also we summarize the previous experiments that have searched for neutrino periodicity. Next, in Section IV, we review the statistical methodologies used in our analysis. In Section V, we describe the simulation strategy, compare statistical methods and introduce the signal-to-noise ratio as a convenient estimation tool. Then in Section VI, we present our resulting projections, and in Section VII, the discussion and conclusions.

II. EVENT RATES AT DIFFERENT DETECTORS

A. Theoretical calculation

Figures 1 and 2 show the electron and nuclear recoil spectra for the solar, atmospheric, and DSNB spectra for Xenon and Argon targets. The nuclear recoil spectrum uses the neutral current coherent elastic neutrino-nucleus scattering (CEvNS) channel, and the electron recoil channel uses charged current neutrino-electron elastic scattering (ES). We refer to previous literature for details of these calculations [19]. Here we simply highlight the components of the spectrum as a function of recoil energy to get a sense of the recoil threshold required to detect each component. For Solar neutrinos, we used the high metallicity model for the normalization [20]. We also show the appropriate experimental background components [21].

In addition to the energy dependence shown in Figure 1 and 2, for several of the neutrino components there is a time variation to the flux. For solar neutrinos, since the time variation due to the eccentricity of the Earth's orbit affects all flavors, it will be present in both the CEvNS and the ES channels. For charged current detection channels, the day-night effect due to oscillations is present in the ES channel. For atmospheric neutrinos, the time variation from the solar modulation of the atmospheric neutrino

TDiff invariant gauge fields in cosmology

Antonio L. Maroto^{*} and Alfredo D. Miravet[†]

*Departamento de Física Teórica and Instituto de Física de Partículas y del Cosmos (IPARCOS-UCM),
Universidad Complutense de Madrid, 28040 Madrid, Spain*

(Dated: February 29, 2024)

We study the dynamics of Abelian gauge fields invariant under transverse diffeomorphisms (TDiff) in cosmological contexts. We show that in the geometric optics approximation, very much as for Diff invariant theories, the corresponding massless gauge bosons propagate along null geodesics and particle number is conserved. In addition, the polarization vectors are orthogonal to the propagation direction and the physical (transverse projection) polarization is parallel transported along the geodesics. We also consider TDiff invariant Dirac spinors, study the coupling to the gauge fields and analyze the conditions in order to avoid violations of Einstein's Equivalence Principle. The contributions to the energy-momentum tensor of the gauge field are also analyzed. We find that, in general, the breaking of Diff invariance makes the electric and magnetic parts of the vector field to gravitate in a different way. In the sub-Hubble regime we recover the standard radiation-like behaviour of the energy density, however in the super-Hubble regime the behaviour is totally different to the Diff case, thus opening up a wide range of possibilities for cosmological model building. In particular, possible effects on the evolution of large-scale primordial magnetic fields are discussed.

I. INTRODUCTION

Einstein's General Relativity (GR) is the best description of gravity we have to date. It has performed exceptionally well in multiple tests ranging from the Solar System orbits to gravitational lensing and has been able to describe purely gravitational phenomena such as black holes and gravitational waves. It also serves as a theoretical framework for the standard Lambda-cold dark matter (Λ CDM) cosmology, which is a phenomenological model that accurately describes the large-scale structure and evolution of the universe with only a handful of parameters. GR relies on invariance under general coordinate transformations, i.e., invariance under diffeomorphisms (Diff) and Einstein's Equivalence Principle [1], which is equivalent to the Weak Equivalence Principle (WEP), Local Lorentz Invariance (LLI) and Local Position invariance (LPI). GR comes with its shortcomings though: Its lack of description of quantum gravity and the unknown fundamental nature of the dark sector of Cosmology have motivated the search for alternatives to GR. Generally, these modifications of GR consist of additional degrees of freedom, implemented in multiple ways, that alter the behaviour of gravity in a certain regime, typically at very long or very short distances.

Over the last decade, there has been a growing interest in theories that break Diff-invariance down to invariance under transverse diffeomorphisms (TDiff), a subgroup restricted to volume-preserving general transformations. Early works include [2, 3], in which a stability analysis of TDiff-invariant theories is performed at classical and one-loop levels. Here it was found that by enhancing the symmetry group with local Weyl invariance (dubbed WTDiff), the additional scalar degree of freedom is removed, thus propagating the same degrees of freedom as GR and preventing possible ghost instabilities. Unimodular gravity [4–11], the most popular TDiff-invariant theory for gravity, falls into this category and features the metric determinant treated as a non-dynamical scalar, so only the traceless part of Einstein's equations contribute to the dynamics. As a matter of fact, unimodular gravity has been proposed as a simple solution to the vacuum energy problem [12]. TDiff models beyond unimodular gravity have also been considered in [2, 13–16]. In these models, the metric determinant is a dynamical field and the corresponding spectrum includes a scalar graviton in addition to the standard massless spin-2 graviton. Also, the cosmological evolution in TDiff-invariant theories propagating a scalar graviton mode was recently investigated in [17].

Breaking down to TDiff was also considered in the coupling to matter in the case of scalar fields in [18, 19] and possible violations of the Einstein Equivalence Principle were found. However, in [20], it was shown that, in the geometric optics approximation, when breaking down to TDiff invariance by a global factor in the matter action, the three types of masses (inertial, active and passive) agree with those of standard Diff invariant theories thus

^{*}Electronic address: maroto@ucm.es

[†]Electronic address: alfrdelg@ucm.es

Gravitational wave memory signatures in identifying transition redshift

Indranil Chakraborty,^{*} Susmita Jana,[†] and S. Shankaranarayanan[‡]

Department of Physics, Indian Institute of Technology Bombay, Mumbai 400076, India

Abstract

Many astrophysical and cosmological observations consistently indicate that the universe is currently accelerating. Despite many possible explanations, the exact cause of this acceleration remains unknown. Therefore, additional observational probes are necessary to pinpoint the cause. Gravitational waves (GWs) have the potential to unravel some of the unresolved mysteries in cosmology. In this work, we highlight the potential utility of *gravitational wave memory* as a tool to identify the cause of this acceleration. We evaluate cosmological memory as a particular case of the master equation for GW memory in Locally Rotationally Symmetric type II spacetimes. Unlike the previous works, the master equation for GW memory contains non-linear dependence of the background quantities. Hence, even though the successive GWs generated are smaller than their predecessors, we demonstrate that their cumulative effect over cosmological time leads to observable signatures, akin to the growth of density perturbations resulting in large-scale structures. Finally, we show that the GW memory exhibits distinct signatures between accelerated and decelerated universes, potentially enabling the identification of the transition redshift from a matter-dominated to a dark-energy-dominated universe.

^{*} indranil.phy@iitb.ac.in; Equal contribution to this work.

[†] susmitajana@iitb.ac.in; Equal contribution to this work.

[‡] shanki@iitb.ac.in

Gravitational Repulsion in an Expanding Ball of Dust

Diogo P. L. Bragança*

*Kavli Institute for Particle Astrophysics and Cosmology - KIPAC,
Department of Physics, Stanford University, Stanford, CA 94305, USA*

In general relativity, there is a velocity dependent term in the gravitational acceleration of a test particle for an observer at infinity. Depending on the direction of motion and the speed, that term can be repulsive. We show that this is also the case in the Parametrized Post-Newtonian (PPN) formalism. We compute the magnitude of that repulsive term for an expanding sphere of dust observed at infinity, and find that it could mimic the effect of a cosmological constant. The time evolution of such an expanding ball of dust for an observer at infinity is calculated, and compared with the standard Λ CDM model. We find that the so-called coincidence problem does not exist for such a model as the energy density attributed to the expansion is always of the same order as the matter energy density.

CONTENTS

I. Introduction	1
II. Gravitational repulsion in Schwarzschild and in the PPN formalism	2
A. Repulsion in Schwarzschild spacetime	2
B. Repulsion in the PPN formalism	3
III. Expanding ball of dust embedded in Schwarzschild spacetime	3
IV. Application to cosmology: cosmological acceleration	4
A. Dynamical analysis	5
B. Comparison with Λ CDM	6
V. Discussion and Conclusion	7
ACKNOWLEDGMENTS	7
References	7

I. INTRODUCTION

Since Milne and McCrea [1–3] found that the Friedmann equations could be derived from Newtonian mechanics, the so-called Newtonian cosmology consisting in the study of an expanding ball of fluid has consistently been explored and interpreted, especially in comparison with relativistic cosmology. Harrison [4] used Newtonian gravity to derive the Friedmann equations from a partitioned Universe. Callan, Dicke, and Peebles [5] also confirmed that a Newtonian mechanics is sufficient to describe the real expanding universe (and not just a crude classical model). Tipler [6, 7] even showed that Newtonian cosmology could be made as rigorous as relativistic cosmology provided that Newtonian gravity is formu-

lated in geometrical language, proving also that Newtonian cosmology is more general than Friedmannian cosmology. Reis [8] showed that even if the background evolution in Newtonian and relativistic cosmology could match, the growth of perturbations in the two regimes is not exactly the same when pressure is non-zero. Ellis and Gibbons [9] built a discrete Newtonian cosmology from the bottom up using only point-particles, again finding the same equations as relativistic cosmology.

Newtonian cosmology has also inspired work in describing an expanding ball of fluid from a fully relativistic perspective. In that regard, Bilić and Tolić [10] showed that this system can reproduce any FLRW cosmology by choosing an appropriate potential. More recently, Faraoni and Atieh [11] studied a similar system, studying quasi-local energy aspects and showing that there is a symmetry correspondence between the Einstein-Friedmann equations and the Newtonian system.

In parallel to this study of Newtonian cosmology, it has also been observed that general relativity contains an effectively repulsive contribution to the gravitational force. Hilbert [12] was the first to make this observation in a Schwarzschild spacetime for an observer at infinity. McVittie [13] also considered such repulsive contributions. Zel’dovich and Novikov [14] claimed that this was merely a coordinate effect (a falling object seems to slow down at the event horizon). McGruder [15] provided a review of this particular discussion in the twentieth century and noticed as Hilbert that if the particle velocity was great enough anywhere in Schwarzschild spacetime then an observer at infinity would always observe a repulsive force. More recently, Gorkavyyi and Vasilkov [16] claimed that there could also be a repulsive force in general relativity if the gravitational mass of the system decreases (for example by gravitational radiation). McGruder [17] even hypothesized that the gravitational repulsion in Schwarzschild spacetime could explain cosmic rays. Grøn [18] showed that if the velocity of the particle is zero, then there is never a gravitational repulsion in the Schwarzschild field.

Given these two research topics (Newtonian cosmology and gravitational repulsion), it then becomes interesting to combine them and analyze the relativistic grav-

* diogobraganca@alumni.stanford.edu

An Axion Pulsarscope

Mariia Khelashvili,^{1,2,3,*} Mariangela Lisanti,^{1,4,†} Anirudh Prabhu,^{5,‡} and Benjamin R. Safdi^{6,7,§}

¹*Department of Physics, Princeton University, Princeton, NJ 08544, USA*

²*Bogolyubov Institute for Theoretical Physics of the NAS of Ukraine, Metrolohichna Str. 14-b, Kyiv, 03143, Ukraine*

³*Goethe Universität, Max-von-Laue Str. 1, Frankfurt am Main, 60438, Germany*

⁴*Center for Computational Astrophysics, Flatiron Institute, New York, NY 10010, USA*

⁵*Princeton Center for Theoretical Science, Princeton University, Princeton, NJ 08544, USA*

⁶*Berkeley Center for Theoretical Physics, University of California, Berkeley, CA 94720, USA*

⁷*Theoretical Physics Group, Lawrence Berkeley National Laboratory, Berkeley, CA 94720, USA*

(Dated: February 29, 2024)

Electromagnetic fields surrounding pulsars may source coherent ultralight axion signals at the known rotational frequencies of the neutron stars, which can be detected by laboratory experiments (*e.g.*, pulsarscopes). As a promising case study, we model axion emission from the well-studied Crab pulsar, which would yield a prominent signal at $f \approx 29.6$ Hz regardless of whether the axion contributes to the dark matter abundance. We estimate the relevant sensitivity of future axion dark matter detection experiments such as DMRadio-GUT, Dark SRF, and CASPER, assuming different magnetosphere models to bracket the uncertainty in astrophysical modeling. For example, depending on final experimental parameters, the Dark SRF experiment could probe axions with any mass $m_a \ll 10^{-13}$ eV down to $g_{a\gamma\gamma} \sim 3 \times 10^{-13}$ GeV⁻¹ with one year of data and assuming the vacuum magnetosphere model. These projected sensitivities may be degraded depending on the extent to which the magnetosphere is screened by charge-filled plasma. The promise of pulsar-sourced axions as a clean target for direct detection experiments motivates dedicated simulations of axion production in pulsar magnetospheres.

Introduction.— The existence of axions is predicted by numerous well-motivated extensions to the Standard Model [1, 2]. While interesting in their own right, these ultralight pseudoscalar bosons can potentially account for the dark matter (DM), as is the case for the quantum chromodynamics (QCD) axion [3–10]. Given their ubiquity in theoretical models, a broad laboratory program exists to search for axions (see [11–13]). This includes haloscope experiments, which search for axion DM in the Milky Way [14–28], helioscope experiments, which search for axions produced by the Sun [29, 30], and “light shining through walls” experiments, which aim to produce axions directly in the lab [31, 32]. This Letter proposes a fourth alternative—the *pulsarscope*—and demonstrates that planned experiments can successfully search for coherent axion signals emitted by nearby pulsars.

Axions are generically expected to couple to Standard Model fields through dimension-five operators, motivating efforts to detect them in the laboratory. For example, the axion field, $a(x)$, couples to electromagnetism through the operator $\mathcal{L} \supset -g_{a\gamma\gamma} a F \tilde{F} / 4 = g_{a\gamma\gamma} a \mathbf{E} \cdot \mathbf{B}$, where $g_{a\gamma\gamma}$ is the coupling constant, F is the quantum electrodynamics (QED) field strength, and \mathbf{E} (\mathbf{B}) is the electric (magnetic) field. The axion may also couple to Standard Model fermions f through the operator $\mathcal{L} \supset (g_{aff}/2m_f) \partial_\mu a \bar{f} \gamma^\mu \gamma^5 f = -(g_{aff}/m_f) \nabla \cdot \mathbf{S}$ (in the non-relativistic limit), where \mathbf{S} is the fermion spin operator, m_f is the fermion mass, and g_{aff} is the coupling constant. These operators may induce observable signatures in laboratory experiments, such as axion-to-photon conversion (*e.g.*, [29, 30, 33–38]) or spin precession (*e.g.*, [39–45]).

Rapidly-rotating neutron stars (NSs), or pulsars, can serve as axion factories because their magnetospheres may possess regions of large, un-screened accelerating electric fields ($\mathbf{E} \cdot \mathbf{B} \neq 0$) [46–48]. In non-axisymmetric pulsar magnetospheres, ultralight axions are efficiently radiated at the rotation frequency of the pulsar, Ω [46]. As illustrated in Fig. 1, this relativistic axion signal travels towards Earth, where it may be detected by a ground-based experiment. While their densities are generally much smaller than the DM density near Earth [12], pulsar-sourced axions benefit from large coherence times and have known frequencies.

We estimate the sensitivity of proposed axion DM detection experiments to pulsar-sourced axions. We consider two extreme models of the pulsar magnetosphere to bracket the uncertainty on the expected signal. The leading sensitivity to low-mass axions is obtained from the CASPER-wind [40–43], Dark SRF [49, 50], and DMRadio-GUT [51, 52] experiments. Most optimistically, these experiments could probe previously unexplored regions of axion parameter space for axion masses $m_a \ll 10^{-13}$ eV; however, if the magnetospheres are heavily screened, then the sensitivities may be subdominant relative to current constraints.

Axion Radiation from Pulsars.— The axion field sourced by a pulsar is determined by the distribution of $\mathbf{E} \cdot \mathbf{B}$ in the magnetosphere according to the Klein-Gordon equation, $(\square + m_a^2) a(x) = g_{a\gamma\gamma} \mathbf{E} \cdot \mathbf{B}$. In the limit where the axion mass $m_a \rightarrow 0$, this equation is analogous to that for the electric potential, interpreted as $a(x)$, in Lorenz gauge with charge density $\rho_{\text{eff}} = g_{a\gamma\gamma} \mathbf{E} \cdot \mathbf{B}$. Thus, one can calculate the radiated axion signal given a model

Measuring Tracers of Planet Formation in the Atmosphere of WASP-77A b: Sub-stellar O/H and C/H ratios, with a stellar C/O ratio and a potentially Super-stellar Ti/H ratio

BILLY EDWARDS^{1,2} AND QUENTIN CHANGEAT^{3,2}

¹*SRON, Netherlands Institute for Space Research, Niels Bohrweg 4, NL-2333 CA, Leiden, The Netherlands*

²*Department of Physics and Astronomy, University College London, Gower Street, WC1E 6BT London, United Kingdom*

³*European Space Agency (ESA), ESA Office, Space Telescope Science Institute (STScI), Baltimore MD 21218, USA*

(Received September 1, 2023; Revised December 18, 2023; Accepted December 19, 2023)

Submitted to ApJ Letters

ABSTRACT

We present a comprehensive atmospheric retrieval study of the hot Jupiter WASP-77A b using eclipse observations from the Hubble Space Telescope (HST) and JWST. Using atmospheric retrievals, the spectral features of H₂O, CO, and TiO are identified, with volume mixing ratios estimated at $\log_{10}(\text{VMR}) = -4.40^{+0.14}_{-0.11}$, $-4.44^{+0.34}_{-0.28}$, and $-6.40^{+0.22}_{-0.23}$, respectively. We derive the atmospheric carbon-to-oxygen ratio – a key planetary formation tracer – to be $\text{C/O} = 0.54 \pm 0.12$, which is consistent with both the stellar host value and previous studies of the planet’s atmosphere, suggesting a relatively close-in formation. Computing other elemental ratios (i.e., C/H, O/H, and Ti/H), we conclude that the general enrichment of the atmosphere (i.e., metallicity) is sub-stellar, is depleted in C and O, but that Ti appears slightly super-stellar. A low C and O content could be obtained, in combination with a stellar C/O ratio, if the planet formed outside of the CO₂ snow line before migrating inwards. Meanwhile, a super-stellar Ti/H could be obtained by late contamination from refractory rich planetesimals. While broadly in agreement with previous works, we do find some differences and discuss these while also highlighting the need for homogeneous analyses when comparative exoplanetology is conducted.

Keywords: Exoplanet atmospheres (487); Hot Jupiters (753); Hubble Space Telescope (761); JWST (2291)

1. INTRODUCTION

Despite being a rare outcome of planetary formation, numerous hot Jupiters have been detected due to the transit technique being biased toward large planets on short orbits. As their size and temperature are favourable for atmospheric characterisation, most atmospheric observational studies using space-based instruments have focused on this class of objects. With the advent of the spatial scanning technique (McCullough & MacKenty 2012), the Wide Field Camera 3 (WFC3) on board the Hubble Space Telescope (HST) has enabled around one hundred of those planets to be characterised via transit (e.g., Tsiaras et al. 2018; Pinhas et al. 2019; Cubillos & Blečić 2021; Kawashima & Min 2021; Edwards et al. 2023) and eclipse (e.g., Mansfield et al. 2021; Changeat et al.

2022) spectroscopy, enabling the search for trends in their atmospheric composition.

More recently, JWST has become the premier facility for space-based exoplanet spectroscopy. The four instruments on board JWST offer a wider simultaneous wavelength coverage than was previously available as well as access to previously uncharted spectral regions. Early studies of giant exoplanets have successfully used each of these JWST instruments for transit (e.g., Dyrek et al. 2023; Feinstein et al. 2023), eclipse (e.g., Bean et al. 2023; Coulombe et al. 2023) and phase-curve observations (e.g., Bell et al. 2023).

Here, we conduct a comprehensive retrieval study on WASP-77A b, an inflated hot Jupiter in a wide binary system (Maxted et al. 2013), using data from HST and JWST. The planet orbits WASP-77A, a G8V star. WASP-77 B, a fainter K-dwarf companion to WASP-77A, is separated by 3”. WASP-77A b has been previously observed in emission with the ground-based high-resolution Immersion GRating Infrared Spectrometer (IGRINS) on Gemini-South (covering wavelengths from $\lambda \in [1.45, 2.55] \mu\text{m}$). Those observa-

A New Probe of Cosmic Birefringence Using Galaxy Polarization and Shapes

Weichen Winston Yin,^{1,*} Liang Dai,¹ Junwu Huang,² Lingyuan Ji,¹ and Simone Ferraro^{3,1}

¹*Department of Physics, 366 Physics North MC 7300,
University of California, Berkeley, CA 94720, USA*

²*Perimeter Institute for Theoretical Physics, 31 Caroline St. N., Waterloo, Ontario N2L 2Y5, Canada*

³*Physics Division, Lawrence Berkeley National Laboratory, Berkeley, CA 94720, USA*

(Dated: February 29, 2024)

We propose a new method to search for parity-violating new physics via measurements of cosmic birefringence and demonstrate its power in detecting the topological effect originating from an axion string network with an axion-photon coupling as a motivated source of cosmic birefringence. The method, using large galaxy samples, exploits an empirical correlation between the polarization direction of the integrated radio emission from a spiral galaxy and its apparent shape. We devise unbiased minimum-variance quadratic estimators for discrete samples of galaxies with both integrated radio polarization and shape measurements. Assuming a synergy with overlapping optical imaging surveys, we forecast the sensitivity to polarization rotation of the forthcoming SKA radio continuum surveys of spiral galaxies out to $z \sim 1.5$. The angular noise power spectrum of polarization rotation using our method can be lower than that expected from CMB Stage-IV experiments, when assuming a wide survey covering $\sim 1000 \text{ deg}^2$ and reaching an RMS flux of $\sim 1 \mu\text{Jy}$. Our method will be complementary to CMB-based methods as it will be subject to different systematics. It can be generalized to probe time-varying or redshift-varying birefringence signals.

Introduction — The question of whether discrete transformations—charge conjugation (C), parity (P), and time reversal (T)—are fundamental symmetries of the Universe has led to important discoveries [1–3]. The axion was originally proposed to solve the strong CP problem in Quantum Chromodynamics [4–7]. More recently, generic axions are shown to arise abundantly in string theory [8, 9]. The Chern-Simons interaction between the axion and electromagnetism leads to the parity-violating cosmic birefringence effect [10]:

$$\mathcal{L} = -\frac{1}{4} g_{a\gamma\gamma} a F^{\mu\nu} \tilde{F}_{\mu\nu} = g_{a\gamma\gamma} a \mathbf{E} \cdot \mathbf{B}, \quad (1)$$

where a is the axion field, $F^{\mu\nu}$ is the electromagnetic field strength tensor, and $\tilde{F}^{\mu\nu} \equiv (1/2) \epsilon_{\mu\nu\rho\sigma} F^{\rho\sigma}$ is its dual. As a photon travels through a background axion field, its plane of polarization rotates by an angle proportional to the net change in the axion field value along the photon’s worldline, multiplied by the axion-photon coupling constant $g_{a\gamma\gamma}$. The rotation is independent of the photon’s frequency due to the topological nature of the interaction [11–13]. Recent analyses of the cosmic microwave background (CMB) have shown hints of a rotation of its polarization anisotropies that is highly coherent across the sky, on the order of a fraction of a degree [14, 15]. Possible contamination from foregrounds is being investigated [16]. On the other hand, searches for anisotropic birefringence have not so far uncovered a signal [17–20].

Measuring birefringence toward any single astrophysical source or along any single sightline is hindered by our lack of knowledge about the *intrinsic* polarization direction of the source. When the CMB is used as the probe,




this fundamental problem is solved statistically. Rotation angles that are correlated across the sky are measurable owing to the state-of-the-art cosmological model that accurately predicts the Gaussian statistics of the primary CMB polarization anisotropies [20–23]. To confidently confirm a signal of cosmic birefringence, it is important to consider alternative methods of detection based on distinct cosmological or astrophysical probes whose systematics are independent of CMB measurements.

In this paper, we propose a new probe of cosmic birefringence that relies on a large sample of spiral galaxies with both radio polarization and apparent shape measurements. This is motivated by empirical findings that the *integrated* radio emission of nearby spiral galaxies, at least at 4.8 GHz, is significantly polarized and aligns on average with the apparent minor axis of the optical galactic disk [24]. A plausible explanation for this alignment is that the polarized radio emission is predominantly synchrotron radiation powered by star-formation feedback and has a polarization direction perpendicular to the local toroidal magnetic field that is ordered on the galactic scale. Integrating over the entire disk results in a non-zero net polarization if the disk is inclined. It seems reasonable to assume that a similar empirical correlation is true for a cosmological population of spiral galaxies. The apparent disk shape can be measured with either optical imaging or interferometric radio imaging, with the former available from existing weak lensing catalogs [25–27] or from upcoming imaging surveys [28, 29].

In reality, the polarization-shape alignment is imperfect either due to the poloidal component of the ordered magnetic field or due to randomly arising asymmetry in the disk structure. Nonetheless, one expects that the mean polarization-shape misalignment angle is zero among a sample of unrelated galaxies, as long as all the physics on the (sub-)galactic scale responsible for the

* winstonyin@berkeley.edu

Primordial Magnetic Fields in Light of Dark Ages Global 21-cm Signal

Vivekanand Mohapatra ¹, Pravin Kumar Natwariya ^{2,3},
Alekha C. Nayak ^{1*}

¹Department of Physics, National Institute of Technology Meghalaya,
Shillong, 793003, Meghalaya, India.

²School of Fundamental Physics and Mathematical Sciences, Hangzhou
Institute for Advanced Study, UCAS, Hangzhou, 310024, China.

³University of Chinese Academy of Sciences, Beijing, 100190, China.

*Corresponding author(s). E-mail(s): acnayak@nitm.ac.in;
Contributing authors: p22ph003@nitm.ac.in; pravin@ucas.ac.cn;

Abstract

We study the constraints on the primordial magnetic fields in light of dark ages global 21-cm signal. An early absorption signal in the redshift of $200 \lesssim z \lesssim 30$ is predicted in the Λ CDM model of cosmology. During the Dark Ages, there were no stars, therefore, measuring the global 21-cm signal can provide pristine cosmological information. However, measuring the Dark Ages global 21-cm signal from ground-based telescopes is challenging. To overcome this difficulty, recently lunar and space-based experiments have been proposed, such as FARSIDE, DAPPER, FarView, etc. Primordial magnetic fields can heat the intergalactic medium gas via magnetohydrodynamic effects. We study the effects of magnetic fields on the Dark Ages global 21-cm signal and constrain the present-day strength of primordial magnetic fields and the spectral index. We find that measuring the Dark Ages signal can provide stronger bounds compared to the existing constraints from Planck 2016. Additionally, we also explore the dark-ages consistency ratio which can identify the magnetic heating of IGM by measuring the 21-cm signal at only three different redshifts in future experiments.

Keywords: 21-cm signal, Dark Ages, Primordial Magnetic Fields

Dark Scattering: accelerated constraints from KiDS-1000 with ReACT and CosmoPower

Karim Carrion,^{1*} Pedro Carrilho,² Alessio Spurio Mancini,^{3,4,5} Alkistis Pourtsidou,^{2,6} Juan Carlos Hidalgo¹

¹ Instituto de Ciencias Físicas, Universidad Nacional Autónoma de México, Cuernavaca, Morelos, 62210, Mexico

² Institute for Astronomy, The University of Edinburgh, Royal Observatory, Edinburgh EH9 3HJ, UK

³ Department of Physics, Royal Holloway, University of London, Egham Hill, Egham, UK

⁴ Mullard Space Science Laboratory, University College London, Holmbury St. Mary, Dorking, Surrey, RH5 6NT, UK

⁵ Department of Physics and Astronomy, University College London, Gower Street, London WC1E 6BT, UK

⁶ Higgs Centre for Theoretical Physics, School of Physics and Astronomy, The University of Edinburgh, Edinburgh EH9 3FD, UK

Accepted XXX. Received YYY; in original form ZZZ

ABSTRACT

We present constraints on the Dark Scattering model through cosmic shear measurements from the Kilo Degree Survey (KiDS-1000), using an accelerated pipeline with novel emulators produced with CosmoPower. Our main emulator, for the Dark Scattering non-linear matter power spectrum, is trained on predictions from the halo model reaction framework, previously validated against simulations. Additionally, we include the effects of baryonic feedback from HMcode2016, whose contribution is also emulated. We analyse the complete set of statistics of KiDS-1000, namely Band Powers, COSEBIs and Correlation Functions, for Dark Scattering in two distinct cases. In the first case, taking into account only KiDS cosmic shear data, we constrain the amplitude of the dark energy – dark matter interaction to be $|A_{\text{ds}}| \lesssim 20$ b/GeV at 68% C.L. Furthermore, we add information from the cosmic microwave background (CMB) from Planck, along with baryon acoustic oscillations (BAO) from 6dFGS, SDSS and BOSS, approximating a combined weak lensing + CMB + BAO analysis. From this combination, we constrain $A_{\text{ds}} = 10.6^{+4.5}_{-7.3}$ b/GeV at 68% C.L. We confirm that with this estimated value of A_{ds} the interacting model considered in this work offers a promising alternative to solve the S_8 tension.

Key words: cosmology: theory – observations – large-scale structure of the Universe – methods: numerical, machine learning, statistical

1 INTRODUCTION

Over the coming years cosmology will be transformed, with enormous amounts of new data being collected by Stage IV surveys such as DESI¹, which recently released its first set of data (Adame et al. 2023), the recently launched Euclid² satellite mission (Laureijs et al. 2011), The Vera Rubin Observatory³ (Abate et al. 2012), and the SKA Observatory⁴ (Bacon et al. 2020). These are going to observe several millions of galaxies over a large fraction of the sky, in the optical and radio wavelengths out to high redshifts. With these instruments it will soon be possible to probe scales approaching the size of the Hubble horizon, and determine with greater accuracy the properties of the Universe.

The standard cosmological model is Λ CDM, consisting of dark energy in the form of a cosmological constant Λ and cold dark matter. Stage IV optical galaxy surveys will use galaxy clustering and weak gravitational lensing to probe the nature of dark energy and aim

to provide sub-percent constraints on the equation of state of dark energy (w).

In recent years, as more data has become available, the Λ CDM model has come into question due to apparent inconsistencies (tensions) between observables. Firstly, the H_0 measurements from early and late-time probes differ significantly, at a level of $\sim 5\sigma$ (Riess 2019; Di Valentino et al. 2021). Secondly, the amplitude of density fluctuations at early times, encoded in the σ_8 value extrapolated to the present day, is inconsistent with the near redshift measurements of that same quantity (see Douspis et al. (2018)). This second tension is most evident in the inferred values of the parameter $S_8 \equiv \sigma_8 \sqrt{\Omega_m/0.3}$: from the latest cosmic microwave background (CMB) measurements of the Planck satellite we have $S_8 = 0.825 \pm 0.011$ (Aghanim et al. 2020b), whereas at low redshifts, weak lensing measurements from the DES collaboration (Abbott et al. 2022) have estimated $S_8 = 0.776 \pm 0.017$ and the Kilo-Degree Survey (KiDS-1000) (Asgari et al. 2021) reports a value of $S_8 = 0.759^{+0.024}_{-0.021}$. Furthermore, the joint analysis of these last two surveys (Abbott et al. 2023) found a value of $S_8 = 0.790^{+0.018}_{-0.014}$. Thus, discrepancies are around $2 - 2.5\sigma$ with respect to Planck. While such discrepancies may be attributed to systematics or unaccounted astrophysical processes, the role of cosmological modelling cannot be entirely ruled out (Cortés & Liddle 2023).

In the pursuit of alternatives to the concordance model, interacting

* E-mail: kcarrion@icf.unam.mx

¹ <https://www.desi.lbl.gov>

² <https://www.euclid-ec.org>

³ <https://www.lsst.org/about>

⁴ <https://www.skatelescope.org/science>

Primordial Rotating Disk Composed of ≥ 15 Dense Star-Forming Clumps at Cosmic Dawn

S. Fujimoto^{1,*}, M. Ouchi^{2,3,4,5}, K. Kohno^{6,7}, F. Valentino^{8,9}, C. Giménez-Arteaga^{9,10}, G. B. Brammer^{9,10}, L. J. Furtak¹¹, M. Kohandel¹², M. Oguri^{13,14}, A. Pallottini¹², J. Richard¹⁵, A. Zitrin¹¹, F. E. Bauer^{16,17,18}, M. Boylan-Kolchin¹, M. Dessauges-Zavadsky¹⁹, E. Egami²⁰, S. L. Finkelstein¹, Z. Ma²⁰, I. Smail²¹, D. Watson^{9,10}, T. A. Hutchison²², J. R. Rigby²², B. D. Welch^{22,23,24}, Y. Ao^{25,26}, L. D. Bradley²⁷, G. B. Caminha²⁸, K. I. Caputi²⁹, D. Espada^{30,31}, R. Endsley¹, Y. Fudamoto¹³, J. González-López^{32,33}, B. Hatsukade^{4,6,34}, A. M. Koekemoer²⁶, V. Kokorev²⁸, N. Laporte³⁵, M. Lee^{9,36}, G. E. Magdis^{9,10,36}, Y. Ono³, F. Rizzo^{9,10}, T. Shibuya³⁷, K. Shimasaku^{6,7}, F. Sun¹⁵, S. Toft^{9,10}, H. Umehata^{38,39,40}, T. Wang^{41,42}, and H. Yajima⁴³

Early galaxy formation, initiated by the dark matter and gas assembly, evolves through frequent mergers and feedback processes into dynamically hot, chaotic structures¹. In contrast, dynamically cold, smooth rotating disks have been observed in massive evolved galaxies merely 1.4 billion years after the Big Bang², suggesting rapid morphological and dynamical evolution in the early Universe. Probing this evolution mechanism necessitates studies of young galaxies, yet efforts have been hindered by observational limitations in both sensitivity and spatial resolution. Here we report high-resolution observations of a strongly lensed and quintuply imaged, low-luminosity, young galaxy at $z = 6.072$ (dubbed *the Cosmic Grapes*), 930 million years after the Big Bang. Magnified by gravitational lensing, the galaxy is resolved into at least 15 individual star-forming clumps with effective radii of $r_e \simeq 10\text{--}60$ parsec (pc), which dominate $\simeq 70\%$ of the galaxy's total flux. The cool gas emission unveils a smooth, underlying rotating disk characterized by a high rotational-to-random motion ratio and a gravitationally unstable state (Toomre $Q \simeq 0.2\text{--}0.3$), with high surface gas densities comparable to local dusty starbursts with $\simeq 10^{3\text{--}5}$ solar mass (M_\odot) per pc². These gas properties suggest that the numerous star-forming clumps are formed through disk instabilities with weak feedback effects. The clumpiness of *the Cosmic Grapes* significantly exceeds that of galaxies at later epochs and the predictions from current simulations for early galaxies. Our findings shed new light on internal galaxy substructures and their relation to the underlying dynamics and feedback mechanisms at play during their early formation phases, potentially explaining the high abundance of bright galaxies observed in the early Universe³ and the dark matter core-cusp problem⁴.

Using the James Webb Space Telescope (JWST) with Near Infrared Camera (NIRCam), we obtained deep near-infrared (NIR) imaging over $1\text{--}5\mu\text{m}$ wavelengths of a gravitationally-lensed star-forming galaxy, the *Cosmic Grapes* at $z = 6.072$. The *Cosmic Grapes* and the arc were initially discovered as multiply lensed images via the bright [C II] $158\mu\text{m}$ emission lines in the Atacama Large Millimeter Array (ALMA) Lensing Cluster Survey behind the massive galaxy cluster RXCJ0600-2007^{5,6}. A total of five multiple images have been spectroscopically confirmed, which provides stringent constraints from their sky positions and morphology, resulting in a well-constrained magnification estimate of $\mu = 32_{-6.8}^{+0.7}$ for the *Cosmic Grapes*, even in this high magni-

On the Age Calibration of Open Clusters using Red Clump Stars

ABIGAIL R. CHRISS ¹ AND GUY WORTHEY ²

¹*Department of Physics and Astronomy, Bowdoin College, 8800 College Station, Brunswick, ME 04011-8488, USA*

²*Department of Physics and Astronomy, Washington State University, 1245 Webster Hall, Pullman, WA 99164-2814, USA*

(Received February 29, 2024; Revised XXX; Accepted YYY)

ABSTRACT

In this study, we extend the dust-independent [Hatzidimitriou \(1991\)](#) relation between cluster age and d_{B-R} color difference between red giant branch (RGB) and red clump (RC) to younger cluster ages. We perform membership analysis on twenty-two open clusters using *Gaia* DR3 astrometry, then compute the difference in color of red giant branch and red clump d_{B-R} using *Gaia* photometry. We find that the trend derived from older clusters does not extrapolate to younger ages and becomes double-valued. We confirm that d_{B-R} is independent of metallicity. Current stellar evolutionary isochrones do not quantitatively reproduce the trend and furthermore predict an increased color gap with a decrease in metallicity that is not echoed in the data. Integrated light models based on current isochrones exaggerate the color change over the $-0.5 < [\text{Fe}/\text{H}] < 0$ interval at the few-percent level.

Keywords: Open star clusters (1160) — Stellar ages (1581) — Red giant clump (1370) — Red giant branch (1368) — Hertzsprung Russell diagram (725)

1. INTRODUCTION

Star clusters represent both a crucial testing ground for the theory of stellar evolution and markers for the chemical and dynamical history of the Milky Way and other galaxies. While massive star clusters typically host multiple stellar populations ([Gratton et al. 2012](#)), lower-mass open clusters are currently presumed to be simple stellar populations (SSPs) of a single age and heavy element abundance pattern. Cluster ages are often derived from the color magnitude diagram (CMD), where, especially, the luminosity of the main sequence turnoff (MSTO) provides a theoretically robust chronometer ([Chaboyer 1995](#)).

Even assuming perfect comparison models, distance uncertainty and line of sight dust extinction add error to age estimates. [Hatzidimitriou \(1991\)](#), hereafter [H91](#), proposed a method that bypasses both dust and distance. The color of the He-burning red clump (RC) is subtracted from the color of the H-burning red giant branch (RGB) at the same luminosity. [H91](#) used Johnson-Cousins B and R filters and thus the color difference is d_{B-R} . Age was found to track d_{B-R} for clusters older than ~ 2 Gyr and for a variety of heavy element abundances. A bonus advantage of this method is that red clump stars are ~ 100 times brighter than MSTO stars, and thus the method could be applied to distant clusters.

The advent of star formation history reconstruction methods, where the entire CMD is fit with a swarm of stellar evolutionary isochrones ([Harris & Zaritsky 2001](#); [Dolphin 2002](#)), might explain why the [H91](#) formula has not seen wide use ([Girardi 2016](#)). [Girardi](#) notes, however, that the reconstructions for older ages rest upon clump and RGB lifetimes, something predicted by stellar evolutionary theory only at the 20% level.

The purpose of the present work is to confirm and extend [H91](#)'s result. The red clump should exist in the CMD for ages as young as ~ 200 Myr, or MSTO masses of $\sim 5 M_{\odot}$. We were curious if [H91](#)'s result extended to younger populations. To that end, we mined *Gaia* open cluster data for additional clusters with red clumps, with particular attention to clusters between 200 Myr and 2 Gyr in age.

We describe cluster membership discrimination and our derivation of isochrone-based ages in §2. The [H91](#) method is addressed in §3, and we discuss the result in §4.

2. CLUSTER SAMPLE AND MEMBERSHIP ANALYSIS

From open cluster lists ([Kharchenko et al. 2013](#); [Cantat-Gaudin et al. 2020](#)) we selected clusters beyond the [H91](#) list, initially in the age range 200 Myr to 2 Gyr. As the project developed, we added a few older clusters to test the repeatability of the [H91](#) method. Ideal clusters lie nearby and bloom richly with stars.

High angular momentum hot differentially rotating equilibrium star evolutions in conformally flat spacetime

Patrick Chi-Kit Cheong ^{1,2,*}, Nishad Muhammed,³ Pavan Chawhan,³ Matthew D. Duez,³ and Francois Foucart¹

¹*Department of Physics & Astronomy, University of New Hampshire, 9 Library Way, Durham NH 03824, USA*

²*Department of Physics, University of California, Berkeley, Berkeley, CA 94720, USA*

³*Department of Physics & Astronomy, Washington State University, Pullman, Washington 99164, USA*

(Dated: February 29, 2024)

The conformal flatness approximation to the Einstein equations has been successfully used in many astrophysical applications such as initial data constructions and dynamical simulations. Although it has been shown that full general relativistic strongly differentially rotating equilibrium models deviate by at most a few percents from their conformally flat counterparts, whether those conformally flat solutions remain stable has not been fully addressed. To further understand the limitations of the conformal flatness approximation, in this work, we construct spatially-conformally-flat hot hypermassive neutron stars with postmerger-like rotation laws, and perform conformally flat evolutions and analysis over dynamical timescales. We found that the stellar profiles of quasi-toroidal models with high angular momentum for $J \gtrsim 9 GM_{\odot}^2/c$ can change significantly over dynamical timescales. In contrast, all the quasi-spherical models considered in this work remain stable even with high angular momentum $J = 9 GM_{\odot}^2/c$. Our investigation suggest that the quasi-spherical models are suitable initial data for long-lived hypermassive neutron star modelings in conformally flat spacetime.

I. INTRODUCTION

The detection of a binary neutron star merger on 17 August 2017 has laid a milestone in multi-messenger astronomy. This event was observed by the coincident detections of gravitational waves GW170817 [1], the short gamma-ray burst GRB170817A [2], and in other spectral bands [3]. Even though this groundbreaking multimessenger detection has confirmed our basic understanding of neutron star merger [4, 5], details of the post-merger evolution are poorly understood. A hypermassive neutron star, which is expected to be hot and supported by strong differential rotation, is one of the possible outcomes of binary neutron star merger. Studying hypermassive neutron star helps us to further understand the nature of the central engine of the relativistic jets [2, 6] and kilonova transients [7–10].

Detailed investigations of the post-merger phase over dynamical and secular timescales are extremely challenging yet significant. Not only does one need to solve Einstein field equations and general-relativistic magneto-hydrodynamics self-consistently [5], neutrino microphysics is also required [11]. Moreover, to better understand the post-merger observational signatures, seconds-long simulations are required. Hence, any simplification of the simulations is highly desirable.

The spatially conformally flat spacetime approximation [12–14] has shown to be useful for modeling neutron star mergers. Binary neutron star merger simulations based on the conformally flat approximation have been successfully carried out (e.g. [15–20], see also the applications in the context of core-collapse supernovae [21–23]






and isolated neutron stars [24–34]). In addition, it has been shown in fully general relativistic simulations that long-lived neutron star merger remnants are qualitatively axisymmetric, and the corresponding spacetime is nearly conformally flat [35, 36]. Mapping such post-merger profiles by assuming conformally flat conditions onto other evolution codes that impose different symmetries or with different input physics has been done recently [35, 36]. Specifically, the multigrid based conformally-flat spacetime solver of Gmnu [37, 38] has been demonstrated to be very effective for the studies of long-lived post-merger neutron star merger remnants over secular timescales [36].

Understanding the limitation of the conformally flat spacetime approximation in the context of hypermassive neutron stars is critical. Despite the success in neutron star modelings (e.g. [15–20]), the conformally flat condition is ultimately an approximation. This approximation is no longer valid in the case of Kerr black hole [39, 40], and it may also fail with systems that have extreme rotations or high angular momentum. Studies have shown that there is at most a few percent difference between fully general relativistic and conformally flat differentially rotating equilibrium models [41–44]. However, whether the full and conformally flat solutions share the same properties of dynamical and secular stabilities is not clearly addressed. Recently, the conformally flat approximated dynamical evolutions of quasi-toroidal models with the J -constant rotation law [45] with polytropic equation of state has been carried out [46]. Nevertheless, the rotation law considered in [46] is very different from neutron star merger. It is still unclear whether post-merger like hypermassive neutron stars can be accurately modeled under the conformal flatness approximation.

In this work, we investigate the limitations of using axisymmetric differentially rotating quasi-equilibrium mod-

* patrick.cheong@berkeley.edu; N3AS Postdoctoral fellow

Bayesian model reconstruction based on spectral line observations

FREDERIK DE CEUSTER ¹, THOMAS CEULEMANS ¹, LEEN DECIN ¹,
TAÏSSA DANILOVICH ^{1,2,3} AND JEREMY YATES ⁴

¹*Institute of Astronomy, Department of Physics & Astronomy, KU Leuven,
Celestijnenlaan 200D, 3001 Leuven, Belgium*

²*School of Physics & Astronomy, Monash University,
Clayton, Victoria, Australia*

³*ARC Centre of Excellence for All Sky Astrophysics in 3 Dimensions (ASTRO 3D),
Clayton, Victoria, Australia*

⁴*Department of Computer Science, University College London,
WC1E 6EA, London, United Kingdom*

ABSTRACT

Spectral line observations encode a wealth of information. A key challenge, therefore, lies in the interpretation of these observations in terms of models to derive the physical and chemical properties of the astronomical environments from which they arise. In this paper, we present POMME: an open-source PYTHON package that allows users to retrieve 1D or 3D models of physical properties, such as chemical abundance, velocity, and temperature distributions of (optically thin) astrophysical media, based on spectral line observations. We discuss how prior knowledge, for instance, in the form of a steady-state hydrodynamics model, can be used to guide the retrieval process, and demonstrate our methods both on synthetic and real observations of cool stellar winds.

Keywords: Radiative transfer (1335) — Astronomy software (1855) — Computational methods (1965) — High resolution spectroscopy (2096)

1. INTRODUCTION

A typical problem in astronomy is that for most of our observations we are restricted to the plane of the sky. As a result, these observations are always mere projections containing only partial information about the distribution of the physical properties of the observed object, especially along the line of sight. Luckily, in some frequency bands, the observed media are optically thin, such that we receive radiation from the

Do galaxy mergers prefer under-dense environments?

U. Sureshkumar^{1,2}, A. Durkalec³, A. Pollo^{2,3}, W. J. Pearson³, D. J. Farrow^{4,5}, A. Narayanan⁶, J. Loveday⁷,
E. N. Taylor⁸, and L. E. Suelves³

¹ Wits Centre for Astrophysics, School of Physics, University of the Witwatersrand, Private Bag 3, Johannesburg 2050, South Africa
e-mail: unnikrishnan.sureshkumar@wits.ac.za

² Astronomical Observatory of the Jagiellonian University, ul. Orla 171, 30-244 Kraków, Poland

³ National Centre for Nuclear Research, ul. Pasteura 7, 02-093 Warsaw, Poland

⁴ Centre of Excellence for Data Science, Artificial Intelligence and Modelling (DAIM), University of Hull, Cottingham Road, Hull, HU6 7RX, UK

⁵ E. A. Milne Centre for Astrophysics, University of Hull, Cottingham Road, Hull, HU6 7RX, UK

⁶ Department of Earth and Space Sciences, Indian Institute of Space Science & Technology, Thiruvananthapuram 695547, Kerala, India

⁷ Astronomy Centre, University of Sussex, Falmer, Brighton BN1 9QH, UK

⁸ Centre for Astrophysics and Supercomputing, Swinburne University of Technology, John Street, Hawthorn, 3122, Australia

Received 11 August 2023 / Accepted YYY

ABSTRACT

Context. Galaxy mergers play a crucial role in galaxy evolution. However, the correlation between mergers and the local environment of galaxies is not fully understood.

Aims. We aim to address the question of whether galaxy mergers prefer denser or less dense environments by quantifying the spatial clustering of mergers and non-mergers. We use two different indicators to classify mergers and non-mergers – classification based on a deep learning technique (f) and non-parametric measures of galaxy morphology, Gini- M_{20} (g).

Methods. We used a set of galaxy samples in the redshift range $0.1 < z < 0.15$ from the Galaxy and Mass Assembly (GAMA) survey with a stellar mass cut of $\log(M_*/M_\odot) > 9.5$. We measured and compared the two-point correlation function (2pCF) of mergers and non-mergers classified using the two merger indicators f and g . We measured the marked correlation function (MCF), in which the galaxies are weighted by f to probe the environmental dependence of galaxy mergers.

Results. We do not observe a statistically significant difference between the clustering strengths of mergers and non-mergers obtained using 2pCF. However, using the MCF measurements with f as a mark, we observe an anti-correlation between the likelihood of a galaxy being a merger and its environment. Our results emphasise the advantage of MCF over 2pCF in probing the environmental correlations.

Conclusions. Based on the MCF measurements, we conclude that the galaxy mergers prefer to occur in the under-dense environments on scales $> 50 h^{-1} \text{kpc}$ of the large-scale structure (LSS). We attribute this observation to the high relative velocities of galaxies in the densest environments that prevent them from merging.

Key words. large-scale structure of Universe – galaxies: statistics – galaxies: evolution – galaxies: interactions – cosmology: observations

1. Introduction

In the hierarchical structure formation scenario, gas cools down at the centre of dark matter haloes to form galaxies (Press & Schechter 1974; White & Rees 1978). These galaxies undergo various processes, of which galaxy mergers play an important role in galaxy evolution. Galaxy mergers occur when two or more galaxies collide into each other, and these events affect the properties of the galaxies involved. For example, galaxy mergers can lead to the transformation of disk galaxies to elliptical ones (e.g. Toomre & Toomre 1972; Schweizer 1982; Barnes 1992) and are expected to influence the star formation activity (e.g. Larson & Tinsley 1978; Barnes & Hernquist 1991; Mihos & Hernquist 1996; Ellison et al. 2008; Patton et al. 2013; Davies et al. 2015; Silva et al. 2018; Pearson et al. 2019a, 2022). The galaxy mergers can also contribute towards the growth of supermassive black holes at the galaxy centres (e.g. Volonteri et al. 2003; Dotti et al. 2012; Ellison et al. 2019). All these effects

make galaxy mergers an important phenomenon in the process of galaxy evolution.

The environment, that is, the local density of galaxies, is expected to be a decisive factor in shaping the evolution of galaxies. However, what remains unclear is the exact role that the environment plays on the merger rates and the post-merger properties of the merging galaxies such as their morphology, star formation rate (SFR), stellar mass, luminosity, and the evolution of their stellar population. The primary question is: do galaxy mergers predominantly take place in the denser or less dense environments of the large-scale structure (LSS)?

As the merging is an assembly of two or more galaxies into one, mergers are expected to have a strong dependence on the environment. That is, we naively expect mergers to occur frequently in denser regions. Some studies have tried to answer this question. Indeed, a strong dependence of galaxy merger rate on the environment was observed in high redshifts ($z \sim 1$), where higher merger rates were found in high density regions (Lin et al. 2010; de Ravel et al. 2011). However, only a weak dependence

Galaxies with grains: unraveling dust evolution and extinction curves with hydrodynamical simulations

Yohan Dubois¹, Francisco Rodríguez Montero², Corentin Guerra³, Maxime Trebitsch⁴, San Han⁵,
Ricarda Beckmann⁶, Sukyoung K. Yi⁵, Joseph Lewis¹, and J. K. Jang⁵

¹ Institut d'Astrophysique de Paris, UMR 7095, CNRS, Sorbonne Université, 98 bis boulevard Arago, 75014 Paris, France
e-mail: dubois@iap.fr

² Sub-department of Astrophysics, University of Oxford, Keble Road, Oxford OX1 3RH, United Kingdom

³ Observatoire de Paris, PSL University, Université de Paris, CNRS, LUTH 5 Place Jules Janssen, 92190 Meudon, France

⁴ Kapteyn Astronomical Institute, University of Groningen, P.O. Box 800, 9700AV Groningen, The Netherlands

⁵ Department of Astronomy and Yonsei University Observatory, Yonsei University, Seoul 03722, Republic of Korea

⁶ Institute of Astronomy and Kavli Institute for Cosmology, University of Cambridge, Madingley Road, Cambridge CB3 0HA, United Kingdom

Received / Accepted

ABSTRACT

Dust in galaxies is an important tracer of galaxy properties and their evolution over time. The physical origin of the grain size distribution, the dust chemical composition and, hence, the associated ultraviolet-to-optical extinctions in diverse galaxies remains elusive. To address this issue, we introduce a model for dust evolution in the RAMSES code for simulations of galaxies with a resolved multiphase interstellar medium. Dust is modelled as a fluid transported with the gas component, and is decomposed into two sizes, 5 nm and 0.1 μm , and two chemical compositions for carbonaceous and silicate grains. This dust model includes the growth of dust by accretion of elements from the gas phase and by the release of dust in stellar ejecta, the destruction by thermal sputtering, supernovae, and astration, and the exchange of dust mass between the two main populations of grain sizes by coagulation and shattering. Using a suite of isolated disc simulations with different masses and metallicities, the simulations can explore the role of these processes in shaping the key properties of dust in galaxies. The simulated Milky Way analogue reproduces the dust-to-metal mass ratio, depletion factors, size distribution and extinction curves of the Milky Way. Galaxies with lower metallicities reproduce the observed decrease in the dust-to-metal mass ratio with metallicity at around a few 0.1 Z_{\odot} . This break in the DTM corresponds to a galactic gas metallicity threshold that marks the transition from an ejecta-dominated to an accretion-dominated grain growth, and that is different for silicate and carbonaceous grains, with $\approx 0.1 Z_{\odot}$ and $\approx 0.5 Z_{\odot}$ respectively. This leads to more Magellanic Cloud-like extinction curves, i.e. with steeper slopes in the ultraviolet and a weaker bump feature at 2175 Å, in galaxies with lower masses and lower metallicities. Steeper slopes in these galaxies are caused by the combination of the higher efficiency of gas accretion by silicate relative to carbonaceous grains, and by the low rates of coagulation that preserves the amount of small silicate grains. Weak bumps are due to the overall inefficient accretion growth of carbonaceous dust at low metallicity, whose growth is mostly supported by the release of large grains in SN ejecta. We also show that the formation of CO molecules is a key component to limit the ability of carbonaceous dust to grow, in particular in low-metallicity gas-rich galaxies.

Key words. Galaxies – Galaxies: ISM – dust, extinction – Methods: numerical

1. Introduction

The spectral energy distribution (SED) of galaxies characterises the distance and properties of galaxies (e.g. [Fioc & Rocca-Volmerange 1997, 2019](#); [Devriendt et al. 1999](#); [Noll et al. 2009](#); [Chevallard & Charlot 2016](#); [Boquien et al. 2019](#)). As dust efficiently absorbs light in the optical or in the ultraviolet (UV), it re-emits this light in the infrared (IR), which is subsequently absorbed and re-emitted in the IR (producing IR multi-scattering). The exact SEDs of galaxies across the entire spectral range are, thus, tied in part to the properties of the dust, and in particular to the size and chemical composition of grains.

While galaxy attenuation curves offer insights into the dust properties ([Calzetti et al. 2000](#)), it is crucial to note that they result from the interplay of complex radiative transfer effects within the intricate geometry of the interstellar medium (ISM) and stellar distribution (e.g., [Gordon et al. 1997](#); [Witt & Gordon 2000](#); [Granato et al. 2000](#); [Inoue 2005](#); [Narayanan et al. 2018](#)). A

key source of knowledge about dust properties comes from the extinction curves of multiple lines-of-sights of individual stars (for which the complexity of dust absorption is better characterised) in the Milky Way or from the Magellanic Clouds. The Milky Way extinction curve is characterised by a moderate extinction in the ultraviolet, as opposed to Magellanic Clouds, and by a significant feature in the optical range, called the 2175 Å bump, very faint in the Large Magellanic Cloud and almost indistinguishable in the Small Magellanic Cloud ([Pei 1992](#)). Thanks to the description with Mie theory of light absorption and scattering by solid spherical bodies, and optical properties of grains, it is possible to interpret the shape of the Milky Way extinction curve by a number density distribution skewed towards small grains (a few nm in size) but dominated by large grains (0.1 μm) in mass, as well as a mixed composition of carbonaceous grains and of silicate grains ([Weingartner & Draine 2001a](#)). Although, the exact nature of the carbonaceous grains

Introducing cuDisc: a 2D code for protoplanetary disc structure and evolution calculations

Alfie Robinson,^{1*} Richard A. Booth² and James E. Owen¹

¹*Astrophysics Group, Imperial College London, Prince Consort Road, London SW7 2AZ, UK*

²*School of Physics and Astronomy, University of Leeds, Leeds, LS2 9JT, UK*

Accepted XXX. Received YYY; in original form ZZZ

ABSTRACT

We present a new 2D axisymmetric code, cuDisc, for studying protoplanetary discs, focusing on the self-consistent calculation of dust dynamics, grain size distribution and disc temperature. Self-consistently studying these physical processes is essential for many disc problems, such as structure formation and dust removal, given that the processes heavily depend on one another. To follow the evolution over substantial fractions of the disc lifetime, cuDisc uses the CUDA language and libraries to speed up the code through GPU acceleration. cuDisc employs a second-order finite-volume Godunov solver for dust dynamics, solves the Smoluchowski equation for dust growth and calculates radiative transfer using a multi-frequency hybrid ray-tracing/flux-limited-diffusion method. We benchmark our code against current state-of-the-art codes. Through studying steady-state problems, we find that including 2D structure reveals that when collisions are important, the dust vertical structure appears to reach a diffusion-settling-coagulation equilibrium that can differ substantially from standard models that ignore coagulation. For low fragmentation velocities, we find an enhancement of intermediate-sized dust grains at heights of ~ 1 gas scale height due to the variation in collision rates with height, and for large fragmentation velocities, we find an enhancement of small grains around the disc mid-plane due to collisional “sweeping” of small grains by large grains. These results could be important for the analysis of disc SEDs or scattered light images, given these observables are sensitive to the vertical grain distribution.

Key words: protoplanetary discs – methods: numerical – stars: pre-main sequence

1 INTRODUCTION

The past few decades have seen the study of young planetary systems and their formation environments become a rapidly evolving field with major interest within the astrophysics community. This is largely due to an unprecedented wealth of observations made possible by recent observatories such as ALMA (Wootten & Thompson 2009) and the continual discovery of diverse exoplanetary systems (e.g Mayor et al. 2011; Batalha et al. 2013; Winn & Fabrycky 2015; Madhusudhan 2019; Zhu & Dong 2021). Protoplanetary discs, the discs of gas and dust that form around young stars, are the birthplace of such planetary systems and have, therefore, been subject to extensive theoretical interest. Various questions relating to their nature have arisen in recent years that remain at least partly unanswered by current theoretical models. Examples of such problems include: the nature of the mechanisms behind “sub-structure” formation in protoplanetary discs, as observations have shown these objects to exhibit diverse features from axisymmetric rings and gaps to non-axisymmetric arcs (Andrews 2020; Bae et al. 2022); the connection between the spatial distribution and evolution of chemical species in discs to the eventual compositions of planetary cores and atmospheres (Öberg et al. 2011; Booth et al. 2017; Madhusudhan 2019; Eistrup 2023); and mechanisms for the dispersal of protoplanetary discs after their observed lifetimes of \sim

a few Myr (Ercolano & Pascucci 2017; Owen & Kollmeier 2019).

Exploring these problems requires sophisticated numerical modelling, given the plethora of physical processes that govern the structure and evolution of protoplanetary discs. Our understanding of discs has primarily been advanced through the use of state-of-the-art codes for studying the dynamics and thermodynamics of the gas and dust that comprise the disc material. 2D and 3D simulations have typically been used to study discs on short, dynamical time-scales, given their computational cost, whilst 1D models have often been used to study discs on longer, secular time-scales. Work done using these models has hugely advanced our understanding of protoplanetary discs; however, it has become evident that for certain problems, the interplay of each of the facets of disc physics - dynamics, thermodynamics and the dust size distribution - must be studied self-consistently over secular time-scales. The 1D code DustPy (Stammler & Birnstiel 2022) is the current state-of-the-art for studying problems of this nature; however, it cannot be used if the problem depends on the intricacies of the disc vertical structure. Examples of such problems include temperature instabilities (Watanabe & Lin 2008; Wu & Lithwick 2021; Fuksman & Klahr 2022) where 2D temperature solvers have been used but dust dynamics and growth neglected, snow line instabilities (Owen 2020) where 1D temperature and dynamics solvers have been used, and problems relating to disc dispersal such as the removal of dust from discs via radiation pressure (Owen &

* E-mail: a.robinson21@imperial.ac.uk

Dissecting a miniature universe: A multi-wavelength view of galaxy quenching in the Shapley supercluster

N. Aghanim^{1*}, T. Tuominen¹, V. Bonjean^{2,3}, C. Gouin¹, T. Bonnaire⁴, and M. Einasto⁵

¹ Université Paris-Saclay, CNRS, Institut d'Astrophysique Spatiale, 91405 Orsay, France

² Littoral, Environnement et Sociétés, Université de La Rochelle, and CNRS (UMR7266), La Rochelle, France

³ Instituto de Astrofísica de Canarias, E-38205 Tenerife, and University of La Laguna, E-38206 Tenerife, Spain

⁴ Laboratoire de Physique de l'École normale supérieure, ENS, Université PSL, CNRS, Sorbonne Université, Université Paris Cité, F-75005 Paris, France

⁵ Tartu Observatory, Tartu University, Observatooriumi 1, 61602 Tõravere, Tartumaa, Estonia

ABSTRACT

Multiple-cluster systems, i.e. superclusters, contain large numbers of galaxies assembled in clusters inter-connected by multi-scale filamentary networks. As such, superclusters are a smaller version of the cosmic web and can hence be considered as miniature universes. In addition to the galaxies, superclusters also contain gas, hot in the clusters and warmer in the filaments. Therefore, they are ideal laboratories to study the interplay between the galaxies and the gas. In this context, the Shapley supercluster (SSC) stands out since it hosts the highest number of galaxies in the local universe with clusters interconnected by filaments. In addition, it is detected in both X-rays and via the thermal Sunyaev-Zel'dovich (tSZ) effect, making it ideal for a multi-wavelength study of the gas and galaxies. Applying for the first time a filament-finder based on graphs, T-REx, on a spectroscopic galaxy catalogue, we uncovered the 3D filamentary network in and around SSC. Simultaneously, we used a large sample of photometric galaxies with information on their star formation rates (SFR) in order to investigate the quenching of star formation in the SSC environments which we define as a function of the gas distribution in the *Planck* tSZ map and the ROSAT X-ray map.

With T-REx, we confirm filaments already observed in the distribution of galaxies of the SSC, and detect new ones. We observe the quenching of star formation as a function of the gas contained in the SSC. We show a general trend of decreasing SFR where the tSZ and X-ray signals are the highest, within the high density environments of the SSC. Within these regions, we also observe a rapid decline of the number of star-forming galaxies, coinciding with an increasing number of transitioning and passive galaxies. Within the SSC filaments, the fraction of passive galaxies is larger than outside filaments, irrespective of the gas pressure. Our results suggest the zone of influence of the SSC, in which galaxies are pre-processed and quenched, is well defined by the tSZ signal that combines the density and temperature of the environments.

Key words. Cosmology: large-scale structure of Universe, Galaxies: clusters: individual: Shapley, Galaxies: evolution

1. Introduction

The cosmic web is an entangled structure made of nodes (galaxy groups and clusters) at the intersection of filaments surrounded by walls and separated by voids. In the cosmic web, galaxy superclusters are defined as the high-density regions in the distribution of galaxies or galaxy groups/clusters (e.g., Einasto et al. 1997; Liivamägi et al. 2012; Chon et al. 2013; Chow-Martínez et al. 2014; Sankhyayan et al. 2023a,b). Superclusters occupy only 1% of the volume of the Universe; however they host around 15% of galaxies including all very rich and luminous galaxy clusters which reside in superclusters or in their high-density cores (e.g., Einasto et al. 2022b, 2024). Furthermore, numerical simulations show that the progenitors of the present-day galaxy superclusters are already seen in the very early Universe (Park et al. 2022; Einasto et al. 2023). Several studies have shown that galaxy superclusters or their high-density cores are the largest objects which are either collapsing now or which will collapse in the future (e.g., Dünner et al. 2006; Kopylova & Kopylov 2007; Luparello et al. 2011; Chon et al. 2015; Einasto

et al. 2016, 2021, 2022b). This property has further been used to define superclusters as in Luparello et al. (2011) and Chon et al. (2015). In their study, Einasto et al. (2022b) compared different definitions of superclusters based on their sizes and masses. They showed that the largest collapsing cores are associated with the richest superclusters, such as the Shapley and the Corona Borealis supercluster in the local Universe, or the BOSS Great Wall at redshift $z = 0.47$. These cores have sizes up to approximately $10 - 12 h^{-1} \text{ Mpc}$ and masses up to $10^{16} M_{\text{sun}}$.

Superclusters embed galaxies, groups, and clusters connected by galaxy filaments, which may extend to their surrounding cosmic web. Supercluster environment is known to impact the evolution of galaxies within them. This was shown in seminal studies (e.g., Einasto & Einasto 1987) and in detailed analyses of a few nearby superclusters (e.g., Luparello et al. 2013; Pearson et al. 2014; Lietzen et al. 2016; Lacerna et al. 2016; Einasto et al. 2018, 2020, 2021; Castignani et al. 2022; Heinämäki et al. 2022). They conclude that galaxies in groups within superclusters have older stellar populations, suggesting that groups in superclusters formed differently from groups in other environments (see e.g., Einasto et al. 2023, for a recent study) with their galax-

* nabila.aghanim@ias.u-psud.fr

Fast and spurious: a robust determination of our peculiar velocity with future galaxy surveys

Fabien Lacasa^{a,b} Camille Bonvin^a Charles Dalang^{c,d} Ruth Durrer^a

^aDépartement de Physique Théorique and Center for Astroparticle Physics, Université de Genève, 24 quai Ernest Ansermet, CH-1211 Geneva, Switzerland

^bUniversité Paris-Saclay, CNRS, Institut d'Astrophysique Spatiale, 91405, Orsay, France

^cQueen Mary University of London, Mile End Road, E1 4NS, London, United Kingdom

^dInstitute of Cosmology and Gravitation, University of Portsmouth, Burnaby Road, Portsmouth PO1 3FX, United Kingdom

E-mail: fabien.lacasa@unige.ch

Abstract. To date, the most precise measurement of the observer's peculiar velocity comes from the dipole in the Cosmic Microwave Background (CMB). This velocity also generates a dipole in the source number counts, whose amplitude is governed not only by the observer velocity, but also by specific properties of the sources, that are difficult to determine precisely. Quantitative studies of the source number counts currently give dipoles which are reasonably well aligned with the CMB dipole, but with a significantly larger amplitude than that of the CMB dipole. In this work, we explore an alternative way of measuring the observer velocity from the source number counts, using correlations between neighboring spherical harmonic coefficients, induced by the velocity. We show that these correlations contain both a term sensitive to the source properties and another one directly given by the observer velocity. We explore the potential of a *Euclid*-like survey to directly measure this second contribution, independently of the characteristics of the population of sources. We find that the method can reach a precision of 4%, corresponding to a detection significance of 24σ , on the observer velocity. This will settle with precision the present "dipole tension".

Keywords: large-scale structure of the Universe – methods: analytical – methods: statistical

Correction method applied to MC simulated LST images affected by clouds

Natalia Żywucka,^{a,b,*} Julian Sitarek,^{a,‡} Dorota Sobczyńska,^a Mario Pecimotika,^{c,d} Dario Hrupec,^e Dijana Dominis Prester,^c Lovro Pavletić^c and Saša Mićanović^c

^aDepartment of Astrophysics, University of Łódź, Pomorska 149, Łódź, Poland

^bNorth-West University, Potchefstroom, South Africa

^cFaculty of Physics, University of Rijeka, Radmile Matejčić 2, Rijeka, Croatia

^dInstitute Ruđer Bošković, Bijenička cesta 54, Zagreb, Croatia

^eDepartment of Physics, J. J. Strossmayer University of Osijek, Trg Ljudevita Gaja 6, Osijek, Croatia

[‡]Now at Institute for Cosmic Ray Research (ICRR), The University of Tokyo, Kashiwa, 277-8582 Chiba

E-mail: natalia.zywucka@fis.uni.lodz.pl

We present the results of a preliminary study of a correction method applied to the Imaging Atmospheric Cherenkov Telescope images affected by clouds. The studied data are Monte Carlo simulations made with CORSIKA, imitating the very high energy events registered by the Large-Sized Telescopes, a type of telescope within the future Cherenkov Telescope Array. We implement the cloud correction method in the ctapepe/lstchain analysis framework. The correction is based on a simple geometrical model of the emission. We show the effect of the correction method on the image parameters and the stereo-reconstructed shower parameters.

High Energy Astrophysics in Southern Africa 2022 - HEASA2022
28 September - 1 October 2022
Brandfort, South Africa

*Speaker

© Copyright owned by the author(s) under the terms of the Creative Commons Attribution-NonCommercial-NoDerivatives 4.0 International License (CC BY-NC-ND 4.0).

<https://pos.sissa.it/>

Correction method applied to MC simulated LST images affected by clouds

Natalia Żywucka

1. Introduction

Since very-high-energy (VHE) gamma-ray sources emit characteristic photon fluxes of $\lesssim 10^{-12}$ erg cm⁻² s⁻¹, large collection areas > 100 m² are required to detect them. Otherwise, the observations are statistically insignificant due to too low rates of observed photons. Presently, it is not feasible for gamma-ray instrumentation with a physical size exceeding ~ 1 m² to be sent into space, severely limiting the performance of direct observations in this energy range. The Imaging Atmospheric Cherenkov Telescopes (IACTs) take advantage of Cherenkov radiation visible in the optical range from 300 to 600 nm and allow indirect, ground-based observations of VHE radiation. The technique relies on the detection of short Cherenkov light flashes lasting 3–4 ns caused by the air showers generated during collisions of ultrarelativistic gamma-ray photons or hadrons with nuclei in the upper layer of the Earth's atmosphere. The ground-based detectors register information, leading to a precise identification of the primary particles, i.e. to measure their initial energy, establish the direction of emission, and determine the nature of the source of radiation.

The Cherenkov telescope array¹ (CTA) [1] is an emerging, ground-based, IACT observatory located in two hemispheres, namely CTA-North on the Canary island of La Palma (Spain) and CTA-South in the Atacama Desert in Chile. The observatory will consist of three types of telescopes, namely large- (LST), medium- (MST), and small- (SST) sized telescopes, having mirror diameters of 23 m, 11.5 m, and 4.3 m, and the fields of view of 4.5°, 7°, and 8°, respectively. In this manner, the CTA observatory tends to cover both hemispheres in a wide range of photon energy between 20 GeV and 300 TeV, improving the sensitivity level at the reference energy of 1 TeV by an order of magnitude in comparison to currently operating Cherenkov observatories. The key scientific goals of the CTA observatory include understanding the origin of VHE emission from astrophysical sources, the existence and the role of relativistic cosmic particles in the Universe, searching for dark matter, and many other topics [2].

The first operating CTA telescope is the LST-1 located in the CTA-North site at the Roque de Los Muchachos Observatory on La Palma [3]. The sub-array scheme assumes the construction of four such telescopes at the central part of the northern array that provides the dominant contribution to the full system sensitivity in the range of 20 to 150 GeV. The inauguration of the LST-1 was held in 2018 and the telescope is currently in the science-engineering phase. The LSTs have a wide scope of observations, including Galactic transients, active galactic nuclei, gamma-ray bursts, and other astrophysical sources. It is worth mentioning that a fraction of observations will be affected by clouds, which cannot be avoided. However, the gathered data can be improved in the analysis process.

We propose a geometrical model correction of an image, which aims to improve the gamma/hadron separation and shower direction reconstruction. The proposed method is enhanced with a bias fit which is independent of energy and impact.

2. Simulations

Based on the physical parameters describing individual particle cascades, such as shape and components, that are later on reflected in their Cherenkov light images, hadronic and electromagnetic

¹<https://www.cta-observatory.org/>

Discovery of an extended Horizontal Branch in the Large Magellanic Cloud globular cluster NGC1835 [★]

Camilla Giusti^{1,2}, Mario Cadelano^{1,2}, Francesco R. Ferraro^{1,2}, Barbara Lanzoni^{1,2}, Cristina Pallanca^{1,2}, Maurizio Salaris³, Emanuele Dalessandro², Enrico Vesperini⁴, and Alessio Mucciarelli^{1,2}

¹ Dipartimento di Fisica & Astronomia, Università degli Studi di Bologna, via Gobetti 93/2, I-40129 Bologna, Italy

² INAF - Astrophysics and Space Science Observatory Bologna, Via Gobetti 93/3, 40129, Bologna, Italy

³ Astrophysics Research Institute, Liverpool John Moores University, Liverpool L3 5RF, UK

⁴ Dept. of Astronomy, Indiana University, Bloomington, IN 47401, USA

February 29, 2024

ABSTRACT

We present a high angular resolution multi-wavelength study of the massive globular cluster NGC 1835 in the Large Magellanic Cloud. Thanks to a combination of optical and near ultraviolet images acquired with the WFC3 on board the HST, we performed a detailed inspection of the stellar population in this stellar system adopting a “UV-guided search” to optimize the detection of relatively hot stars. This allowed us to discover a remarkably extended horizontal branch (HB), spanning more than 4.5 magnitudes in both magnitude and colour from the region redder than the instability strip, up to effective temperatures of 30,000 K, and including a large population of RR Lyrae (67 confirmed variables, and 52 new candidates). This is the first time that such a feature has been detected in an extra-Galactic cluster, demonstrating that the physical conditions responsible for the formation of extended HBs are ubiquitous. The acquired dataset has been also used to redetermine the cluster distance modulus, reddening, and absolute age, yielding $(m - M)_0 = 18.58$, $E(B - V) = 0.08$, and $t = 12.5$ Gyr, respectively.

1. Introduction

The Large Magellanic Cloud (LMC) is the most massive ($\sim 10^{11} M_{\odot}$; Erkal et al. 2019) satellite of the Milky Way. It hosts a rich system of star clusters, including massive globular clusters (GCs) with properties similar to those of the Milky Way, and lower-mass stellar systems similar to the Galactic open clusters. As in the case of our Galaxy, the study of the LMC stellar systems provides deep insights into the star formation history (Olszewski et al. 1996; Olsen et al. 1998; Brocato et al. 1996; Mackey & Gilmore 2003; Baumgardt et al. 2013), the chemical enrichment (e.g., Hill et al. 2000; Pietrzynski & Udalski 2000; Ferraro et al. 2006; Mucciarelli et al. 2010; Glatt et al. 2010; Cadelano et al. 2022a), and the past merger history (e.g., Mucciarelli et al. 2021) of the host galaxy. The LMC GCs cover a metallicity range comparable to that sampled by Galactic clusters, but show a much broader range of ages (from a few million, to several billion years), thus providing the ideal laboratory to empirically calibrate the so-called “red giant branch (RGB) and asymptotic giant branch (AGB) Phase Transitions” (see, e.g., Ferraro et al. 1995, 2004; Mucciarelli et al. 2006). These are two crucial events in a star cluster life that are expected to induce significant changes in the spectral energy distribution (SED) as a function of time. The empirical calibration of theoretical SEDs is a mandatory step for the proper interpretation of the spectra of unresolved galaxies through cosmic time (see Maraston 2005).

To the same purpose, also the accurate characterization of the horizontal branch (HB) morphology of stellar systems is extremely important. In fact, it is well known that this can have a strong impact on the integrated light of stellar populations, affecting their colours and line indices (Lee et al. 2002; Schiavon et al. 2004; Percival & Salaris 2011; Dalessandro et al. 2012). In particular, HBs with extended blue tails imply the presence of very hot stars that, in unresolved stellar systems, can mimic the existence of young populations even in cases where star formation stopped several Gyr ago. Indeed, the so-called “UV upturn” or “UV excess” observed in early-type galaxies is mainly explained as due to blue HB stars (e.g., Greggio & Renzini 1990; Dorman et al. 1993, 1995; Brown 2004). In addition, peculiar populations of “slowly cooling white dwarfs” have been recently identified in GCs with extended blue HBs, while they are not observed in stellar systems where the HB is restricted to the red (cold) region (Chen et al. 2021, 2022, 2023a). The link between the HB morphology and the presence/lack of slowly cooling white dwarfs is due to the fact that, because of their small mass, the bluest HB stars skip the asymptotic giant branch phase and therefore keep a relatively massive residual hydrogen envelope around the degenerate carbon-oxygen core. Hydrogen thermonuclear burning in this residual envelope then acts as an extra-energy source during the white dwarf phase, thus slowing down the evolution and resulting in observable populations of “slowly cooling white dwarfs” (Chen et al. 2021). In spite of its astrophysical importance, we still have an incomplete understanding of the physical origin of the HB morphology (the so-called “second parameter problem”; see e.g. Catelan 2009; Gratton et al. 2010; Milone et al. 2014) and it is therefore important to keep

[★] Based on observations with the NASA/ESA HST, obtained under program GO 16361 (PI: Ferraro). The Space Telescope Science Institute is operated by AURA, Inc., under NASA contract NAS5-26555

A measurement of cluster masses using *Planck* and SPT-SZ CMB lensing

Alexandre Huchet and Jean-Baptiste Melin

Université Paris-Saclay, CEA, Département de Physique des Particules, 91191, Gif-sur-Yvette, France.
e-mail: alexandre.huchet@cea.fr, jean-baptiste.melin@cea.fr

Received ; accepted

ABSTRACT

We used an unbiased CMB lensing mass estimator on 468 SPT-SZ clusters from the SPT-SZ and the *Planck* public data, the first such estimation using combined ground- and space-based data. We measured the average ratio between CMB lensing and SZ mass to be $M_{\text{CMB lens}}/M_{\text{SZ}} = 0.98 \pm 0.19$ (stat.) ± 0.03 (syst.). The average CMB lensing mass from the combination of the two data sets is measured at 4.8σ , which is a significant gain with respect to the measurement performed on the SPT-SZ only (3.9σ) or the *Planck* only (3.7σ) data set. We showed that the combination not only takes advantage of the two different ranges of spatial scales (i.e. Fourier modes) observed but also exploits the lensing induced correlation between scales observed by one experiment and the other. This result demonstrates the importance of measuring a large range of spatial scales for CMB lensing mass estimation, from arcmin to degrees. This large range of scales will most probably be provided by the combination of various data sets, such as from the large and small aperture telescopes of the upcoming Simons Observatory and future CMB-S4 experiment, and *Planck*. In this context, the *Planck* data will remain a key element for CMB lensing cluster studies in the years to come.

Key words. galaxies: clusters: general – cosmic background radiation – Gravitational lensing: weak – methods: statistical

1. Introduction

Clusters of galaxies, located at the nodes of the cosmic web, are very useful objects for studying both astrophysics and cosmology. They have played an important role in shaping and reinforcing the Λ CDM concordance model and have been used in many works to derive constraints on cosmological parameters (e.g., White et al. 1993; Carlberg et al. 1996; Bahcall et al. 1997; Allen et al. 2002). Among these approaches, the most promising way to constrain cosmological parameters with clusters is through cluster counts as a function of redshift and mass, which are very sensitive to cosmological parameters, particularly Ω_m and σ_8 (Albrecht et al. 2006; Vikhlinin et al. 2009; Allen et al. 2011). Clusters thus have the statistical power to be as efficient as other major cosmological probes but their constraints unfortunately suffer from uncertainty in the relation between cluster masses and directly observable quantities. This uncertainty on the cluster mass scale dominates current analyses (e.g., Hasefield et al. 2013; Planck Collaboration et al. 2016c; Bocquet et al. 2019; Abbott et al. 2020). However, the situation will change in the next few years with the advent of the large optical facilities *Euclid*¹ and the Vera Rubin Observatory². These facilities will improve the accuracy and number of measurements of cluster masses thanks to weak gravitational lensing, up to redshifts of the order of one (Laureijs et al. 2011; LSST Science Collaboration et al. 2009). The major uncertainty for cosmology with clusters at $z < 1$ will, therefore, be overcome in the next decade. Extending cosmological studies with clusters at redshift $z > 1$ will not be possible with the weak gravitational lensing

on galaxies due to the lack of background sources at these redshifts. The cosmic microwave background (CMB) is hoped to be a new background source for studying the weak lensing of clusters at higher redshift. Located at $z \sim 1100$ and having precisely known statistical properties, it makes it possible to measure masses of galaxy clusters by weak gravitational lensing in the redshift range $0 < z < 3$. (Zaldarriaga & Seljak 1999; Seljak & Zaldarriaga 2000; Holder & Kosowsky 2004; Dodelson 2004; Vale et al. 2004; Lewis & King 2006; Lewis & Challinor 2006).

The first tools were proposed in the mid-2000s to detect this effect (Maturi et al. 2005; Hu et al. 2007; Yoo & Zaldarriaga 2008; Yoo et al. 2010), but the first data sets for which the lensing signal became detectable only appeared in the early 2010s (Ruhl et al. 2004; Swetz et al. 2011; Planck Collaboration et al. 2020a). The signal-to-noise for CMB lensing mass measurement is very low in these data sets. Thus, it is not possible to make individual measurements and it is necessary to average the signal over several hundred clusters to pull the signal out of the noise. The first measurements were carried out almost jointly by the ACT, SPT and *Planck* collaborations shortly before the mid-2010s (Madhavacheril et al. 2015; Baxter et al. 2015; Planck Collaboration et al. 2016c). These detections were made possible thanks to the pioneering work cited above and improved tools (see Melin & Bartlett 2015). The improvement of existing tools and the development of new tools are currently active research fields (Raghunathan et al. 2017; Madhavacheril & Hill 2018; Raghunathan et al. 2019a; Horowitz et al. 2019; Patil et al. 2020; Gupta & Reichardt 2021; Levy et al. 2023; Chan et al. 2023). The motivation is to be ready to analyze data from the new generation of CMB instruments which will provide data sets that will enable individual mass measurements for the first time, the Simons Observatory (SO, Ade et al. 2019) and CMB-S4 (Abazajian et al. 2019).

¹ https://www.esa.int/Science_Exploration/Space_Science/Euclid & <https://www.euclid-ec.org>

² <https://rubinobservatory.org> & <https://lsstdesc.org>

Calibration requirement for Epoch of Reionization 21-cm signal observation - III. Bias and variance in uGMRT ELAIS-N1 field power spectrum

Saikat Gayen^a Rashmi Sagar^b Sarvesh Mangla^{c,b} Prasun Dutta^a
Nirupam Roy^d Arnab Chakraborty^e Jais Kumar^f Abhirup Datta^b
Samir Choudhuri^g

^aDepartment of Physics, Indian Institute of Technology (Banaras Hindu University), Varanasi - 221005, India

^bDepartment of Astronomy, Astrophysics and Space Engineering, Indian Institute of Technology, Indore, Madhya Pradesh, 453552, India

^cNational Centre for Radio Astrophysics, Tata Institute of Fundamental Research, Pune 411007, India

^dDepartment of Physics, Indian Institute of Science, Bangalore 560012, India

^eDepartment of Physics and McGill Space Institute, McGill University, Montreal, QC, Canada H3A 2T8

^fDepartment of Physics, K. N. Government P. G. College, Gyanpur, Bhadohi - 221304, India

^gCentre for Strings, Gravitation and Cosmology, Department of Physics, Indian Institute of Technology, Madras, Chennai 600036, India

E-mail: saikatgayen.rs.phy22@itbhu.ac.in, phd2101121003@iiti.ac.in,
phd1801121006@iiti.ac.in, pdutta.phy@itbhu.ac.in, nroy@iisc.ac.in,
arnab.chakraborty2@mail.mcgill.ca, jaisk.rs.phy16@itbhu.ac.in,
abhirup.datta@iiti.ac.in, samir@iitm.ac.in

Abstract. Power spectrum of diffuse HI 21 cm background radiation is one of the promising probes to study large scale structure of the universe and understand the evolution of the galaxies. Presence of orders of magnitude larger foregrounds in the frequency range for such observations has been one of the largest challenge. The foreground contamination also hinders the calibration procedures and introduce residual calibration errors in the interferometric data. It has been shown that the calibration errors can introduce bias in the 21-cm power spectrum estimates and introduce systematics. There have been several efforts to understand and improve on the calibration errors. In this work we use an analytical estimate of the bias and variance in redshifted 21-cm power spectrum in presence of time-correlated residual gain errors and foreground. We use the uGMRT Band-3 observations of the ELAIS-N1 field and estimate the bias and variance in the power spectrum from these observation. We first access the statistics of the gain errors and based on the quality of calibration we flag a set of additional antennae. The latter reduce the bias and variance of power spectrum significantly and we found it to be recommended for such analysis. These estimates demonstrate that the majority of the systematics at the lower angular scales are due to the residual gain errors. We observe that for the uGMRT baseline configuration and system parameters, the variance is always higher than the bias in the power spectrum estimates. The excess variance in the power spectrum reduces with increase of the angular scales and at about $\ell \sim 6000$ the effects from residual gain errors are negligible. Based on our analysis we observe that for an angular multipole of $\ell \sim 3000$, 2000 hours of ‘on source time’ is required with uGMRT to detect redshifted 21-cm signal at $3 - \sigma$ significance from a redshift of 2.55. In this work we only consider the power spectrum measurement in the plane of the sky, an assessment of residual gain statistics and its effect on multifrequency angular power spectrum estimation will be presented in a companion paper.

Keywords: statistical sampling techniques, reionization, power spectrum

Grey Two-moment Neutrino Transport: Comprehensive Tests and Improvements for Supernova Simulations

Haakon Andresen^{1*}, Evan P. O'Connor¹, Oliver Eggenberger Andersen¹, and Sean M. Couch^{2,3,4}

¹ The Oskar Klein Centre, Department of Astronomy

Stockholm University, AlbaNova, SE-106 91 Stockholm, Sweden

² Department of Physics and Astronomy, Michigan State University,

East Lansing, MI 48824, USA

³ Department of Computational Mathematics, Science, and Engineering, Michigan State University,

East Lansing, MI 48824, USA

⁴ Facility for Rare Isotope Beams, Michigan State University,

East Lansing, MI 48824, USA

ABSTRACT

Aims. In this work, we extended an energy-integrated neutrino transport method to facilitate efficient, yet precise, modeling of compact astrophysical objects. We focus particularly on core-collapse supernovae.

Methods. We implemented the framework of Foucart et al. (2016) into FLASH and performed a detailed evaluation of its accuracy in core-collapse supernova simulations. Based on comparisons with results from simulations using energy-dependent neutrino transport, we incorporated several improvements to the original scheme.

Results. Our analysis shows that our grey neutrino transport method successfully reproduces key aspects from more complex energy-dependent transport across a variety of progenitors and equations of state. We find both qualitative and reasonable quantitative agreement with multi-group M1 transport simulations. However, the grey scheme tends to slightly favor shock revival. In terms of gravitational wave and neutrino signals, there is a good alignment with the energy-dependent transport, although we find 15-30 per cent discrepancies in the average energy and luminosity of heavy-lepton neutrinos. Simulations using the grey transport are around four times faster than those using energy-dependent transport.

Key words. supernovae: general – Neutrinos – Radiative transfer – Hydrodynamics – Gravitational waves

1. Introduction

Core-collapse supernovae are important for several facets of astrophysics, they play key role in the chemical (Edmunds 2017; Thielemann et al. 2018) and dynamical evolution (Smith et al. 2018; Bacchini et al. 2023) of galaxies and they are the progenitors of every binary system observed so far by LIGO-Virgo-KAGRA collaboration (Abbott et al. 2016b,a,c, 2017b,a,c,d, 2019, 2020c,b,a,d, 2021a,b,b, 2024, 2023). To thoroughly understand core-collapse supernovae and their impact in astrophysics, it is essential to systematically examine the varied outcomes that occur in the final stages of the evolution of massive stars.

In the last decade, the efforts of the modelling community have led to several successful supernova explosions in three-dimensional simulations with state-of-the-art microphysics (Melson et al. 2015a,b; Roberts et al. 2016; Summa et al. 2018; Vartanyan et al. 2019; Burrows et al. 2019; Vartanyan et al. 2019; Burrows et al. 2020; Vartanyan et al. 2022). Despite recent advances, there are still several open questions and challenges left to tackle in the core-collapse field. The ultimate goal is to simulate a star from the onset of iron-core collapse, through shock revival, until the shock breaks out of the star and self-consistently predicting every aspect of the observables. Reaching this goal will require an improved understanding of the stellar progenitors (Arnett & Meakin 2011; Couch & Ott 2015; Cristini et al. 2017; Jones et al. 2017; Müller et al. 2016),

understanding the importance of neutrino oscillations (Izaguirre et al. 2017; Chakraborty et al. 2016; Capozzi et al. 2019; Johns et al. 2020; Chakraborty & Chakraborty 2020; Bhattacharyya & Dasgupta 2021; Capozzi et al. 2020; Martin et al. 2021; Johns 2023; Capozzi et al. 2022; Xiong et al. 2023b; Richers & Sen 2022; Dedin Neto et al. 2023; Liu et al. 2023; Xiong et al. 2023a; Cornelius et al. 2023; Shalgar & Tamborra 2023; Ehring et al. 2023; Dedin Neto et al. 2023; Cornelius et al. 2023; Shalgar & Tamborra 2023; Akaho et al. 2024), accurate microphysics (Sumiyoshi et al. 2005; Hempel et al. 2012; Fischer et al. 2014; Oertel et al. 2017; da Silva Schneider et al. 2020; Pascal et al. 2022; Suleiman et al. 2023), understanding the impact of rotation and magnetic fields (Kotake et al. 2011; Takiwaki & Kotake 2018; Summa et al. 2018; Jardine et al. 2022; Obergaulinger & Aloy 2021; Bugli et al. 2021; Reichert et al. 2023; Bugli et al. 2023; Buellet et al. 2023), and the ability to accurately simulate all the aforementioned aspects. The input physics underlying core-collapse supernovae are complex and subject to active research. Consequently, the underpinning of supernova simulations comes with inherent uncertainty.

On one hand, state-of-the-art simulations are necessary to move the field forward and the inclusion of ever more detailed physics in numerical simulations is sure to yield interesting results in the future. On the other hand, the most complex simulations are ill suited for systematically studying the effects of the uncertainties in the input physics due to their high computational cost. First among the computationally expensive parts of

* e-mail: haakon.andresen@astro.su.se

Origin of broad He II 4686 Å emission in early spectra of type IIP supernovae

© 2024 N. N. Chugai¹ and V. P. Utrobin^{2,1}

¹ *Institute of astronomy, Russian Academy of Sciences, Moscow*

² *SRC “Kurchatov institute”, Moscow*

Submitted 05.10.2023

Keywords: stars – supernovae; stars – stellar wind

PACS codes:

arXiv:2402.18299v1 [astro-ph.HE] 28 Feb 2024

¹email: nchugai@inasan.ru

Molecular gas scaling relations for local star forming galaxies in the low- M_* regime

B. Hagedorn¹, C. Cicone¹, M. Sarzi², A. Saintonge³, P. Severgnini⁴, C. Vignali^{5,6}, S. Shen¹, K. Rubinur¹, A. Schimek¹, and A. Lasrado¹

¹Institute of Theoretical Astrophysics, University of Oslo, P.O. Box 1029, Blindern, 0315 Oslo, Norway

²Armagh Observatory and Planetarium, College Hill, Armagh BT61 9DG, UK

³Department of Physics and Astronomy, University College London, London, WC1E 6BT, UK

⁴INAF - Osservatorio Astronomico di Brera, Via Brera 28, 20121 Milano, Italy

⁵Dipartimento di Fisica e Astronomia Augusto Righi, Università degli Studi di Bologna, via Gobetti 93/2, 40129 Bologna, Italy

⁶INAF – Osservatorio di Astrofisica e Scienza dello Spazio di Bologna, Via Gobetti 101, 40129 Bologna, Italy

e-mail: bendix.hagedorn@astro.uio.no

Received xx xx xx / Accepted: xx xx xx

ABSTRACT

We derive molecular gas fractions ($f_{\text{mol}} = M_{\text{mol}}/M_*$) and depletion times ($\tau_{\text{mol}} = M_{\text{mol}}/\text{SFR}$) for 353 galaxies representative of the local star-forming population with $10^{8.5} M_{\odot} < M_* < 10^{10.5} M_{\odot}$ drawn from the ALLSMOG and xCOLDGASS surveys of CO(2-1) and CO(1-0) line emission. By adding constraints from low-mass galaxies and upper limits for CO non-detections, we find the median molecular gas fraction of the local star-forming population to be constant at $f_{\text{mol}} = -1.04 \pm 0.04$ challenging previous reports of increased molecular gas fractions in low mass galaxies. Above $M_* \sim 10^{10.5} M_{\odot}$ we find the M_* vs f_{mol} relation to be sensitive to the selection criteria for star-forming galaxies. We test the robustness of our results against different prescriptions for the CO-to- H_2 conversion factor and different selection criteria for star-forming galaxies. The depletion timescale τ_{mol} depends weakly on M_* , following a power law with a best-fit slope of 0.24 ± 0.03 . This suggests that small variations in specific SFR (sSFR = SFR/ M_*) across the local main sequence of star forming galaxies with $M_* < 10^{10.5} M_{\odot}$ are driven mainly by differences in the efficiency of converting the available molecular gas into stars. We test these results against a possible dependence of f_{mol} and τ_{mol} on the surrounding (group) environment of the targets by splitting them into centrals, satellites, and isolated galaxies, and find no significant variation between these populations. We conclude that the group environment is unlikely to have a large systematic effect on the molecular gas content of star-forming galaxies in the local universe.

Key words. galaxies: general – galaxies: ISM – galaxies: evolution

1. Introduction

The tight correlations found between the cold molecular gas content of galaxies and other physical galaxy properties, such as stellar mass (M_*) and star formation rate (SFR) are powerful and widely used tools in the study of galaxy evolution. These quantities are inextricably linked because stars form in clouds of cold molecular gas. However, the exact physical processes governing the interplay of cloud collapse and feedback are not fully understood and may vary among galaxy populations (e.g. Sun et al. 2020). Scaling relations have the potential to reveal any systematic differences across regimes in M_* , SFR, and environment, but this requires data covering the associated parameter ranges. Due to observational challenges, molecular line data in low-mass, low-metallicity galaxies is lacking. As a consequence, scaling relations have so far been largely based on massive ($M_* > 10^{10} M_{\odot}$), metal rich galaxies (see Saintonge & Catinella 2022 for a review).

Recent studies have made efforts to push observations of cold molecular gas to lower masses with statistically significant sample sizes (Cicone et al. 2017; Saintonge et al. 2017; Wylezalek et al. 2022), but there is no clear picture of the behaviour of molecular gas scaling relations in the low-mass regime ($M_* < 10^9 M_{\odot}$) yet. Particularly in the case of intensive properties (i.e.

those that do not directly depend on the size of the system), such as the molecular gas fraction ($f_{\text{mol}} = M_{\text{mol}}/M_*$), the results reported in the literature differ significantly. Some recent studies find f_{mol} to be anti-correlated with stellar mass following a simple power-law across the entire mass range studied (e.g. Hunt et al. 2020), while others report a shallow or flat relation at lower masses (e.g. Calette et al. 2018; Saintonge et al. 2017) with a downturn above a certain stellar mass. This feature is sometimes attributed to the larger fraction of passive galaxies at higher masses (Jiang et al. 2015), but it appears even in samples selected to exclude passive galaxies (e.g. Saintonge et al. 2017; Calette et al. 2018). The situation is similar for the molecular gas depletion time ($\tau_{\text{mol}} = M_{\text{mol}}/\text{SFR}$), which is a measure of how rapidly galaxies convert their molecular gas into stars. Some authors report that τ_{mol} is independent of M_* for main-sequence galaxies (e.g. Accurso et al. 2017; Boselli et al. 2014), but others find τ_{mol} and M_* to correlate, at least above $M_* = 10^9 M_{\odot}$ (e.g. Hunt et al. 2020; Saintonge et al. 2017). A lack of relation between τ_{mol} and M_* would indicate that star formation proceeds at a universal rate in galaxies, while a correlation has been argued to be a consequence of global galaxy properties affecting processes on cloud scales (Sun et al. 2020; Saintonge & Catinella 2022).

Lighting Dark Ages with Tomographic ISW Effect

Deng Wang* and Olga Mena†

Instituto de Física Corpuscular (CSIC-Universitat de València), E-46980 Paterna, Spain

The integrated Sachs-Wolfe effect (ISW) describes how CMB photons pick up a net blue or redshift when traversing the time-varying gravitational potentials between the last scattering surface and us. Deviations from its standard amplitude could hint new physics. We show that reconstructing the amplitude of the ISW effect as a function of the redshift may provide a unique tool to probe the gravity sector during the era of dark ages, inaccessible via other cosmological observables. Exploiting Planck CMB temperature, polarization and lensing observations, we find a 2σ deviation from the standard ISW amplitude at redshift $z = 500$. Barring a systematic origin, our findings could point to either possibly new physics or a departure from the standard picture of structure formation under the General Relativity framework. Assuming the simplest two-redshift-bin scenario, we ensure 38σ and 2σ evidences of the early and late ISW effects, respectively, despite a priori possible degeneracy with the CMB lensing amplitude. Using a multiple tomographic method, we present the first complete characterization of the ISW effect over space and time. Future tomographic ISW analyses are therefore crucial to probe the dark ages at redshifts otherwise unreachable via other probes.

Introduction. The cosmic dark ages, which encode a wealth of cosmological information, lie between the recombination epoch when the CMB photons decoupled from matter at $z \sim 1090$ and the appearance of the first light sources at $z \sim 30$. The line absorption due to the 21cm spin-flip transition in neutral hydrogen can extract physical information at $30 \lesssim z \lesssim 300$ [1]. However, an important question is how to dig up useful information at $300 \lesssim z \lesssim 1090$ in current cosmological observations. A viable solution is the integrated Sachs-Wolfe (ISW) effect [2], one class of secondary CMB temperature fluctuations, which is a powerful probe of dark energy, the nature of gravity, neutrinos and other extra degrees of freedom present at recombination. This effect is originated from the interaction between CMB photons and the time-dependent gravitational potentials along the line of sight between us and the last scattering surface. Given the fact that the gravitational potentials will remain constant unless the expansion of the universe is not entirely driven by a non-relativistic matter component, there can be identified two ISW effects at two distinct periods in the expansion of the universe. Namely, the early ISW effect is sensitive to relativistic particles at the recombination epoch, such as neutrinos, axions or other cosmic relics contributing to the dark radiation of the universe. On the contrary, the late ISW effect is a test of the late-time density perturbations, depending on the dark energy evolution, on modifications of the gravity sector, or on any other modification to the growth of perturbations (curvature, massive neutrinos, among others). Notice that since the ISW effect is always subdominant with respect to primary sources in the CMB, it has to be measured by cross correlating the large scale structure (LSS) [3, 4], or from CMB polarization induced by intra-cluster electron scattering [5]. Progresses in precise CMB measurements and large scale galaxy surveys enable detections of the ISW-LSS cross correlation and confirm the decay of the cosmological gravitational potential [6–21].

The Planck collaboration [22] reports a 4σ detection by cross-correlating CMB temperature maps with different LSS tracers. Reference [23] shows a 36σ detection of the early ISW effect using Planck 2015 CMB data and finds a correlation between the early ISW amplitude and the lensing amplitude, interfering with the measurement of the ISW amplitude. 21cm surveys [24] can also be used to detect the ISW effect, for instance, cross correlating their measurements at high redshifts with galaxies [25]. Moreover, ISW effects are studied in a number of dark energy and alternative gravity models [26–28].

In this *letter*, we shall consider several tomographic parameterizations of the ISW effect, finding that CMB data only are able to measure the late ISW effect with a significance above 2σ independently of parameter degeneracies, as shown in Fig. 1. The novelty of our study also resides on the exploration of the redshift and scale dependence of the ISW effect. Crucially, we demonstrate that our tomographic method, reconstructing the ISW effect amplitude as a function of redshift, can serve as a powerful probe of the dark ages, inaccessible via other observables. A larger value of $A_{\text{ISW}} > 1$ points to a stronger time variation of the gravitational potentials during the dark ages. Indeed, we find a 2σ deviation of the ISW amplitude ($A_{\text{ISW}} > 1$) at redshift $z = 500$, which could be signaling either new physics beyond the Λ CDM cosmology, a signal beyond the standard structure formation, or unidentified systematical errors.

Basics. The ISW effect leads to a CMB temperature perturbation given by the line-of-sight integral between us and the last scattering surface:

$$\Theta_\ell(k, \eta_0) = \int_0^{\eta_0} d\eta e^{-\tau(\eta)} [\dot{\Psi}(k, \eta) - \dot{\Phi}(k, \eta)] j_\ell[k(\eta_0 - \eta)], \quad (1)$$

where dot refers to conformal time derivative, τ is the optical depth, η_0 is the present conformal time and Ψ and Φ are the gravitational potentials in the Newtonian gauge. Before recombination the factor $e^{-\tau(\eta)}$ is negli-

Evidence for axion miniclusters with an increased central density

Benedikt Eggemeier,^{1,*} Ananthu Krishnan Anilkumar,^{1,†} and Klaus Dolag^{2,3,‡}

¹*Institut für Astrophysik, Georg-August-Universität Göttingen, D-37077 Göttingen, Germany*

²*Universitäts-Sternwarte, Fakultät für Physik, Ludwig-Maximilians-Universität München, Scheinerstr.1, 81679 München, Germany*

³*Max-Planck-Institut für Astrophysik, Karl-Schwarzschild-Straße 1, 85741 Garching, Germany*

(Dated: February 29, 2024)

We identify axion miniclusters collapsing in the radiation-dominated era and follow them to redshift $z = 99$ with N-body simulations. We find that the majority of the densest miniclusters end up in the center of larger minicluster halos at late times. Soon after their formation, the miniclusters exhibit NFW profiles but they subsequently develop a steeper inner slope approaching $\rho \sim r^{-2}$ on small scales. Using the so far most highly resolved axion structure formation simulation with 2048³ particles we examine the structure of previously studied minicluster halos. While the density profiles of their subhalos are NFW-like we confirm that a modified NFW profile with a steeper inner slope provides a better description for minicluster halos with masses above $\sim 10^{-12} M_{\odot}$. We show that miniclusters with a higher central density might be in contrast to pure NFW halos dense enough to induce gravitational microlensing. Likewise, more compact minicluster halos will have immediate implications for direct and indirect axion detection.

I. INTRODUCTION

The QCD axion is a hypothetical particle and results from a spontaneously broken global $U(1)$ symmetry that was introduced by Peccei and Quinn to provide a solution to the so-called strong CP problem [1–8]. Since the axion is stable and only very weakly coupled to the Standard Model it is an attractive dark matter candidate [9]. The point in time of symmetry-breaking is crucial for the subsequent evolution of the axion and thus affects the phenomenology of axion dark matter.

In the post-inflationary symmetry-breaking scenario the early axion field is characterized by small-scale inhomogeneities which further leads to the formation of a cosmic string network [10]. When the axion mass becomes relevant compared to the expansion rate of the universe, domain walls start to build between the axion strings. This initializes the collapse of the string network producing both relativistic and nonrelativistic axions. As highly nonlinear processes are involved, the generation of axions from the decay of axion strings can only be studied numerically which is done via cosmological lattice simulations [11–20]. This is a highly non-trivial and challenging task that allows for the prediction of axion model parameters and the dark matter abundance. While there are some simulation scheme-dependent systematic uncertainties concerning the axion mass (see for example Ref. [21] for a discussion), the occurrence of large overdensities in the axion field as a consequence of the collapse of axion strings is a firm prediction.

Eventually, gravity becomes the dominant force and the axion overdensities collapse into gravitationally

bound axion *miniclusters* (MCs) [22–26]. In contrast to the usual structure formation scenarios with cold dark matter (CDM), axion MCs form already during the radiation-dominated era of cosmic history with typical masses of $M \sim 10^{-12} M_{\odot}$ and merge hierarchically into larger structures known as axion *minicluster halos* (MCHs) [27, 28]. Since MCs are particularly dense objects it is expected that a large fraction survives the merging processes. Hence, axion MCs should exist as dark matter substructures within galaxy-sized halos at present if they are not tidally disrupted by encounters with stars [29–34].

Their presence in Milky Way-like dark matter halos is of significance for axion searches relying on direct and indirect detection techniques. If a large fraction of dark matter is bound in axion MCs, opportunities for indirect axion detection arise from gravitational microlensing [26, 27, 35] and transient radio signals originating from collisions of axion MCs with the magnetospheres of neutron stars [36–38]. Conversely, this decreases the chances of a direct axion detection in haloscope experiments significantly as an encounter of an MC with the Earth is presumably a rare event taking place only once every 10^5 years [29, 39]. Nevertheless, the probability of detecting axions directly is enhanced by the possible tidal disruption of MCs and MCHs leading to tidal streams that cover a larger volume with axions.

To make reliable quantitative predictions about the distribution of axion MCs and their structure, the gravitational growth and collapse of axion overdensities need to be studied numerically. Starting from initial conditions produced by lattice simulations of the early axion field evolution using the methods from Ref. [15], the first N-body simulations addressing the formation of axion MCHs were presented in Ref. [28]. They found that at their final redshift of $z = 99$ roughly 75% of axions are gravitationally bound in MCHs covering a mass range from $10^{-15} M_{\odot}$ to $10^{-9} M_{\odot}$ and they analyzed the

* benedikt.eggemeier@phys.uni-goettingen.de

† a.anilkumar@stud.uni-goettingen.de

‡ kdolag@mpa-garching.mpg.de

Studying The Effect of Radiation Pressure on Evolution of a Population III Stellar Cluster

SUKALPA KUNDU¹ AND JAYANTA DUTTA¹

¹*Harish Chandra Research Institute, Chhatnag Rd, Jhusi, Prayagraj, Uttar Pradesh 211019*

ABSTRACT

Recent numerical simulations have shown that the unstable disk within the central regime of the primordial gas cloud fragments to form multiple protostars on several scales. Their evolution depends on the mass accretion phenomenon, interaction with the surrounding medium and radiative feedback respectively. In this work, we use a fast semi-analytical framework in order to model multiple protostars within a rotating cloud, where the mass accretion is estimated via a Bondi-Hoyle flow and the feedback process is approximated through radiation pressure. We observe that while some of the evolving protostars possibly grow massive ($\approx 1 - 24M_{\odot}$) via accretion and mergers, a fraction of them ($\approx 20\%$) are likely to be ejected from the parent cloud with a mass corresponding to $M_* \lesssim 0.8M_{\odot}$. These low-mass protostars may be considered as the potential candidates to enter the zero-age-main-sequence (ZAMS) phase and possibly survive till the present epoch.

Keywords: Pop III stars – Semi-numerical simulation – Radiation Pressure – Survival

1. INTRODUCTION

In the standard framework of cosmology, primordial fluctuations in the density field of the universe grow into dark matter (DM) minihalos (of virial mass $\approx 10^5 - 10^6 M_{\odot}$) as a consequence of the hierarchical structure formation (Navarro et al. 1996; Haiman 2011; Wise 2019; Wang et al. 2020; Springel et al. 2021). Baryonic matter including the electrons from the recombination era settles into the potential wells of these minihalos to form the primordial gas clouds, which are the sites of the Population III (or Pop III) stars (see e.g., the reviews Barkana & Loeb 2001; Bromm & Larson 2004; Ciardi & Ferrara 2005; Klessen & Glover 2023). Subsequently, this unstable gas undergoes nonlinear collapse as a result of self-gravity and thermodynamical instabilities through the primordial chemical network (Palla et al. 1983; Glover & Abel 2008; Turk et al. 2011; Bovino et al. 2014; Dutta 2015; Barkana 2018), eventually giving rise to a disk-like structure that fragments to form multiple protostars (Stacy et al. 2010; Clark et al. 2011; Greif et al. 2011; Dutta et al. 2015; Sharda et al. 2019; Inoue & Yoshida 2020; Wollenberg et al. 2020; Chiaki

& Yoshida 2022). At some epoch, the mass accretion process of these protostars is affected by the radiative feedback that becomes a crucial factor influencing their mass evolution (Hosokawa et al. 2011; Stacy et al. 2012; Hirano et al. 2015; Latif et al. 2022).

Depending on the initial configuration such as rotation, thermal and chemical instabilities, some of these protostars continue to grow massive either through accretion (Haemmerlé et al. 2017; Woods et al. 2017) or through merger (Kulkarni et al. 2019; Susa 2019). The other can even explode as pair-instability-supernovae (PISN) (Chen et al. 2014; Yoshii et al. 2022; Padmanabhan & Loeb 2022; Venditti et al. 2024) or collapse to form the seed of the blackhole (Smith et al. 2018; Safarzadeh & Haiman 2020; Santoliquido et al. 2023) or undergo runaway merger with other stars (Vergara et al. 2021; Alister Seguel et al. 2020). A fraction of the fragments can also lead to the formation of low-mass stars that may even go out of the cluster (Marigo et al. 2001; Komiya et al. 2015; Ishiyama et al. 2016; Dutta 2016a; Raghuvanshi & Dutta 2023).

However, to investigate the initial mass function (IMF), we need to follow the evolution for hundreds of thousands of years, which seems to be non-trivial in existing 3D numerical simulations. This is mainly due to complexities such as complicated chemical networks and the high dynamic range in densities. Besides, introducing the radiative transfer to account for the feed-

sukalpa.k123@gmail.com

Corresponding author: Sukalpa Kundu

Corresponding author: Jayanta Dutta

Concise Spectrotemporal Studies of Magnetar SGR J1935+2154 Bursts

ÖZGE KESKIN ¹, ERSIN GÖĞÜŞ ¹, YUKI KANEKO ¹, MUSTAFA DEMIRER ¹,
SHOTARO YAMASAKI ², MATTHEW G. BARING ³, LIN LIN ⁴, OLIVER J. ROBERTS ⁵ AND
CHRYSSA KOUVELIOTOU ^{6,7}

¹*Sabanci University, Faculty of Engineering and Natural Sciences, İstanbul 34956 Turkey*

²*Department of Physics, National Chung Hsing University, 145 Xingda Rd., South Dist., Taichung 40227, Taiwan*

³*Department of Physics and Astronomy - MS 108, Rice University, 6100 Main Street, Houston, Texas 77251-1892, USA*

⁴*Department of Astronomy, Beijing Normal University, Beijing 100875, China*

⁵*Science and Technology Institute, Universities Space and Research Association, 320 Sparkman Drive, Huntsville, AL 35805, USA.*

⁶*Department of Physics, The George Washington University, 725 21st Street NW, Washington, DC 20052, USA*

⁷*Astronomy, Physics, and Statistics Institute of Sciences (APSYS), The George Washington University, Washington, DC 20052, USA*

ABSTRACT

SGR J1935+2154 has truly been the most prolific magnetar over the last decade: It has been entering into burst active episodes once every 1-2 years since its discovery in 2014, it emitted the first Galactic fast radio burst associated with an X-ray burst in 2020, and has emitted hundreds of energetic short bursts. Here, we present the time-resolved spectral analysis of 51 bright bursts from SGR J1935+2154. Unlike conventional time-resolved X-ray spectroscopic studies in the literature, we follow a two-step approach to probe true spectral evolution. For each burst, we first extract spectral information from overlapping time segments, fit them with three continuum models, and employ a machine learning based clustering algorithm to identify time segments that provide the largest spectral variations during each burst. We then extract spectra from those non-overlapping (clustered) time segments and fit them again with the three models: the cutoff power-law model, the sum of two blackbody functions, and the model considering the emission of a modified black body undergoing resonant cyclotron scattering, which is applied systematically at this scale for the first time. Our novel technique allowed us to establish the genuine spectral evolution of magnetar bursts. We discuss the implications of our results and compare their collective behavior with the average burst properties of other magnetars.

Keywords: Neutron Stars (1108), Magnetars (992), X-ray bursts (1814)

Identifying changing-look AGNs using variability characteristics

SHU WANG,¹ JONG-HAK WOO,¹ ELENA GALLO,² HENGXIAO GUO,³ DONGHOON SON,¹ MINZHI KONG,⁴
AMIT KUMAR MANDAL,¹ HOJIN CHO,¹ CHANGSEOK KIM,¹ AND JAEJIN SHIN^{5,6}

¹*Department of Physics & Astronomy, Seoul National University, Seoul 08826, Republic of Korea; wangshu100002@gmail.com; woo@astro.snu.ac.kr*

²*Department of Astronomy, University of Michigan, Ann Arbor, MI 48109, USA*

³*Key Laboratory for Research in Galaxies and Cosmology, Shanghai Astronomical Observatory, Chinese Academy of Sciences, 80 Nandan Road, Shanghai 200030, People's Republic of China; hengxiaoguo@gmail.com*

⁴*Department of Physics, Hebei Normal University, No. 20 East of South 2nd Ring Road, Shijiazhuang 050024, People's Republic of China*

⁵*Korea Astronomy and Space Science Institute, Daejeon 34055, Republic of Korea*

⁶*Major in Astronomy and Atmospheric Sciences, Kyungpook National University, Daegu 41566, Republic of Korea*

ABSTRACT

Changing-look (CL) Active Galactic Nuclei (AGNs), characterized by appearance/disappearance of broad emission lines in the span of a few years, present a challenge for the AGN unified model, whereby the Type 1 vs. Type 2 dichotomy results from orientation effects alone. We present a systematic study of a large sample of spectroscopically classified AGNs, using optical variability data from the Zwicky Transient Facility (ZTF) as well as follow-up spectroscopy data. We demonstrate that Type 1 vs. Type 2 AGN can be neatly separated on the basis of the variability metric σ_{QSO} , which quantifies the resemblance of a light curve to a damped random walk model. For a small sub-sample, however, the ZTF light curves are inconsistent with their previous classification, suggesting the occurrence of a CL event. Specifically, we identify 35 (12) turn-on (turn-off) CL AGN candidates at $z < 0.35$. Based on follow-up spectroscopy, we confirm 17 (4) turn-on (turn-off) CL AGNs out of 21 (5) candidates, presenting a high success rate of our method. Our results suggest that the occurrence rate of CL AGNs is $\sim 0.3\%$ over timescales of 5 to 20 years, and confirm that the CL transition typically occurs at the Eddington ratio of $\lesssim 0.01$.

Keywords: Active galactic nuclei (16) — Quasars (1319)

1. INTRODUCTION

Active Galactic Nuclei (AGNs) are classified as either Type 1 or Type 2, respectively, based on the presence or absence of broad emission lines, which are typically defined with a full-width-at-half-maxima larger than $\sim 1000 \text{ km s}^{-1}$ in their ultra-violet (UV), optical, and near-IR spectra. Intermediate classes, i.e., Type 1.8 or 1.9 AGNs are characterized by broad H α and weak or absent broad H β lines (Osterbrock 1981). In the AGN unified model, this dichotomy is purely driven by orientation effects (Antonucci 1993; Urry & Padovani 1995), depending on whether or not the observer's line of sight is intercepted by a dusty torus. This scenario is supported by multiple lines of evidence, including the discovery of broad lines in the polarized spectra of some Type 2 AGNs (Antonucci & Miller 1985; Zakamska et al. 2005) and the higher fraction of Compton-thick AGNs amongst Type 2 AGNs (Mulchaey et al. 1992).

At the same time, the unified model faces significant challenges, particularly with the discovery of a small population of AGNs with emerging/disappearing broad emission lines over timescales of several years. Approximately 150 such changing-look (CL) AGNs have been reported so far, based on H β and/or H α (e.g., LaMassa et al. 2015; MacLeod et al. 2016; Runnoe et al. 2016; Ruan et al. 2016; Runco et al. 2016; Yang et al. 2018; MacLeod et al. 2019; Wang J. et al. 2019; Green et al. 2022; Zeltyn et al. 2022; Hon et al. 2022; López-Navas et al. 2022, 2023b; Guo W. et al. 2023; Neustadt et al. 2023). These CL AGNs demonstrate that the orientation-based unified model might be too simplistic.

The growing sample of CL AGNs provides insights to the physics underlying the phenomenon. CL AGNs are rare, with an occurrence rate of ~ 1 per cent or lower, estimated using multi-epoch spectra from large-area spectroscopic surveys (e.g., MacLeod et al. 2016, 2019; Yang et al. 2018). The timescale of CL events is

From Simulations to Reality: Dark Energy Reconstruction with Simulated SNIa data from the Vera C. Rubin Observatory

Ayan Mitra^{1,2,3,*}, Isidro Gómez-Vargas^{4,5,†} and Vasilios Zarikas^{6,‡}

¹*Center for AstroPhysical Surveys, National Center for Supercomputing Applications, University of Illinois Urbana-Champaign, Urbana, IL, 61801, USA*

²*Department of Astronomy, University of Illinois at Urbana-Champaign, Urbana, IL 61801, USA*

³*Kazakh-British Technical University, 59 Tole Bi Street, 050000 Almaty, Kazakhstan*

⁴*Instituto de Ciencias Físicas, Universidad Nacional Autónoma de México, 62210, Cuernavaca, Morelos, México.*

⁵*Department of Astronomy of the University of Geneva, 51 Chemin Pegasi, 1290 Versoix, Switzerland.*

⁶*Department of Mathematics, University of Thessaly, Lamia 35132, Greece*

(Dated: February 29, 2024)

In this paper, we present an Artificial Neural Network (ANN) based reconstruction analysis of the Supernova Ia (SNIa) distance moduli ($\mu(z)$), and hence dark energy, using LSST simulated three-year SNIa data. Our ANN reconstruction architecture can model both the distance moduli and their corresponding error estimates. For this we employ astroANN and incorporate Monte Carlo dropout techniques to quantify uncertainties in our predictions. We tune our hyperparameters through advanced genetic algorithms, including elitism, utilizing the DEAP library. We compared the performance of the ANN based reconstruction with two theoretical descriptions of dark energy models, Λ CDM and Chevallier-Linder-Polarski (CPL). We perform a Bayesian analysis for these two theoretical models using the LSST simulations and also compare with observations from Pantheon and Pantheon+ SNIa real data. We show that our model-independent reconstruction using ANN is consistent with both of them. We assessed the performance using mean squared error (MSE) and showed that the ANN can produce distance estimates in better agreement with the LSST dataset than either Λ CDM or CPL, albeit very small. We included an additional residual analysis and a null test with F -scores to show that the reconstructed distances from the ANN model, are in excellent agreement with the Λ CDM or CPL model.

arXiv:2402.18124v1 [astro-ph.CO] 28 Feb 2024

* ayan@illinois.edu

† isidro.gomezvargas@unige.ch

‡ vzarikas@uth.gr

Locating heating channels of the solar corona in a plage region with the aid of high-resolution 10830 Å filtergrams

PARIDA HASHIM,¹ FANGYU XU,² YA WANG,³ WEIJIE MENG,^{2,4} JINHUA SHEN,¹ YINGNA SU,³ JIANPING LI,³ ZHENYU JIN,²
AND HAISHENG JI³

¹*Xinjiang Astronomical Observatory, CAS, Urumqi, 830011, China*

²*Yunnan Astronomical Observatory, CAS, Kunming, 650216, China*

³*Purple Mountain Observatory, CAS, Nanjing, 210023, China*

⁴*University of CAS, Beijing, 100049, China*

ABSTRACT

In this paper, with a set of high-resolution He I 10830 Å filtergrams, we select an area in a plage, very likely an EUV moss area, as an interface layer to follow the clues of coronal heating channels down to the photosphere. The filtergrams are obtained from the 1-meter aperture New Vacuum Solar Telescope (NVST). We make a distinction between the darker and the brighter regions in the selected area and name the two regions enhanced absorption patches (EAPs) and low absorption patches (LAPs). With well-aligned, nearly simultaneous data from multiple channels of the AIA and the continuum of the HMI on board SDO, we compare the EUV/UV emissions, emission measure, mean temperature, and continuum intensity in the two kinds of regions. The following progress is made: 1) The mean EUV emissions over EAPs are mostly stronger than the corresponding emissions over LAPs except for the emission at 335 Å. The UV emissions at 1600 and 1700 Å fail to capture the difference between the two regions. 2) In the logarithmic temperature range of 5.6-6.2, EAPs have higher EUV emission measure than LAPs, but they have lower mean coronal temperature. 3) The mean continuum intensity over EAPs is lower. Based on the above progress, we suggest that the energy for coronal heating in the moss region can be traced down to some areas in intergranular lanes with enhanced density of both cool and hot material. The lower temperature over the EAPs is due to the greater fraction of cool material over there.

Keywords: Solar corona — Solar transition region — Solar Chromosphere — Solar photosphere

1. INTRODUCTION

How the solar or stellar corona is heated to millions of degrees is an unsolved problem in the field of astrophysics (Klimchuk 2006; Schrijver & Zwaan 2000; Aschwanden 2005). Most researchers agree that the corona is probably heated in two primary ways: dissipation of MHD waves and nano-flares (Parker 1988) that occur directly in the corona. The latter was believed to be caused by magnetic reconnection in the braided coronal magnetic field. Nanoflares are often associated with impulsive heating (Warren et al. 2003; Patsourakos & Klimchuk 2006; Tripathi et al. 2010), while wave heating is believed to be in a steady state (Reale et al. 2000; Antiochos et al. 2003; Brooks & Warren 2009). Both kinds of heating mechanisms have their support from contemporary observations, e.g., even with the highest observations from Hi-C in the extreme-ultraviolet (EUV), the opinions regarding steady-state heating or impulsive heating are co-existing (Testa et al. 2013; Graham et al. 2019; Warren et al. 2020). Aschwanden et al. (2007) pointed out that energy for heating the corona certainly comes from the lower atmosphere, which includes the lower transition region (TR), the chromosphere, and the photosphere. Also, more and more high-resolution observations from the lower atmosphere reveal that the heating process is at small spatial and temporal scales via hot expulsions, spicules, or waves generated directly from the photosphere, leaving responses in the TR and chromosphere (Tian et al. 2014;

Galaxy clustering at cosmic dawn from JWST/NIRCam observations to redshift $z \sim 11$

Nicolò Dalmaso^{1,2*}, Nicha Leethochawalit³, Michele Trenti^{1,2}, Kristan Boyett^{1,2}

¹*School of Physics, University of Melbourne, Parkville, Vic 3010, Australia*

²*ARC Centre of Excellence for All Sky Astrophysics in 3 Dimensions (ASTRO 3D), Australia*

³*National Astronomical Research Institute of Thailand (NARIT), Mae Rim, Chiang Mai, 50180, Thailand*

Accepted XXX. Received YYY; in original form ZZZ

ABSTRACT

We report measurements of the galaxy two-point correlation function at cosmic dawn, using photometrically-selected sources from the JWST Advanced Deep Extragalactic Survey (JADES). The JWST/NIRCam dataset comprises approximately $N_g \simeq 7000$ photometrically-selected Lyman Break Galaxies (LBGs), spanning from $z = 5.5$ up to $z = 10.6$. The primary objective of this study is to extend clustering measurements beyond redshift $z > 10$, finding a galaxy bias $b = 9.6 \pm 1.7$ for the sample at $\bar{z} = 10.6$. The result suggests that the observed sources are hosted by dark matter halos of approximately $M_h \sim 10^{10.5} M_\odot$, in broad agreement with theoretical and numerical modelling of early galaxy formation during the epoch of reionization. Furthermore, the JWST JADES dataset enables an unprecedented investigation of clustering of dwarf galaxies two orders of magnitude fainter than the characteristic L_* luminosity (i.e. with $M_{F200W} \simeq -14.5$) during the late stages of the epoch of reionization at $z \sim 6$. By measuring clustering versus luminosity, we observe that $b(M_{F200W})$ initially decreases with M_{F200W} as theoretically expected, but a turning point of the relationship is seen at $M_{F200W} \sim -16$. We interpret the rise of clustering of the faintest dwarf as evidence of multiple halo occupation (i.e. as a one-halo term in bias modelling). These initial results demonstrate the potential for further quantitative characterisation of the interplay between assembly of dark matter and light during cosmic dawn that the growing samples of JWST observations are enabling.

Key words: cosmology: observations – galaxies: general – galaxies: high-redshift – galaxies: evolution

1 INTRODUCTION

The Universe we observe today formed from primordial fluctuations emerged during an inflationary epoch, subsequently amplified by gravitational instability shaping matter distribution. Gas dissipated over time, gravitating towards dark matter halos' central regions, intricately linking the growth and spatial arrangement of galaxies to their dark matter halos (Peebles 1980; Persic & Salucci 1992; Bullock et al. 2001).

The conceptualization of the galaxy–halo connection coincided with the realization that the spatial distribution of galaxies can yield insights into their formative properties. Early studies such as Peebles (1980) focused on the two-point statistics of galaxies, as well as investigations on signal strength sensitivity to measure galaxy mass and luminosity (e.g., Bahcall & Soneira 1980; Davis & Peebles 1983).

Recognizing that measuring these clustering properties could furnish information about the masses of the dark matter halos housing these galaxies was a pivotal insight due to the pronounced dependence of halo clustering on halo mass (e.g., Bardeen et al. 1986; Mo & White 1996; Klypin et al. 1996; Sheth & Tormen 1999; Jenkins et al. 2001; Tinker et al. 2010).

A key tool to quantify clustering is the two-point correlation func-

tion ($\xi(r)$; Peebles 1980), which quantifies the excess probability of finding a galaxy at a given separation distance "r" compared to a random distribution. Given that precise redshift are not always available (e.g. in the case of photometrically selected samples), this function is often replaced by the Angular Two-Point Correlation Function (ACF), which expresses the excess as a function of the angular separation denoted by (θ) instead. The ACF can then be mapped to an two-point correlation function in physical space based on the (estimated) redshift distribution of the sample, leading to a characteristic correlation length (r_0 ; Davis & Peebles 1983). This parameter r_0 represents the typical separation distance at which galaxies exhibit significant correlation or clustering. The value of r_0 may vary depending on the specific sample of galaxies, the redshift range under investigation, and the cosmological model applied.

The correlation length is closely tied to determining another crucial parameter: galaxy bias (b ; Peebles 1980), representing the systematic deviation or clustering of galaxies compared to the underlying matter distribution in the Universe. A rising trend in galaxy bias suggests stronger clustering and in-turn this implies that the galaxy population is hosted in more massive dark-matter halos.

Clustering, when combined with information on the galaxy luminosity function, can also provide insight on the typical occupation fraction of dark-matter halos that host luminous galaxies. This fraction is known as the duty cycle (ϵ_{DC}). The duty cycle is typically

* e-mail: ndalmaso@student.unimelb.edu.au

A study of 10 Rotating Radio Transients using Parkes radio telescope

Xinhui Ren^{1,2,3}, Jingbo Wang³, Wenming Yan^{1,4}, Jintao Xie⁵, Shuangqiang Wang¹, Yirong Wen^{1,2,3}, Yong Xia^{1,2,3}

¹ Xinjiang Astronomical Observatory, Chinese Academy of Sciences, Urumqi, Xinjiang 830011, People's Republic of China

² University of Chinese Academy of Sciences, Beijing 100049, People's Republic of China

³ Institute of Optoelectronic Technology, Lishui University, Lishui, Zhejiang, 323000, People's Republic of China; 1983wangjingbo@163.com

⁴ Xinjiang Key Laboratory of Radio Astrophysics, Urumqi, Xinjiang, 830011, People's Republic of China

⁵ Research Center for Intelligent Computing Platforms, Zhejiang Laboratory, Hangzhou, Zhejiang 311100, China

Received 20XX Month Day; accepted 20XX Month Day

Abstract Rotating Radio Transients (RRATs) are a relatively new subclass of pulsars that emit detectable radio bursts sporadically. We conducted an analysis of 10 RRATs observed using the Parkes telescope, with 8 of these observed via the Ultra-Wideband Receiver. We measured the burst rate and produced integrated profiles spanning multiple frequency bands for 3 RRATs. We also conducted a spectral analysis on both integrated pulses and individual pulses of 3 RRATs. All of their integrated pulses follow a simple power law, consistent with the known range of pulsar spectral indices. Their average spectral indices of single pulses are -0.9, -1.2, and -1.0 respectively, which are within the known range of pulsar spectral indices. Additionally, we find that the spreads of single-pulse spectral indices for these RRATs (ranging from -3.5 to +0.5) are narrower compared to what has been observed in other RRATs (Shapiro-Albert et al. 2018; Xie et al. 2022). It is notable that the average spectral index and scatter of single pulses are both relatively small. For the remaining 5 RRATs observed at the UWL receiver, we also provided the upper limits on fluence and flux density. In addition, we obtained the timing solution of PSR J1709-43. Our analysis shows that PSRs J1919+1745, J1709-43 and J1649-4653 are potentially nulling pulsars or weak pulsars with sparse strong pulses.

Characterization of the Astrophysical Diffuse Neutrino Flux using Starting Track Events in IceCube

R. Abbasi,¹⁷ M. Ackermann,⁶⁴ J. Adams,¹⁸ S. K. Agarwalla,^{40,*} J. A. Aguilar,¹² M. Ahlers,²² J.M. Alameddine,²³ N. M. Amin,⁴⁴ K. Andeen,⁴² G. Anton,²⁶ C. Argüelles,¹⁴ Y. Ashida,⁵³ S. Athanasiadou,⁶⁴ L. Ausborn,¹ S. N. Axani,⁴⁴ X. Bai,⁵⁰ A. Balagopal V.,⁴⁰ M. Baricevic,⁴⁰ S. W. Barwick,³⁰ S. Bash,²⁷ V. Basu,⁴⁰ R. Bay,⁸ J. J. Beatty,^{20,21} J. Becker Tjus,^{11,†} J. Beise,⁶² C. Bellenghi,²⁷ C. Benning,¹ S. BenZvi,⁵² D. Berley,¹⁹ E. Bernardini,⁴⁸ D. Z. Besson,³⁶ E. Blaufuss,¹⁹ S. Blot,⁶⁴ F. Bontempo,³¹ J. Y. Book,¹⁴ C. Boscolo Meneguolo,⁴⁸ S. Böser,⁴¹ O. Botner,⁶² J. Böttcher,¹ J. Braun,⁴⁰ B. Brinson,⁶ J. Brostean-Kaiser,⁶⁴ L. Brusa,¹ R. T. Burley,² R. S. Busse,⁴³ D. Butterfield,⁴⁰ M. A. Campana,⁴⁹ I. Caracas,⁴¹ K. Carloni,¹⁴ J. Carpio,^{34,35} S. Chattopadhyay,^{40,*} N. Chau,¹² Z. Chen,⁵⁶ D. Chirkin,⁴⁰ S. Choi,⁵⁷ B. A. Clark,¹⁹ A. Coleman,⁶² G. H. Collin,¹⁵ A. Connolly,^{20,21} J. M. Conrad,¹⁵ P. Coppin,¹³ R. Corley,⁵³ P. Correa,¹³ D. F. Cowen,^{60,61} P. Dave,⁶ C. De Clercq,¹³ J. J. DeLaunay,⁵⁹ D. Delgado,¹⁴ S. Deng,¹ K. Deoskar,⁵⁵ A. Desai,⁴⁰ P. Desiati,⁴⁰ K. D. de Vries,¹³ G. de Wasseige,³⁷ T. DeYoung,²⁴ A. Diaz,¹⁵ J. C. Díaz-Vélez,⁴⁰ M. Dittmer,⁴³ A. Domi,²⁶ L. Draper,⁵³ H. Dujmovic,⁴⁰ M. A. DuVernois,⁴⁰ T. Ehrhardt,⁴¹ L. Eidenschink,²⁷ A. Eimer,²⁶ P. Eller,²⁷ E. Ellinger,⁶³ S. El Mentawi,¹ D. Elsässer,²³ R. Engel,^{31,32} H. Erpenbeck,⁴⁰ J. Evans,¹⁹ P. A. Evenson,⁴⁴ K. L. Fan,¹⁹ K. Fang,⁴⁰ K. Farrag,¹⁶ A. R. Fazely,⁷ A. Fedynitch,⁵⁸ N. Feigl,¹⁰ S. Fiedlschuster,²⁶ C. Finley,⁵⁵ L. Fischer,⁶⁴ D. Fox,⁶⁰ A. Franckowiak,¹¹ P. Fürst,¹ J. Gallagher,³⁹ E. Ganster,¹ A. Garcia,¹⁴ E. Genton,³⁷ L. Gerhardt,⁹ A. Ghadimi,⁵⁹ C. Girard-Carillo,⁴¹ C. Glaser,⁶² T. Glüsenkamp,^{26,62} J. G. Gonzalez,⁴⁴ S. Goswami,^{34,35} A. Granados,²⁴ D. Grant,²⁴ S. J. Gray,¹⁹ O. Gries,¹ S. Griffin,⁴⁰ S. Griswold,⁵² K. M. Groth,²² C. Günther,¹ P. Gutjahr,²³ C. Ha,⁵⁴ C. Haack,²⁶ A. Hallgren,⁶² R. Halliday,²⁴ L. Halve,¹ F. Halzen,⁴⁰ H. Hamdaoui,⁵⁶ M. Ha Minh,²⁷ M. Handt,¹ K. Hanson,⁴⁰ J. Hardin,¹⁵ A. A. Harnisch,²⁴ P. Hatch,³³ A. Haungs,³¹ J. Häußler,¹ K. Helbing,⁶³ J. Hellrung,¹¹ J. Hermannsgabner,¹ L. Heuermann,¹ N. Heyer,⁶² S. Hickford,⁶³ A. Hidvegi,⁵⁵ C. Hill,¹⁶ G. C. Hill,² K. D. Hoffman,¹⁹ S. Hori,⁴⁰ K. Hoshina,^{40,‡} M. Hostert,¹⁴ W. Hou,³¹ T. Huber,³¹ K. Hultqvist,⁵⁵ M. Hünnefeld,²³ R. Hussain,⁴⁰ K. Hymon,²³ A. Ishihara,¹⁶ W. Iwakiri,¹⁶ M. Jacquart,⁴⁰ O. Janik,²⁶ M. Jansson,⁵⁵ G. S. Japaridze,⁵ M. Jeong,⁵³ M. Jin,¹⁴ B. J. P. Jones,⁴ N. Kamp,¹⁴ D. Kang,³¹ W. Kang,⁵⁷ X. Kang,⁴⁹ A. Kappes,⁴³ D. Kappesser,⁴¹ L. Kardum,²³ T. Karg,⁶⁴ M. Karl,²⁷ A. Karle,⁴⁰ A. Katil,²⁵ U. Katz,²⁶ M. Kauer,⁴⁰ J. L. Kelley,⁴⁰ M. Khanal,⁵³ A. Khatee Zathul,⁴⁰ A. Kheirandish,^{34,35} J. Kiryluk,⁵⁶ S. R. Klein,^{8,9} A. Kochocki,²⁴ R. Koirala,⁴⁴ H. Kolanoski,¹⁰ T. Kontrimas,²⁷ L. Köpke,⁴¹ C. Kopper,²⁶ D. J. Koskinen,²² P. Koundal,⁴⁴ M. Kovacevich,⁴⁹ M. Kowalski,^{10,64} T. Kozynets,²² J. Krishnamoorthi,^{40,*} K. Kruiswijk,³⁷ E. Krupczak,²⁴ A. Kumar,⁶⁴ E. Kun,¹¹ N. Kurahashi,⁴⁹ N. Lad,⁶⁴ C. Lagunas Gualda,⁶⁴ M. Lamoureux,³⁷ M. J. Larson,¹⁹ S. Latseva,¹ F. Lauber,⁶³ J. P. Lazar,³⁷ J. W. Lee,⁵⁷ K. Leonard DeHolton,^{60,61} A. Leszczyńska,⁴⁴ J. Liao,⁶ M. Lincetto,¹¹ M. Liubarska,²⁵ E. Lohfink,⁴¹ C. Love,⁴⁹ C. J. Lozano Mariscal,⁴³ L. Lu,⁴⁰ F. Lucarelli,²⁸ W. Luszczak,^{20,21} Y. Lyu,^{8,9} J. Madsen,⁴⁰ E. Magnus,¹³ K. B. M. Mahn,²⁴ Y. Makino,⁴⁰ E. Manao,²⁷ S. Mancina,^{40,48} W. Marie Sainte,⁴⁰ I. C. Mariş,¹² S. Marka,⁴⁶ Z. Marka,⁴⁶ M. Marsee,⁵⁹ I. Martinez-Soler,¹⁴ R. Maruyama,⁴⁵ F. Mayhew,²⁴ T. McElroy,²⁵ F. McNally,³⁸ J. V. Mead,²² K. Meagher,⁴⁰ S. Mechbal,⁶⁴ A. Medina,²¹ M. Meier,¹⁶ Y. Merckx,¹³ L. Merten,¹¹ J. Micallef,²⁴ J. Mitchell,⁷ T. Montaruli,²⁸ R. W. Moore,²⁵ Y. Morii,¹⁶ R. Morse,⁴⁰ M. Moulai,⁴⁰ T. Mukherjee,³¹ R. Naab,⁶⁴ R. Nagai,¹⁶ M. Nakos,⁴⁰ U. Naumann,⁶³ J. Necker,⁶⁴ A. Negi,⁴ M. Neumann,⁴³ H. Niederhausen,²⁴ M. U. Nisa,²⁴ A. Noell,¹ A. Novikov,⁴⁴ S. C. Nowicki,²⁴ A. Obertacke Pollmann,¹⁶ V. O'Dell,⁴⁰ B. Oeyen,²⁹ A. Olivas,¹⁹ R. Orsoe,²⁷ J. Osborn,⁴⁰ E. O'Sullivan,⁶² H. Pandya,⁴⁴ N. Park,³³ G. K. Parker,⁴ E. N. Paudel,⁴⁴ L. Paul,⁵⁰ C. Pérez de los Heros,⁶² T. Pernice,⁶⁴ J. Peterson,⁴⁰ S. Philippen,¹ A. Pizzuto,⁴⁰ M. Plum,⁵⁰ A. Pontén,⁶² Y. Popovych,⁴¹ M. Prado Rodriguez,⁴⁰ B. Pries,²⁴ R. Procter-Murphy,¹⁹ G. T. Przybylski,⁹ C. Raab,³⁷ J. Rack-Helleis,⁴¹ K. Rawlins,³ Z. Rechav,⁴⁰ A. Rehman,⁴⁴ P. Reichherzer,¹¹ E. Resconi,²⁷ S. Reusch,⁶⁴ W. Rhode,²³ B. Riedel,⁴⁰ A. Rifaie,¹ E. J. Roberts,² S. Robertson,^{8,9} S. Rodan,⁵⁷ G. Roellinghoff,⁵⁷ M. Rongen,²⁶ A. Rosted,¹⁶ C. Rott,^{53,57} T. Ruhe,²³ L. Ruohan,²⁷ D. Ryckbosch,²⁹ I. Safa,⁴⁰ J. Saffer,³² D. Salazar-Gallegos,²⁴ P. Sampathkumar,³¹ A. Sandrock,⁶³ M. Santander,⁵⁹ S. Sarkar,²⁵ S. Sarkar,⁴⁷ J. Savelberg,¹ P. Savina,⁴⁰ P. Schaile,²⁷ M. Schaufel,¹ H. Schieler,³¹ S. Schindler,²⁶ B. Schlüter,⁴³ F. Schlüter,¹² N. Schmeisser,⁶³ T. Schmidt,¹⁹ J. Schneider,²⁶ F. G. Schröder,^{31,44} L. Schumacher,²⁶ S. Sclafani,¹⁹ D. Seckel,⁴⁴ M. Seikh,³⁶ M. Seo,⁵⁷ S. Seunarine,⁵¹ P. Seville Myhr,³⁷ R. Shah,⁴⁹ S. Shefali,³² N. Shimizu,¹⁶ M. Silva,⁴⁰ B. Skrzypek,⁸ B. Smithers,⁴ R. Snihur,⁴⁰ J. Soedingrekso,²³ A. Sjøgaard,²² D. Soldin,⁵³ P. Soldin,¹ G. Sommani,¹¹ C. Spannfellner,²⁷ G. M. Spiczak,⁵¹ C. Spiering,⁶⁴ M. Stamatikos,²¹ T. Stanev,⁴⁴ T. Stezelberger,⁹ T. Stürwald,⁶³ T. Stuttard,²² G. W. Sullivan,¹⁹ I. Taboada,⁶ S. Ter-Antonyan,⁷ A. Terliuk,²⁷ M. Thiesmeyer,¹ W. G. Thompson,¹⁴ J. Thwaites,⁴⁰ S. Tilav,⁴⁴ K. Tollefson,²⁴ C. Tönnis,⁵⁷ S. Toscano,¹² D. Tosi,⁴⁰ A. Trettin,⁶⁴ R. Turcotte,³¹ J. P. Twagirayezu,²⁴ M. A. Unland Elorrieta,⁴³ A. K. Upadhyay,^{40,*} K. Upshaw,⁷ A. Vaidyanathan,⁴² N. Valtonen-Mattila,⁶² J. Vandenbroucke,⁴⁰ N.

arXiv:2402.18026v1 [astro-ph.HE] 28 Feb 2024

3

⁴⁶Columbia Astrophysics and Nevis Laboratories,
Columbia University, New York, NY 10027, USA

⁴⁷Dept. of Physics, University of Oxford, Parks Road, Oxford OX1 3PU, United Kingdom

⁴⁸Dipartimento di Fisica e Astronomia Galileo Galilei,
Università Degli Studi di Padova, I-35122 Padova PD, Italy

⁴⁹Dept. of Physics, Drexel University, 3141 Chestnut Street, Philadelphia, PA 19104, USA

⁵⁰Physics Department, South Dakota School of Mines and Technology, Rapid City, SD 57701, USA

⁵¹Dept. of Physics, University of Wisconsin, River Falls, WI 54022, USA

⁵²Dept. of Physics and Astronomy, University of Rochester, Rochester, NY 14627, USA

⁵³Department of Physics and Astronomy, University of Utah, Salt Lake City, UT 84112, USA

⁵⁴Dept. of Physics, Chung-Ang University, Seoul 06974, Republic of Korea

⁵⁵Oskar Klein Centre and Dept. of Physics, Stockholm University, SE-10691 Stockholm, Sweden

⁵⁶Dept. of Physics and Astronomy, Stony Brook University, Stony Brook, NY 11794-3800, USA

⁵⁷Dept. of Physics, Sungkyunkwan University, Suwon 16419, Republic of Korea

⁵⁸Institute of Physics, Academia Sinica, Taipei, 11529, Taiwan

⁵⁹Dept. of Physics and Astronomy, University of Alabama, Tuscaloosa, AL 35487, USA

⁶⁰Dept. of Astronomy and Astrophysics, Pennsylvania State University, University Park, PA 16802, USA

⁶¹Dept. of Physics, Pennsylvania State University, University Park, PA 16802, USA

⁶²Dept. of Physics and Astronomy, Uppsala University, Box 516, SE-75120 Uppsala, Sweden

⁶³Dept. of Physics, University of Wuppertal, D-42119 Wuppertal, Germany

⁶⁴Deutsches Elektronen-Synchrotron DESY, Platanenallee 6, D-15738 Zeuthen, Germany

(Dated: February 29, 2024)

A measurement of the diffuse astrophysical neutrino spectrum is presented using IceCube data collected from 2011-2022 (10.3 years). We developed novel detection techniques to search for events with a contained vertex and exiting track induced by muon neutrinos undergoing a charged-current interaction. Searching for these starting track events allows us to not only more effectively reject atmospheric muons but also atmospheric neutrino backgrounds in the southern sky, opening a new window to the sub-100 TeV astrophysical neutrino sky. The event selection is constructed using a dynamic starting track veto and machine learning algorithms. We use this data to measure the astrophysical diffuse flux as a single power law flux (SPL) with a best-fit spectral index of $\gamma = 2.58_{-0.09}^{+0.10}$ and per-flavor normalization of $\phi_{\text{per-flavor}}^{\text{Astro}} = 1.68_{-0.22}^{+0.19} \times 10^{-18} \times \text{GeV}^{-1} \text{cm}^{-2} \text{s}^{-1} \text{sr}^{-1}$ (at 100 TeV). The sensitive energy range for this dataset is 3 - 550 TeV under the SPL assumption. This data was also used to measure the flux under a broken power law, however we did not find any evidence of a low energy cutoff.

CONTENTS

	A. Quality cuts	8
	B. Starting track veto	9
I. Introduction	C. Starting tracks boosted decision tree	11
II. Measurement Motivation		
A. Astrophysical neutrinos	VI. Measurement Methodology	12
B. Starting track morphology	A. Statistical analysis	12
III. Detector and Simulations	B. Systematic uncertainties	12
A. Detector configuration	1. Atmospheric Flux Systematics	12
B. Simulation of neutrinos and atmospheric muons	2. Detector systematics	13
IV. Reconstructed Observables	VII. Diffuse Flux Measurement	15
A. Directional reconstruction	A. Measurement of the diffuse flux assuming a single power law flux	15
B. Energy reconstruction	B. Measurement of the diffuse flux assuming a segmented power law	16
V. Event Selection	C. Measurement of the diffuse flux assuming a broken power law	17
	D. Measurement of the diffuse flux assuming a non-isotropic diffuse flux	18
	E. Search for prompt atmospheric neutrinos	19
	F. Diffuse flux measurement summary and outlook	19
	VIII. Conclusion	20

* also at Institute of Physics, Sachivalaya Marg, Sainik School Post, Bhubaneswar 751005, India

† also at Department of Space, Earth and Environment, Chalmers University of Technology, 412 96 Gothenburg, Sweden

‡ also at Earthquake Research Institute, University of Tokyo, Bunkyo, Tokyo 113-0032, Japan

Received 2023 October XX; accepted XXXX July XX

How to coadd images: II. Anti-aliasing and PSF deconvolution

Lei Wang^{145*}, Huanyuan Shan³¹⁰¹¹, Lin Nie²⁴, Dezi Liu⁶⁷¹¹, Zhaojun Yan³, Guoliang Li¹⁴⁵,
Cheng Cheng⁸⁹, Yushan Xie³, Han Qu¹⁴⁵, Wenwen Zheng¹⁴⁵, Xi Kang⁵

¹ Purple Mountain Observatory, Chinese Academy of Sciences, No. 10 Yuan Hua Road, Nanjing 210023, China;

² Department of Information Engineering, Wuhan Institute of City, Wuhan, Hubei 430083, China;

³ Shanghai Astronomical Observatory, Nandan Road 80, Shanghai 200030, China;

⁴ National Basic Science Data Center, Building No.2, 4, Zhongguancun South 4th Street, Haidian District, Beijing 190, China;

⁵ Zhejiang University-Purple Mountain Observatory Joint Research Center for Astronomy, Zhejiang University, Hangzhou 327, China;

⁶ South-Western Institute for Astronomy Research, Yunnan University, Kunming, 650500, China;

⁷ The Shanghai Key Lab for Astrophysics, Shanghai Normal University, Shanghai, 200234, China;

⁸ Chinese Academy of Sciences South America Center for Astronomy, National Astronomical Observatories, CAS, Beijing 100101, China;

⁹ CAS Key Laboratory of Optical Astronomy, National Astronomical Observatories, Chinese Academy of Sciences, Beijing 100101, China;

¹⁰ Key Laboratory of Radio Astronomy and Technology, Chinese Academy of Sciences, A20 Datun Road, Chaoyang District, Beijing, 100101, China;

¹¹ University of Chinese Academy of Sciences, Beijing 100049, China

Abstract We have developed a novel method for co-adding multiple under-sampled images that combines the iteratively reweighted least squares and divide-and-conquer algorithms. Our approach not only allows for the anti-aliasing of the images but also enables PSF deconvolution, resulting in enhanced restoration of extended sources, the highest PSNR, and reduced ringing artefacts. To test our method, we conducted numerical simulations that replicated observation runs of the CSST/VST telescope and compared our results to those obtained using previous algorithms. The simulation showed that our method outperforms previous approaches in several ways, such as restoring the profile of extended sources and minimizing ringing artefacts. Additionally, because our method relies on the inherent advantages of least squares fitting, it is more versatile and does not depend on the local uniformity hypothesis for the PSF. However, the new method consumes much more computation than the other approaches.

Key words: Methods: analytical – Techniques: image processing – Gravitational lensing:

Impact of Systematic Redshift Errors on the Cross-correlation of the Lyman- α Forest with Quasars at Small Scales Using DESI Early Data

Abby Bault,^{1,a} David Kirkby,¹ Julien Guy,² Allyson Brodzeller,³ J. Aguilar,² S. Ahlen,⁴ S. Bailey,² D. Brooks,⁵ L. Cabayol-Garcia,⁶ J. Chaves-Montero,⁶ T. Claybaugh,² A. Cuceu,^{7,8,9} K. Dawson,³ R. de la Cruz,¹⁰ A. de la Macorra,¹¹ A. Dey,¹² P. Doel,⁵ S. Filbert,^{3,9} A. Font-Ribera,⁶ J. E. Forero-Romero,^{13,14} E. Gaztañaga,^{15,16,17} S. Gontcho A Gontcho,² C. Gordon,⁶ H. K. Herrera-Alcantar,¹⁰ K. Honscheid,^{7,8,9} V. Irsiĉ,¹⁸ N. G. Karaĉaylı,^{7,8,9,19} R. Kehoe,²⁰ T. Kisner,² A. Kremin,² A. Lambert,² M. Landriau,² L. Le Guillou,²¹ M. E. Levi,² M. Manera,^{6,22} P. Martini,^{7,9,19} A. Meisner,¹² R. Miquel,^{6,23} P. Montero-Camacho,²⁴ J. Moustakas,²⁵ A. Muñoz-Gutiérrez,¹¹ J. Nie,²⁶ G. Niz,^{10,27} N. Palanque-Delabrouille,^{2,28} W. J. Percival,^{29,30,31} I. Pérez-Ràfols,³² C. Poppett,^{2,33,34} F. Prada,³⁵ C. Ramírez-Pérez,⁶ C. Ravoux,^{28,36} M. Rezaie,³⁷ G. Rossi,³⁸ E. Sanchez,³⁹ E. F. Schlafly,⁴⁰ D. Schlegel,² M. Schubnell,^{41,42} J. Silber,² T. Tan,²⁸ G. Tarlé,⁴² M. Walther,^{43,44} B. A. Weaver,¹² Z. Zhou²⁶

¹Department of Physics and Astronomy, University of California, Irvine, 92697, USA

²Lawrence Berkeley National Laboratory, 1 Cyclotron Road, Berkeley, CA 94720, USA

³Department of Physics and Astronomy, The University of Utah, 115 South 1400 East, Salt Lake City, UT 84112, USA

⁴Physics Dept., Boston University, 590 Commonwealth Avenue, Boston, MA 02215, USA

⁵Department of Physics & Astronomy, University College London, Gower Street, London, WC1E 6BT, UK

^aCorresponding author.

³⁰Perimeter Institute for Theoretical Physics, 31 Caroline St. North, Waterloo, ON N2L 2Y5, Canada

³¹Waterloo Centre for Astrophysics, University of Waterloo, 200 University Ave W, Waterloo, ON N2L 3G1, Canada

³²Departament de Física, EEBE, Universitat Politècnica de Catalunya, c/Eduard Maristany 10, 08930 Barcelona, Spain

³³Space Sciences Laboratory, University of California, Berkeley, 7 Gauss Way, Berkeley, CA 94720, USA

³⁴University of California, Berkeley, 110 Sproul Hall #5800 Berkeley, CA 94720, USA

³⁵Instituto de Astrofísica de Andalucía (CSIC), Glorieta de la Astronomía, s/n, E-18008 Granada, Spain

³⁶Aix Marseille Univ, CNRS/IN2P3, CPPM, Marseille, France

³⁷Department of Physics, Kansas State University, 116 Cardwell Hall, Manhattan, KS 66506, USA

³⁸Department of Physics and Astronomy, Sejong University, Seoul, 143-747, Korea

³⁹CIEMAT, Avenida Complutense 40, E-28040 Madrid, Spain

⁴⁰Space Telescope Science Institute, 3700 San Martin Drive, Baltimore, MD 21218, USA

⁴¹Department of Physics, University of Michigan, Ann Arbor, MI 48109, USA

⁴²University of Michigan, Ann Arbor, MI 48109, USA

⁴³Excellence Cluster ORIGINS, Boltzmannstrasse 2, D-85748 Garching, Germany

⁴⁴University Observatory, Faculty of Physics, Ludwig-Maximilians-Universität, Scheinerstr. 1, 81677 München, Germany

E-mail: abault@uci.edu

Abstract. The Dark Energy Spectroscopic Instrument (DESI) will measure millions of quasar spectra by the end of its 5 year survey. Quasar redshift errors impact the shape of the Lyman- α forest correlation functions, which can affect cosmological analyses and therefore cosmological interpretations. Using data from the DESI Early Data Release and the first two months of the main survey, we measure the systematic redshift error from an offset in the cross-correlation of the Lyman- α forest with quasars. We find evidence for a redshift dependent bias causing redshifts to be underestimated with increasing redshift, stemming from improper modeling of the Lyman- α optical depth in the templates used for redshift estimation. New templates were derived for the DESI Year 1 quasar sample at $z > 1.6$ and we found the redshift dependent bias, Δr_{\parallel} , increased from $-1.94 \pm 0.15 h^{-1} \text{ Mpc}$ to $-0.08 \pm 0.04 h^{-1} \text{ Mpc}$ ($-205 \pm 15 \text{ km s}^{-1}$ to $-9.0 \pm 4.0 \text{ km s}^{-1}$). These new templates will be used to provide redshifts for the DESI Year 1 quasar sample.

The fundamental plane of black hole activity for low-luminosity radio active galactic nuclei across $0 < z < 4$

Yijun Wang^{1,2} , Tao Wang^{1,2} , Luis C. Ho^{3,4} , Yuxing Zhong⁵, Bin Luo^{1,2}

¹ School of Astronomy and Space Science, Nanjing University, Nanjing 210093, China
e-mail: wangyijun@nju.edu.cn taowang@nju.edu.cn

² Key Laboratory of Modern Astronomy and Astrophysics (Nanjing University), Ministry of Education, Nanjing 210093, China

³ Kavli Institute for Astronomy and Astrophysics, Peking University, Beijing 100871, China

⁴ Department of Astronomy, School of Physics, Peking University, Beijing 100871, China

⁵ Department of Pure and Applied Physics, Waseda University, 3-4-1 Okubo, Shinjuku, Tokyo 169-8555, Japan

February 29, 2024

ABSTRACT

Context. The fundamental plane of black hole activity describes the correlation between radio luminosity (L_R), X-ray luminosity (L_X), and black hole mass (M_{BH}). It reflects a connection between accretion disc and jet. However, the dependence of the fundamental plane on various physical properties of active galactic nuclei (AGNs) and host galaxies remains unclear, especially for low-luminosity AGNs, which is important for understanding the accretion physics in AGNs.

Aims. Here we explore the dependence of the fundamental plane on radio-loudness, Eddington-ratio (λ_{Edd}), redshift, and galaxy star-formation properties (star forming galaxies and quiescent galaxies) across $0.1 < z \leq 4$ for radio AGNs. Based on current deep and large surveys, our studies can extend to lower luminosities and higher redshifts.

Methods. From the deep and large multi-wavelength surveys in the GOODS-N, GOODS-S, and COSMOS/UltraVISTA fields, we constructed a large and homogeneous radio AGN sample consisting of 208 objects with available estimates for L_R and L_X . Then we divided the radio AGN sample into 141 radio-quiet AGNs and 67 radio-loud AGNs according to the radio-loudness defined by the ratio of L_R to L_X , and explored the dependence of the fundamental plane on different physical properties of the two populations, separately.

Results. The ratio of L_R to L_X shows a bimodal distribution which is well described by two single gaussian models. The cross point between these two gaussian components corresponds to a radio-loudness threshold of $\log(L_R/L_X) = -2.73$. The radio-quiet AGNs have significantly larger Eddington ratio than the radio-loud AGNs. Our radio-quiet and radio-loud AGNs show significantly different fundamental plane which is $\log L_R = (0.55 \pm 0.05) \log L_X + (0.28 \pm 0.06) \log M_{BH} + (13.54 \pm 2.27)$ for the radio-quiet AGNs, and $\log L_R = (0.82 \pm 0.08) \log L_X + (0.07 \pm 0.08) \log M_{BH} + (5.24 \pm 3.33)$ for the radio-loud AGNs. For both radio-quiet and radio-loud AGNs, the fundamental plane does not show a significant dependence on redshift and galaxy star-formation properties, while it shows a significant dependence on λ_{Edd} .

Conclusions. The fundamental plane sheds important light on the accretion physics of central engines. Radio-quiet AGNs at $0.01 < \lambda_{Edd} < 0.1$ are consistent with a combination of advection dominated accretion flow (ADAF) and a synchrotron jet model, while at $0.1 < \lambda_{Edd} < 1$, they mainly follow the synchrotron jet model. Radio-loud AGNs are consistent with a combination of ADAF and the synchrotron jet model at $\lambda_{Edd} < 0.01$, and agree with the synchrotron jet model at $0.01 < \lambda_{Edd} < 0.1$, and follow a combination of the standard thin disc and a jet model at $\lambda_{Edd} > 0.1$.

Key words. galaxies: active – galaxies: general – galaxies: nuclei – radio continuum: galaxies – X-rays: galaxies

1. Introduction

Accreting supermassive black holes (SMBHs), also known as active galactic nuclei (AGNs), emit immense energy across the whole electromagnetic spectrum which are believed to have a great impact on the growth and evolution of host galaxies (Fabian 2012; King & Pounds 2015, for reviews). Thus, AGNs are ideal laboratories to explore both accretion physics around black holes and their connection with host galaxies. Accretion physics around black holes are found to be scale-invariant across black hole mass scale from ~ 10 solar masses of X-ray binaries (XRBs) to $10^6 \sim 10^{10}$ solar masses of SMBHs (Merloni et al. 2003; Falcke et al. 2004; Done & Gierliński 2005; McHardy et al. 2006; Kording 2014; Ruan et al. 2019). One of the most prominent pieces of evidences to support the unification of XRBs and SMBHs is the fundamental plane of black

hole activity (Merloni et al. 2003; Falcke et al. 2004, and references therein) that is characterized by a non-linear empirical relation given by radio luminosity, X-ray luminosity and black hole mass. The radio luminosity is thought to be related with jet activities (Begelman et al. 1984), while the ratio of X-ray luminosity to black hole mass is usually taken as a tracer for accretion rate of disc (Haardt & Maraschi 1991; Liu & Qiao 2022). Thus, the fundamental plane connecting XRBs and SMBHs suggests a similar disc-jet connection across different mass scales (e.g., Merloni et al. 2003; Falcke et al. 2004; Plotkin et al. 2012; Dong et al. 2014). The fundamental plane also provides an approach to estimating black hole mass directly through radio luminosity and X-ray luminosity (e.g., Merloni et al. 2003, and references therein).

However, a growing number of studies focusing only on the fundamental plane of AGNs demonstrate that different types

SDHDF: A new file format for spectral-domain radio astronomy data

Toomey, L. J.^{Ⓜ^a}, Hobbs, G.^{Ⓜ^a}, Price, D. C.^{Ⓜ^b}, Dawson, J. R.^{Ⓜ^{a,c}}, Wenger, T.^{h,l}, Lagoy, D.^h,
 Staveley-Smith, L.^{d,e}, Green, J. A.^{f,j}, Carretti, E.^g, Hafner, A.^a, Huynh, M.^j, Kaczmarek, J.^{Ⓜ^{a,i}},
 Mader, S.ⁱ, McIntyre, V.^a, Reynolds, J.^a, Robishaw, T.^{Ⓜ^h}, Sarkissian, J.ⁱ, Thompson, A.^j,
 Tremblay, C.^{Ⓜ^{j,k}}, Zic, A.^a

^aCSIRO Space & Astronomy, P.O. Box 76, Epping, 1710, NSW, Australia

^bInternational Centre for Radio Astronomy Research, Curtin University, Bentley, 6102, WA, Australia

^cSchool of Mathematical and Physical Sciences and MQ Research Centre in Astronomy, Astrophysics, and
 Astrotechnology, Macquarie University, 2109, NSW, Australia

^dInternational Centre for Radio Astronomy Research (ICRAR), University of Western
 Australia, 6009, WA, Australia

^eARC Centre of Excellence for All Sky Astrophysics in 3 Dimensions (ASTRO 3D), Australia

^fSKA Observatory, SKA-LOW Science Operations Centre, ARRC Building, 26 Dick Perry Avenue, Technology
 Park, Kensington, 6151, WA, Australia

^gINAF, Istituto di Radioastronomia, Via Gobetti 101, Bologna, 40129, Italy

^hDominion Radio Astrophysical Observatory, Herzberg Astronomy and Astrophysics Research Centre, National
 Research Council Canada, PO Box 248, Penticton, BC V2A 6J9, Canada

ⁱCSIRO Space & Astronomy, Parkes Observatory, Parkes, 2870, NSW, Australia

^jCSIRO Space & Astronomy, PO Box 1130, Bentley, 6102, WA, Australia

^kSETI Institute, Mountain View, CA 94043, USA

^lNSF Astronomy & Astrophysics Postdoctoral Fellow, Department of Astronomy, University of
 Wisconsin, Madison, WI 53706, USA

Abstract














Radio astronomy file formats are now required to store wide frequency bandwidths and multiple simultaneous receiver beams and must be able to account for versatile observing modes and numerous calibration strategies. The need to capture and archive high-time and high frequency-resolution data, along with the comprehensive metadata that fully describe the data, implies that a new data format and new processing software are required. This requirement is suited to a well-defined, hierarchically-structured and flexible file format. In this paper we present the Spectral-Domain Hierarchical Data Format (‘SDHDF’) — a new file format for radio astronomy data, in particular for single dish or beam-formed data streams. Since 2018, SDHDF has been the primary format for data products from the spectral-line and continuum observing modes at Murrumbidgee, the CSIRO Parkes 64-m radio telescope, and we demonstrate that this data format can also be used to store observations of pulsars and fast radio bursts.

Keywords: Radio astronomy Astronomy data acquisition

1. INTRODUCTION

With increasing instantaneous bandwidth and higher data volumes output from modern receivers on radio telescopes, such as the Ultra-Wide-Bandwidth Low Frequency (UWL, [1]) receiver, and the

Spatial Distribution of Intracluster Light versus Dark Matter in Horizon Run 5

JAEWON YOO ¹, CHANGBOM PARK ², CRISTIANO G. SABIU ³, ANKIT SINGH ², JONGWAN KO ^{4,5},
JAEHYUN LEE ^{4,2}, CHRISTOPHE PICHON ^{2,6,7}, M. JAMES JEE ^{8,9}, BRAD K. GIBSON ¹⁰, OWAIN SNAITH,¹¹
JUHAN KIM ¹², JIHYE SHIN ⁴, YONGHWI KIM ¹³ AND HYOWON KIM ^{4,5}

¹Quantum Universe Center, Korea Institute for Advanced Study, 85 Hoegi-ro, Dongdaemun-gu, Seoul 02455, Korea

²School of Physics, Korea Institute for Advanced Study, 85 Hoegiro, Dongdaemun-gu, Seoul 02455, Korea

³Natural Science Research Institute (NSRI), University of Seoul, Seoul 02504, Korea

⁴Korea Astronomy and Space Science Institute (KASI), Daedeokdae-ro, Daejeon 34055, Korea

⁵University of Science and Technology (UST), Gajeong-ro, Daejeon 34113, Korea

⁶CNRS and Sorbonne Université, UMR 7095, Institut d'Astrophysique de Paris, 98 bis, Boulevard Arago, F-75014 Paris, France

⁷IPhT, DRF-INP, UMR 3680, CEA, L'Orme des Merisiers, Bât 774, F-91191 Gif-sur-Yvette, France

⁸Department of Astronomy, Yonsei University, 50 Yonsei-ro, Seoul 03722, Korea

⁹Department of Physics, University of California, Davis, One Shields Avenue, Davis, CA 95616, USA

¹⁰Astrophysics Group, Keele University, Keele, Staffordshire, ST5 5BG, UK

¹¹University of Exeter, School of Physics and Astronomy, Stocker Road, Exeter, EX4 4QL, UK

¹²Center for Advanced Computation, Korea Institute for Advanced Study, 85 Hoegiro, Dongdaemun-gu, Seoul 02455, Korea

¹³Korea Institute of Science and Technology Information, 245 Daehak-ro, Yuseong-gu, Daejeon, 34141, Korea

ABSTRACT

One intriguing approach for studying the dynamical evolution of galaxy clusters is to compare the spatial distributions among various components, such as dark matter, member galaxies, gas, and intracluster light (ICL). Utilizing the recently introduced Weighted Overlap Coefficient (WOC) (Yoo et al. 2022), we analyze the spatial distributions of components within 174 galaxy clusters ($M_{\text{tot}} > 5 \times 10^{13} M_{\odot}$, $z = 0.625$) at varying dynamical states in the cosmological hydrodynamical simulation Horizon Run 5. We observe that the distributions of gas and the combination of ICL with the brightest cluster galaxy (BCG) closely resembles the dark matter distribution, particularly in more relaxed clusters, characterized by the half-mass epoch. The similarity in spatial distribution between dark matter and BCG+ICL mimics the changes in the dynamical state of clusters during a major merger. Notably, at redshifts > 1 , BCG+ICL traced dark matter more accurately than the gas. Additionally, we examined the one-dimensional radial profiles of each component, which show that the BCG+ICL is a sensitive component revealing the dynamical state of clusters. We propose a new method that can approximately recover the dark matter profile by scaling the BCG+ICL radial profile. Furthermore, we find a recipe for tracing dark matter in unrelaxed clusters by including the most massive satellite galaxies together with BCG+ICL distribution. Combining the BCG+ICL and the gas distribution enhances the dark matter tracing ability. Our results imply that the BCG+ICL distribution is an effective tracer for the dark matter distribution, and the similarity of spatial distribution may be a useful probe of the dynamical state of a cluster.

Keywords: galaxies: clusters: general — galaxies: halos — (cosmology:) dark matter

1. INTRODUCTION

Galaxy clusters lie at a unique crossroads in the field of astrophysics and cosmology, enabling us to probe the large-scale structure formation and the influences of dark matter and dark energy on the expansion history of the universe

Missing Titanium in the Asymmetric Supernova Remnant W49B

TOSHIKI SATO,¹ MAKOTO SAWADA,² KEIICHI MAEDA,³ JOHN P. HUGHES,⁴ AND BRIAN J. WILLIAMS⁵

¹*Department of Physics, School of Science and Technology, Meiji University, 1-1-1 Higashi Mita, Tama-ku, Kawasaki, Kanagawa 214-8571, Japan*

²*Department of Physics, Rikkyo University, 3-34-1 Nishi-Ikebukuro, Toshima-ku Tokyo 171-8501, Japan*

³*Department of Astronomy, Kyoto University, Kitashirakawa-Oiwake-cho, Sakyo-ku, Kyoto 606-8502 Japan*

⁴*Department of Physics and Astronomy, Rutgers University, 136 Frelinghuysen Road, Piscataway, NJ 08854-8019, USA*

⁵*NASA, Goddard Space Flight Center, 8800 Greenbelt Road, Greenbelt, MD 20771, USA*

ABSTRACT

The progenitor of the W49B supernova remnant is still under debate. One of the candidates is a jet-driven core-collapse supernova. In such a highly asymmetric explosion, a strong α -rich freezeout is expected in local high entropy regions, which should enrich elements synthesized by the capture of α -particles such as ^{44}Ti and ^{48}Cr (decaying to ^{44}Ca and ^{48}Ti , respectively). In the present work, in order to infer the progenitor of the W49B remnant, we constrain the amount of stable Ti (^{48}Ti) synthesized, using the *Suzaku* observation. We found no firm evidence for the Ti line and set the upper limit of $M_{\text{Ti}}/M_{\text{Fe}} < 8.2 \times 10^{-4}$ (99% limit using Xspec) and $M_{\text{Ti}}/M_{\text{Fe}} < 1.9 \times 10^{-3}$ (99% limit using SPEX), and thus excluded almost all hypernova/jet-driven supernova models. Our results, as complemented by some previous studies, suggest that a Type Ia supernova from a near- M_{Ch} (Chandrasekhar mass) white dwarf is the most favorable candidate for the origin of W49B. Future observations with X-ray calorimeter missions, such as XRISM, will give us a stronger constraint on the progenitor.

Keywords: X-ray astronomy — Supernova remnants — ISM: individual objects (W49B) — Nucleosynthesis — Explosive nucleosynthesis

1. INTRODUCTION

W49B is a peculiar supernova remnant (SNR) that exhibits highly asymmetric ejecta distribution (e.g., Lopez et al. 2009, 2011, 2013) and recombining plasma (e.g., Ozawa et al. 2009; Miceli et al. 2010; Yamaguchi et al. 2018; Sun & Chen 2020; Holland-Ashford et al. 2020). While the progenitor of the remnant has been a focus of much attention, a firm conclusion has not yet been reached. The elongated structure of Fe-rich ejecta has been suggested to be related to a bipolar/jet-driven Type Ib/Ic explosion and/or interactions between the shock and a surrounding interstellar cloud (Keohane et al. 2007; Lopez et al. 2013). On the other hand, X-ray spectral studies have argued for the Type Ia supernova origin of W49B from its element abundances (Hwang et al. 2000; Zhou & Vink 2018; Siegel et al. 2020). The main difficulty in inferring the progenitor comes from the lack of emissions below 1 keV due to

strong interstellar absorption ($N_{\text{H}} \sim 5 \times 10^{22} \text{ cm}^{-2}$); without information from O-Ne-Mg-rich ejecta seen in soft X-rays that can characterize a massive progenitor for a core-collapse SN, it is difficult to distinguish from one progenitor scenario to another, since the abundance pattern from Si to Fe is strongly dependent on explosive nucleosynthesis.

W49B is also known as the remnant with the brightest Fe-K α line in the Galaxy (Yamaguchi et al. 2014), providing a unique opportunity to test the explosive nucleosynthesis around Fe-group elements. The Fe-group elements are mainly synthesized by Si burning around the core of exploding stars. This allows us to investigate the differences in the central environment of core-collapse supernovae and Type Ia supernovae (e.g., Woosley et al. 1973). In particular, asymmetric/energetic explosions of massive stars are believed to produce a large amount of ^{44}Ti , since the stronger α -rich freeze-out could occur in the region where the larger energy is deposited (Nagataki et al. 1998; Nakamura et al. 2001; Maeda & Nomoto 2003).



UNIVERSITY OF TABRIZ

FACULTY OF PHYSICS

DEPARTMENT OF THEORETICAL PHYSICS AND ASTROPHYSICS

DOCTORAL DISSERTATION

Exoplanets Prediction in Multi-Planetary Systems and Determining the Correlation Between the Parameters of Planets and Host Stars Using Artificial Intelligence

Author:

Mahdiyar MOUSAVI-SADR

Supervisors:

Prof. Davood M. JASSUR

Dr. Ghassem GOZALIASL

A thesis submitted in fulfillment of the requirements

for the degree of Doctor of Philosophy

in the

Astronomy and Astrophysics

February 2024

iii

"Our posturings, our imagined self-importance, the delusion that we have some privileged position in the Universe, are challenged by this point of pale light. Our planet is a lonely speck in the great enveloping cosmic dark."

Carl Sagan



The Pale Blue Dot: This is a photograph of Earth taken in 1990 by the Voyager 1 at a distance of 6 billion kilometers from the Sun.

Interacting galaxies in the IllustrisTNG simulations - VI: Reconstructed orbits, close encounters and mergers

David R. Patton,¹★ Lawrence Faria,^{1,2} Maan H. Hani,³ Paul Torrey,⁴ Sara L. Ellison,³ Shivani D. Thakur,¹ and Raven I. Westlake¹

¹*Department of Physics and Astronomy, Trent University, 1600 West Bank Drive, Peterborough, ON, K9L 0G2, Canada*

²*Department of Physics, Engineering Physics and Astronomy, Queen's University, Kingston, ON, K7L 3N6, Canada*

³*Department of Physics and Astronomy, University of Victoria, Finnerty Road, Victoria, BC, V8P 1A1, Canada*

⁴*Department of Astronomy, University of Virginia, 530 McCormick Road, Charlottesville, VA 22903, USA*

29 February 2024

ABSTRACT

Cosmological simulations have been used to study interacting galaxies as a function of galaxy pair separation, enabling comparisons with observational studies of galaxy pairs. The study of interacting galaxies as a function of time (i.e. merger stage) has mostly been limited to high resolution merger simulations, due to the poor time sampling available in cosmological simulations. Building on an earlier study of galaxy pairs in the IllustrisTNG cosmological simulations, we reconstruct the orbits of galaxy pairs involving massive galaxies ($M_* > 10^{10} M_\odot$) at redshifts of $0 \leq z < 1$, using a novel kinematic interpolation scheme to model the orbits in between the IllustrisTNG snapshots (which are separated by 162 Myr on average). We assess the accuracy of these interpolations using a pre-existing suite of merger simulations, and find that kinematic interpolations provide a remarkable improvement in accuracy compared with interpolations that use only radial separations or 3D positions. We find that nearly 90 per cent of the closest pairs ($r < 25$ kpc) have had a pericentre encounter within the past Gyr. Many of these close pairs are found on rapidly shrinking orbits, and roughly 85 per cent of these pairs will merge within 1 Gyr. However, approximately 3 per cent of these close pairs appear to be flyby systems that will never merge. These reconstructed orbits will be used in future studies to investigate how and when galaxy properties change during close encounters and mergers between galaxies in IllustrisTNG.

Key words:

galaxies: interactions – galaxies: evolution – galaxies: kinematics and dynamics

1 INTRODUCTION

Early studies of galaxy properties showed that strongly interacting galaxies have morphologies, colours and star formation rates that are significantly different from those of relatively isolated galaxies (Arp 1966; Toomre & Toomre 1972; Larson & Tinsley 1978; Kennicutt et al. 1987). Large statistical studies of galaxy pairs have subsequently shown clear correlations between pair separation and numerous galaxy properties, suggesting that the degree to which galaxy properties are perturbed may be closely tied to the proximity of the encounters. For example, the star formation rates of galaxies in close pairs (with typical projected separations less than about 30 kpc) are found to be enhanced by a factor of roughly 2-3 with respect to relatively isolated galaxies (Ellison et al. 2008; Scudder et al. 2012; Barrera-Ballesteros et al. 2015; Stierwalt et al. 2015; Pan et al. 2018; Garduño et al. 2021; Steffen et al. 2021; Shah et al. 2022), with smaller enhancements extending out to separations of about 150 kpc (Patton et al. 2013, 2020; Brown et al. 2023). Galaxies in close pairs have also been found to have lower gas-phase metallicities (Ellison et

al. 2008; Rupke, Kewley, & Chien 2010; Scudder et al. 2012; Bustamante et al. 2020; Garduño et al. 2021), higher asymmetries (Patton et al. 2005; De Propriis et al. 2007; Casteels et al. 2014; Patton et al. 2016), and higher active galactic nuclei (AGN) fractions (Ellison et al. 2011, 2013; Silverman et al. 2011; Satyapal et al. 2014; Ellison et al. 2019; Steffen et al. 2023; Bickley et al. 2024) than matched control samples of galaxies without close companions. All of these differences have been shown to diminish and then disappear at larger pair separations.

Simulations of merging galaxies have been used to interpret correlations between galaxy properties and pair separation, in attempts to identify the physical mechanisms by which these perturbed galaxy properties may arise. In general, these correlations can be explained by a model in which gravitational and hydrodynamical interactions trigger morphological disturbances and cause the infall of gas into the central regions of galaxies, leading to a dilution of gas-phase metallicity, enhanced star formation, and elevated accretion of gas on the central supermassive black hole (Mihos & Hernquist 1996; Di Matteo, Springel, & Hernquist 2005; Hopkins et al. 2008; Torrey et al. 2012; Renaud et al. 2014; Moreno et al. 2019). These simulations allow researchers to track changes in galaxy properties as a function

★ E-mail: dpatton@trentu.ca

Outshining in the Spatially Resolved Analysis of a Strongly-Lensed Galaxy at $z = 6.072$ with *JWST* NIRC*am*

C. Giménez-Arteaga^{1,2}, S. Fujimoto³, F. Valentino^{4,1}, G. B. Brammer^{1,2}, C. A. Mason^{1,2}, F. Rizzo^{1,2}, V. Rusakov^{1,2}, L. Colina⁵, G. Prieto-Lyon^{1,2}, P. A. Oesch^{1,2,6}, D. Espada^{7,8}, K. E. Heintz^{1,2}, K. K. Knudsen⁹, M. Dessauges-Zavadsky⁶, N. Laporte^{10,11}, M. Lee^{1,12}, G. E. Magdis^{1,2,12}, Y. Ono¹³, Y. Ao^{14,15}, M. Ouchi^{13,16,17,18}, K. Kohno^{19,20}, A. M. Koekemoer²¹

(Affiliations can be found after the references)

February 29, 2024

ABSTRACT

We present *JWST*/NIRC*am* observations of a strongly-lensed, sub- L^* , multiply-imaged galaxy at $z = 6.072$, with magnification factors $\mu \gtrsim 20$ across the galaxy. The galaxy has rich *HST*, *MUSE* and *ALMA* ancillary observations across a broad wavelength range. Aiming to quantify the reliability of stellar mass estimates of high redshift galaxies, we perform a spatially-resolved analysis of the physical properties at scales of ~ 200 pc, inferred from SED modelling of 5 *JWST*/NIRC*am* imaging bands covering $0.16 \mu\text{m} < \lambda_{\text{rest}} < 0.63 \mu\text{m}$ on a pixel-by-pixel basis. We find young stars surrounded by extended older stellar populations. By comparing $\text{H}\alpha$ + $[\text{N II}]$ and $[\text{O III}]$ + $\text{H}\beta$ maps inferred from the image analysis with our additional NIRS*pec* IFU data, we find that the spatial distribution and strength of the line maps are in agreement with the IFU measurements. We explore different parametric star formation history forms with BAGPIPES on the spatially-integrated photometry, finding that a double power-law star formation history retrieves the closest value to the spatially-resolved stellar mass estimate, and other SFH forms suffer from the dominant outshining emission from the youngest stars, thus underestimating the stellar mass – up to ~ 0.5 dex-. On the other hand, the DPL cannot match the IFU measured emission lines. Additionally, the ionizing photon production efficiency may be overestimated in a spatially-integrated approach by ~ 0.15 dex, when compared to a spatially-resolved analysis. The agreement with the IFU measurements implies that our pixel-by-pixel results derived from the broadband images are robust, and that the mass discrepancies we find with spatially-integrated estimates are not just an effect of SED-fitting degeneracies or lack of NIRC*am* coverage. Additionally, this agreement points towards the pixel-by-pixel approach as a way to mitigate the general degeneracy between the flux excess from emission lines and underlying continuum, especially when lacking photometric medium-band coverage and/or IFU observations. This study stresses the importance of studying galaxies as the complex systems that they are, resolving their stellar populations when possible, or using more flexible SFH parameterisations. This can aid our understanding of the early stages of galaxy evolution by addressing the challenge of inferring robust stellar masses and ionizing photon production efficiencies of high redshift galaxies.

Key words. extragalactic astronomy – high-redshift galaxies – star forming regions – gravitational lensing

1. Introduction

One of the most critical problems in the study of high-redshift galaxies is the challenge of inferring robust stellar masses. Recent spatially-unresolved works using the first data obtained with *JWST* have found surprisingly large stellar masses, which may be in conflict with the early growth of structure within the Λ CDM cosmological model (Labbé et al. 2023; Xiao et al. 2023). Various studies have found that varying the star formation history (SFH) parameterisation, or other assumptions such as the initial mass function (IMF), can have a significant impact in the inferred physical properties, potentially solving this conflict (see e.g., Suess et al. 2022; Whittle et al. 2023; Tacchella et al. 2023; Pacifici et al. 2023; Steinhardt et al. 2023; Endsley et al. 2023; Wang et al. 2023; Woodrum et al. 2023).

The superb spatial resolution and sensitivity of the Near-Infrared Camera (NIRC*am*; Rieke et al. 2005, 2023) onboard *JWST*, allows us to extend spatially-resolved studies to high redshifts. Previous analyses have suggested that stellar mass estimates in spatially-integrated studies could be significantly underestimated, emphasising the tension with predictions from theoretical models. This has so far been addressed at lower redshifts ($z < 2.5$), such as the work by Sorba & Sawicki (2018) on a statistically significant sample of ~ 1200 galaxies, finding that

resolved stellar masses can be up to five times larger than unresolved estimates. This effect has also been recently observed at high redshift ($5 < z < 9$), albeit on a limited sample of five galaxies in the SMACS0723 ERO field (Giménez-Arteaga et al. 2023).

When resolving extended galaxies and studying their stellar populations on a pixel-by-pixel basis, one can partially disentangle the problem of *outshining* (Sawicki & Yee 1998; Papovich et al. 2001; Shapley et al. 2001; Trager et al. 2008; Graves & Faber 2010; Maraston et al. 2010; Pforr et al. 2013; Sorba & Sawicki 2015), where young stellar populations (< 10 Myr) completely dominate the integrated light, hiding underlying older stellar populations ($\gtrsim 100$ Myr), thus leading to an underestimation of the total mass of the stellar population. This is particularly a problem when the coverage is limited to the UV-optical range (e.g., Paulino-Afonso et al. 2022), with redder wavelengths mitigating this effect (e.g., Zibetti et al. 2009; Bisigello et al. 2019). Outshining has also been studied in simulations (see e.g., Narayanan et al. 2023). Given the frequent degeneracy encountered between age and dust obscuration, similar stellar mass biases can be found due to dust reddening variations within a source (e.g., Smail et al. 2023).

New Insight Concerning Primordial Lithium Production

Tahani Makki^{1*}, Mounib El Eid² and Grant Mathews³

^{1*}Department of Physics, American University of Beirut (Alumna), Bliss street, Beirut, Lebanon.

²Department of Physics, American University of Beirut (emiritus), Bliss street, Beirut, Lebanon.

³Department of Physics, Center for Astrophysics, University of Notre Dame, Notre Dame, South Bend, 46556, Indiana, USA.

*Corresponding author(s). E-mail(s): trm03@mail.aub.edu;
Contributing authors: meid@aub.edu.lb; gmathews@nd.edu;

Abstract

To constrain the universe before recombination (380000 years after the Big Bang), we mostly rely on the measurements of the primordial abundances that indicate the first insight into the thermal history of the universe. The first production of elements is obtained by the Big Bang Nucleosynthesis (BBN). The production of the elements (D, ³He, ⁴He) during the BBN matches well the observations; however, the production of lithium (⁷Li) based on the Standard Big Bang Nucleosynthesis (SBBN) is found to be higher by about a factor of three than the observed abundance from metal-poor halo stars. This so-called "Cosmological Lithium Problem" is still elusive and needs to be resolved. One important attempt to get more insight into this problem is to invoke a non-standard description of the SBBN to decrease the lithium abundance. In our previous work, we encountered a problem that the decrease in the ⁷Li abundance requires an increase in the deuterium abundance to maximum values that are not accepted by observations. In the present work, a decrease in the lithium abundance could be achieved without maximizing the deuterium abundance by modifying the time-temperature relation in the range $(4.3 - 9.1) \times 10^8$ K during the nucleosynthesis process. This range is crucial to reduce the strong correlation between lithium and deuterium production. The main conclusion of the present work is that ⁷Li abundance in the atmospheres of metal-poor stars cannot be analyzed without considering possible modification of the primordial nucleosynthesis.

Status and plans for the instrumentation of the IceCube Surface Array Enhancement

The IceCube Collaboration

(a complete list of authors can be found at the end of the proceedings)

E-mail: shefali.shefali@kit.edu, frank.schroeder@kit.edu

The surface array of IceCube, IceTop, operates primarily as a cosmic-ray detector, as well as a veto for astrophysical neutrino searches for the IceCube in-ice instrumentation. However, the snow accumulation on top of the IceTop detectors increases the detection threshold and attenuates the measured IceTop signals. Enhancing IceTop by a hybrid array of scintillation detectors and radio antennas will lower the energy threshold for air-shower measurements, provide more efficient veto capabilities, enable more accurate cosmic-ray measurements, and improve the detector calibration by compensating for snow accumulation. After the initial commissioning period, a prototype station at the South Pole has been recording air-shower data and has successfully observed coincident events of both the scintillation detectors and the radio antennas with the IceTop array. The production and calibration of the detectors for the full planned array has been ongoing. Additionally, one station each has been installed at the Pierre Auger Observatory and the Telescope Array for further R&D of these detectors in different environmental conditions. This contribution will present the status and future plans of the hybrid detector stations for the IceCube Surface Array Enhancement.

Corresponding authors: S. Shefali^{1*}, Frank G. Schroeder^{2,3}

¹ *Institute of Experimental Particle Physics, Karlsruhe Institute of Technology (KIT), Germany*

² *Institute for Astroparticle Physics, Karlsruhe Institute of Technology (KIT), Germany*

³ *Bartol Research Institute and Dept. of Physics and Astronomy, University of Delaware, USA*

* Presenter

The 38th International Cosmic Ray Conference (ICRC2023)
26 July – 3 August, 2023
Nagoya, Japan



© Copyright owned by the author(s) under the terms of the Creative Commons Attribution-NonCommercial-NoDerivatives 4.0 International License (CC BY-NC-ND 4.0).

<https://pos.sissa.it/>

Surface Array Enhancement: IceCube

1. Introduction

IceTop [1], the surface array of the IceCube Neutrino Observatory [2], is a unique cosmic-ray detector, which contributes significantly to the veto against the atmospheric background for the In-Ice detector. It consists of 81 pairs of Ice-Cherenkov tanks, placed on the surface of the antarctic ice covering an area of 1 km². The complementary information from the surface and the In-Ice detector allows for a range of cosmic ray studies, including mass composition, energy spectra, muon density [3] [4] etc., in the energy range of 250 TeV to EeV. Since their deployment, non-uniform snow accumulation on the IceTop tanks has resulted in an increase in the detection threshold, due to attenuation in the IceTop signals. To lower this threshold, and develop a multi-component cosmic-ray detection infrastructure, an enhancement of the surface array has been proposed [5].

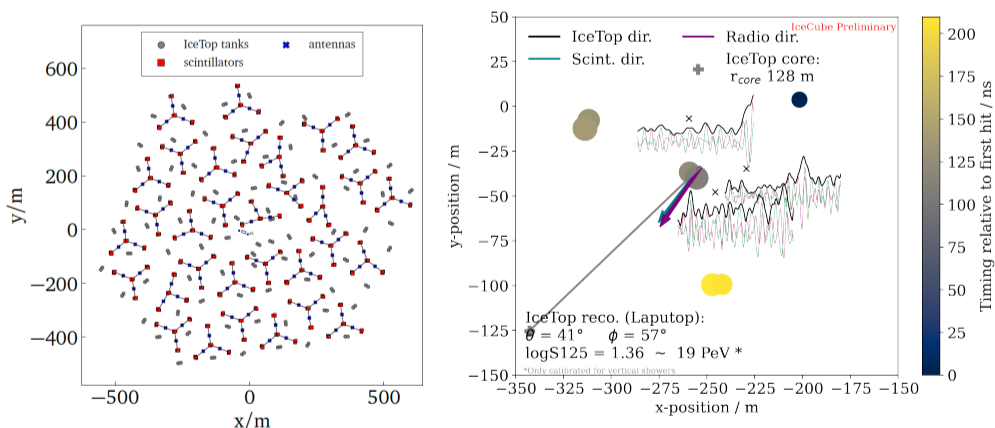


Figure 1: Left: The planned Surface Array Enhancement within the IceTop footprint; Right: An example event with 3-fold coincidence observed by IceTop, scintillation and radio detectors.

The enhancement is planned as a hybrid detector array, consisting of 32 stations within the footprint of IceTop (Fig. 1 (left)). Each station will comprise 8 scintillation detectors, 3 radio detectors and a central fieldhub data acquisition (DAQ) system. Following the intermediate R&D deployments, a fully functional prototype station was operational at the South Pole from January 2020 to December 2022. With the air-shower measurements from the prototype station alone, 3-fold coincident events with the IceTop array were already reconstructed [6]. An example of such an event is presented in Fig. 1 (right). Events coincidentally observed within 2 μ s by all 3 detectors are considered to be a single coincident event. The timestamp of the first scintillation detector hit is taken as the reference time for the coincidence for the scintillator channel, while for the radio detection their trigger time is used. For the IceTop data the timestamp corresponds to when the shower is expected to hit the surface.

Efforts to significantly improve the isolation of the radio emission of the air showers from that of the Galactic and extragalactic background noise, using machine learning methods called convolution neural networks, are ongoing [7]. A successful implementation on a 2 month data set from the prototype station has been achieved. The method is able to successfully distinguish and denoise the air-shower signals, and is found to be in agreement with the traditional IceTop reconstruction. Furthermore, the X_{\max} analysis of the air showers, which can be used to facilitate mass composition studies, using this data set is also in progress. Preliminary results can be found in [8].

A possible relation between global CO excitation and massive molecular outflows in local ULIRGs

I. Montoya Arroyave¹, C. Cicone¹, P. Andreani², A. Weiss³, C. De Breuck², A. Lundgren^{4,2}, P. Severgnini⁵, B. Hagedorn¹, Rubinur K.¹, B. Baumschlager¹, and E. Makroleivaditi^{3,6}

¹ Institute of Theoretical Astrophysics, University of Oslo, P.O. Box 1029, Blindern, 0315 Oslo, Norway
e-mail: isabemo@uio.no

² European Southern Observatory, Karl-Schwarzschild-Strasse 2, 85748 Garching, Germany

³ Max-Planck-Institut für Radioastronomie, Auf dem Hügel 69, D-53121 Bonn, Germany

⁴ Aix Marseille Université, CNRS, LAM, Marseille, F-13388, France

⁵ INAF - Osservatorio Astronomico di Brera, Via Brera 28, I-20121 Milano, Italy

⁶ Rheinische Friedrich-Wilhelms-Universität Bonn, Regina-Pacis-Weg 3, 53113 Bonn, Germany

Received 2023-10-17; Accepted 2024-02-22

ABSTRACT

Local ultra-luminous infrared galaxies (ULIRGs) have been observed to host ubiquitous molecular outflows, including the most massive and powerful ever detected. These sources have also exceptionally excited global, galaxy-integrated CO ladders. A connection between outflows and molecular gas excitation has however never been established, since previous multi- J CO surveys were limited in spectral resolution and sensitivity and so could only probe the global molecular gas conditions. In this work, we address this question using new, ground-based, sensitive heterodyne spectroscopy of multiple CO rotational lines (up to CO(7–6)) in a sample of 17 local ULIRGs. We used the Atacama Pathfinder Experiment (APEX) telescope to survey the CO($J_{\text{up}} \geq 4$) lines at a high signal-to-noise ratio, and complemented these data with CO($J_{\text{up}} \leq 3$) APEX and Atacama Large Millimeter Array (ALMA and ACA) observations presented in Montoya Arroyave et al. (2023). We detected a total of 74 (out of 75) CO lines, with up to six transitions per source. The resulting CO spectral line energy distributions (SLEDs) show a wide range in gas excitation, in agreement with previous studies on ULIRGs. Some CO SLEDs peak at $J_{\text{up}} \sim 3, 4$, which we classify as ‘lower excitation’, while others plateau or keep increasing up to the highest- J CO transition probed, and we classify these as ‘higher excitation’. Our analysis includes for completeness the results of CO SLED fits performed with a single large velocity gradient component, but our main focus is the investigation of possible links between global CO excitation and the presence of broad and/or high-velocity CO spectral components that can contain outflowing gas. We discovered an increasing trend of line width as a function of J_{up} of the CO transition, which is significant at the 4σ level and appears to be driven by the eight sources that we classified as ‘higher excitation’. We further analysed such higher-excitation ULIRGs, by performing a decomposition of their CO spectral profiles into multiple components, and derived CO ladders that are clearly more excited for the spectral components characterised by higher velocities and/or velocity dispersion. Because these sources are known to host widespread molecular outflows, we favour an interpretation whereby the highly excited CO-emitting gas in ULIRGs resides in galactic-scale massive molecular outflows whose emission fills a large fraction of the beam of our APEX high- J CO observations. On the other hands, our results challenge alternative scenarios for which the high CO excitation in ULIRGs can be explained by classical component of the ISM, such as photon- or X-ray dominated regions around the nuclear sources.

Key words.

1. Introduction

In the local universe ($z \leq 0.2$), most (ultra) luminous infrared galaxies ((U)LIRGs), defined by their high infrared luminosities ($L_{\text{IR}}(8 - 1000\mu\text{m}) \geq 10^{11}L_{\odot}$), correspond to galaxy mergers that can trigger accelerated star formation (starbursts, SBs) or accretion of matter onto the supermassive black hole (SMBH) in the center of the galaxy (active galactic nuclei, AGN) (Sanders & Mirabel 1996; Genzel et al. 1998; Lonsdale et al. 2006; Pérez-Torres et al. 2021; U 2022). The stellar and AGN feedback in these sources generate the most powerful galactic outflows known, which can embed gas in different phases and affect the host galaxy from scales of a few parsecs in the interstellar medium (ISM) to several tens of kiloparsecs out to the circumgalactic medium (CGM) (Cicone et al. 2015).

The molecular gas phase of the ISM is the raw material from which stars form, and so constraining its physical prop-

erties in different gas environments, and in particular diffuse and extended outflowing gas, is important to understand the evolution of galaxies. Being rich in dense gas and dust, (U)LIRGs are ideal targets for (sub)millimeter observations of the molecular gas phase. Indeed, in the past decade, thanks to *Herschel* and ground-based sub-mm observatories, massive molecular (H_2) outflows have been detected in the majority of local (U)LIRGs (see Veilleux et al. (2020) for a review). In the recent years, observations of different gas tracers, such as CO, HCN, HCO+ (among others) of these sources have also allowed to study the implications of galactic outflows in the galaxy evolution scheme. Galactic outflows may be the culprits of either removing large fractions of gas from the host galaxy, and hence decrease the star formation rate (SFR; negative feedback; e.g., Di Matteo et al. 2005; Tumlinson et al. 2017), or compressing the available gas, resulting in increased SFR (positive feedback; e.g., Maiolino et al. 2017; Gallagher et al. 2019). Despite extensive theoretic-

The cold interstellar medium of a normal sub- L^* galaxy at the end of reionization

F. Valentino^{1,2}, S. Fujimoto³, C. Giménez-Arteaga^{2,4}, G. Brammer^{2,4}, K. Kohno^{5,6}, F. Sun⁷, V. Kokorev⁸, F. E. Bauer^{9,10,11,12}, C. Di Cesare^{13,14,15}, D. Espada^{16,17}, M. Lee^{2,18}, M. Dessauges-Zavadsky¹⁹, Y. Ao^{20,21}, A. M. Koekemoer²², M. Ouchi^{23,24,25}, J. F. Wu^{22,26}, E. Egami⁷, J.-B. Jolly²⁷, C. del P. Lagos^{28,29,2}, G. E. Magdis^{2,4,18}, D. Schaerer¹⁹, K. Shimasaku^{5,6}, H. Umehata^{30,31,32}, W.-H. Wang³³

(Affiliations can be found after the references)

Received –; accepted –

ABSTRACT

We present the results of a ~60-hour multiband observational campaign with the Atacama Large Millimeter Array targeting a spectroscopically confirmed and lensed sub- L^* galaxy at $z = 6.07$, first identified during the ALMA Lensing Cluster Survey (ALCS). We sampled the dust continuum emission from rest frame 90 to 370 μm at six different frequencies and set constraining upper limits on the molecular gas line emission and content by targeting the CO (7 – 6) and [C I] ($^3P_2 - ^3P_1$) transitions in two lensed images with $\mu \gtrsim 20$. Complementing these submillimeter observations with deep optical and near-IR photometry and spectroscopy with JWST, we find this galaxy to form stars at a rate of $\text{SFR} \sim 7 M_\odot \text{ yr}^{-1}$, ~50–70% of which is obscured by dust. This is consistent with what one would predict for a $M_\star \sim 7.5 \times 10^8 M_\odot$ object by extrapolating the relation between the fraction of the obscured star formation rate and stellar mass at $z < 2.5$ and with observations of IR-detected objects at $5 < z < 7$. The light-weighted dust temperature of $T_{\text{dust}} \sim 50 \text{ K}$ is similar to that of more massive galaxies at similar redshifts, although with large uncertainties and with possible negative gradients. We measure a dust mass of $M_{\text{dust}} \sim 1.5 \times 10^6 M_\odot$ and, by combining [C I], [C II], and a dynamical estimate, a gas mass of $M_{\text{gas}} \sim 2 \times 10^9 M_\odot$. Their ratio (δ_{DGR}) is in good agreement with predictions from models and empirical relations in the literature. The dust-to-stellar mass fraction of $f_{\text{dust}} \sim 0.002$ and the young stellar age (100 – 200 Myr) are consistent with efficient dust production via supernovae, as predicted by existing models and simulations of dust evolution. Also, the expected number density of galaxies with $M_{\text{dust}} \sim 10^6 M_\odot$ at $z = 6$ from a subset of these models is in agreement with the observational estimate that we set from the parent ALCS survey. The combination of gravitational lensing and deep multiwavelength observations allowed us to probe luminosity and mass regimes up to two orders of magnitude lower than what has been explored so far for field galaxies at similar redshifts. Our results serve as a benchmark for future observational endeavors of the high-redshift and faint sub- L^* galaxy population that might have driven the reionization of the Universe.

Key words. Galaxies: high-redshift, ISM, star formation, formation, evolution; Gravitational lensing: strong

1. Introduction

Over the past few years, the number of galaxies confirmed at redshift $z > 6$ and deeper into the reionization epoch has soared. Interferometric (sub)millimeter observations and ground-based and, more recently, space-based optical and near-IR spectroscopy have been instrumental in allowing us to start exploring the physics regulating the growth of the first galaxies. Truly multiwavelength studies proved to be necessary to observe and connect all components in galaxies and provide a complete view of these systems. However, for reasons of opportunity and observing time cost, priority has been given to the brightest and rarest targets that could maximize the detection rates – but in doing so we have been missing more numerous, typical galaxy populations at $z > 6$.

In light of the possible preponderant role played by average, rather than exceptional, galaxy populations in the reionization of the Universe (Robertson 2022), there has been a renewed focus on spectroscopic studies of faint sources around or below the knee of the luminosity function (L^*) and on the main sequence of star formation (Daddi et al. 2007) at these redshifts, particularly after the launch of the *James Webb* Space Telescope (JWST). Moreover, observational campaigns of faint objects are even more affordable when the Universe comes to our aid with the gravitational lensing effect. This phenomenon provides a

unique window onto the formation of faint galaxies on small scales, which would otherwise be impossible to probe without the presence of massive objects along the line of sight.

Here we attempt to push the existing boundaries for deep multiwavelength extragalactic studies at high redshifts by leveraging state-of-the-art instruments and the lensing effect. Our primary objective is to start exploring a new portion of the cold gas and dust parameter space at intrinsic low stellar masses, star formation rates (SFRs), and metallicities. These regimes are critical to understanding the first phases of galaxy formation. The availability of cold gas reservoirs and the impact of intense, hard radiation feedback from young stars with low metallicities ultimately regulate the growth of the numerous population of low-mass galaxies and their ability to reionize the Universe. Furthermore, these processes are intricately linked to the rate at which metals and dust accumulate, and the relationship between these two components in the earliest phases of galaxy assembly remains itself a debated topic (see, e.g., Péroux & Howk 2020; Popping et al. 2023; Heintz et al. 2023a; Konstantopoulou et al. 2024; Schneider & Maiolino 2023, for a few recent examples). Fortunately, both dust and metals can now be traced in early galaxies. Thanks to JWST, we can directly measure the metallicity of large samples of very distant sources (e.g., Curti et al. 2023). In contrast, over the past few years, observations with the Atacama Large Millimeter Array (ALMA) have

Unveiling [C II] clumps in a lensed star-forming galaxy at $z \sim 3.4$

A. Zanella¹, E. Iani², M. Dessauges-Zavadsky³, J. Richard⁴, C. De Breuck⁵, J. Vernet⁵, M. Kohandel⁶, F. Arrigoni Battaia⁷, A. Bolamperti^{8, 1, 5}, F. Calara⁹, C.-C. Chen¹⁰, T. Devereaux⁸, A. Ferrara⁶, V. Mainieri⁵, A. Pallottini⁶, G. Rodighiero⁸, L. Vallini⁹, and E. Vanzella⁹

¹ Istituto Nazionale di Astrofisica (INAF), Vicolo dell'Osservatorio 5, I-35122 Padova, Italy
e-mail: anita.zanella@inaf.it

² Kapteyn Astronomical Institute, University of Groningen, NL-9700 AV Groningen, the Netherlands

³ Département d'Astronomie, Université de Genève, Chemin Pegasi 51, CH-1290 Versoix, Switzerland

⁴ Univ. Lyon, Univ. Lyon1, ENS de Lyon, CNRS, Centre de Recherche Astrophysique de Lyon UMR5574, 69230, Saint-Genis-Laval, France

⁵ European Southern Observatory, Karl Schwarzschild Strasse 2, 85748, Garching, Germany

⁶ Scuola Normale Superiore, Piazza dei Cavalieri 7, 56126 Pisa, Italy

⁷ Max-Planck-Institut für Astrophysik, Karl-Schwarzschild-Str 1, 85748, Garching bei München, Germany

⁸ Dipartimento di Fisica e Astronomia, Università degli Studi di Padova, Vicolo dell'Osservatorio 3, I-35122 Padova, Italy

⁹ INAF - Osservatorio Astronomico di Bologna, Via Gobetti 93/3, I-40129 Bologna, Italy

¹⁰ Academia Sinica Institute of Astronomy and Astrophysics (ASIAA), No. 1, Sec. 4, Roosevelt Road, Taipei 10617, Taiwan

Received XXX; accepted XXX

ABSTRACT

Context. Observations at UV and optical wavelengths have revealed that galaxies at $z \sim 1 - 4$ host star-forming regions, dubbed “clumps,” which are believed to form due to the fragmentation of gravitationally unstable, gas-rich disks. However, the detection of the parent molecular clouds that give birth to such clumps is still possible only in a minority of galaxies, mostly at $z \sim 1$.

Aims. We investigated the [C II] and dust morphology of a $z \sim 3.4$ lensed galaxy hosting four clumps detected in the UV continuum. We aimed to observe the [C II] emission of individual clumps that, unlike the UV, is not affected by dust extinction, to probe their nature and cold gas content.

Methods. We conducted ALMA observations probing scales down to ~ 300 pc and detected three [C II] clumps. One (dubbed “NE”) coincides with the brightest UV clump, while the other two (“SW” and “C”) are not detected in the UV continuum. We do not detect the dust continuum.

Results. We converted the [C II] luminosity of individual clumps into molecular gas mass and found $M_{\text{mol}} \sim 10^8 M_{\odot}$. By complementing it with the star formation rate (SFR) estimate from the UV continuum, we estimated the gas depletion time (t_{dep}) of clumps and investigated their location in the Schmidt-Kennicutt plane. While the NE clump has a very short $t_{\text{dep}} = 0.16$ Gyr, which is comparable with high-redshift starbursts, the SW and C clumps instead have longer $t_{\text{dep}} > 0.65$ Gyr and are likely probing the initial phases of star formation. The lack of dust continuum detection is consistent with the blue UV continuum slope estimated for this galaxy ($\beta \sim -2.5$) and it indicates that dust inhomogeneities do not significantly affect the detection of UV clumps in this target.

Conclusions. We pushed the observation of the cold gas content of individual clumps up to $z \sim 3.4$ and showed that the [C II] line emission is a promising tracer of molecular clouds at high redshift, allowing the detection of clumps with a large range of depletion times.

Key words. galaxies: high-redshift – galaxies: ISM – galaxies: structure – galaxies: formation – galaxies: evolution

1. Introduction

In the last decades, rest-frame ultraviolet (UV) and optical observations have shown that star-forming galaxies at redshift $z \sim 1 - 4$ have irregular morphologies (e.g., Conselice et al. 2004; Conselice 2014; Shibuya et al. 2016; Huertas-Company et al. 2023), dominated by active sites of star formation, dubbed “clumps” (e.g., Elmegreen & Elmegreen 2005; Elmegreen et al. 2008; Förster Schreiber et al. 2011; Guo et al. 2015; Zanella et al. 2015). Spatially resolved observations taken with ground-based adaptive optics facilities (e.g., SINFONI on the Very Large Telescope, VLT), the *Hubble* Space Telescope (*HST*), and more recently the *James Webb* Space Telescope (*JWST*), revealed that clumps typically have stellar masses $M_{\star} \sim 10^7 - 10^9 M_{\odot}$, star formation rates (SFRs) $\sim 0.1 - 10 M_{\odot} \text{yr}^{-1}$, and mostly unresolved sizes

< 1 kpc (e.g., Förster Schreiber et al. 2011; Guo et al. 2018; Zanella et al. 2019; Kalita et al. 2023). By combining the angular resolution of state-of-the-art telescopes with strong lensing, it has been possible to study clumps in the low-mass and low-SFR regime (Livermore et al. 2015; Vanzella et al. 2017a,b; Cava et al. 2018; Vanzella et al. 2021). Such studies have revealed that when magnification (and hence spatial resolution and sensitivity) increases, clumps with smaller sizes are uncovered (Vanzella et al. 2022; Meštrić et al. 2022; Claeysens et al. 2023; Messa et al. 2022). In particular, clumps in lensed galaxies have effective radii $R_{\text{e}} \sim 10 - 100$ pc, stellar masses $M_{\star} \sim 10^6 - 10^8 M_{\odot}$, and SFRs $\sim 0.01 - 10 M_{\odot} \text{yr}^{-1}$ (Meštrić et al. 2022; Claeysens et al. 2023). They have blue UV continuum β slopes, in several cases approaching extreme values ($\beta \sim -3$), indicating that they are active sites of star formation hosting young stellar populations with

DUVET: sub-kiloparsec resolved star formation driven outflows in a sample of local starbursting disk galaxies

Bronwyn Reichardt Chu,^{1,2,3,4*} Deanne B. Fisher,^{1,2} John Chisholm,⁵ Danielle Berg,⁵ Alberto Bolatto,⁶ Alex J. Cameron,⁷ Drummond B. Fielding,⁸ Rodrigo Herrera-Camus,⁹ Glenn G. Kacprzak,^{1,2} Miao Li,¹⁰ Anna F. McLeod,^{3,4} Daniel K. McPherson,^{1,2} Nikole M. Nielsen,^{1,2} Ryan Rickards Vaught,¹¹ Sophia G. Ridolfo,^{12,1,2} and Karin Sandstrom¹¹

¹Centre for Astrophysics and Supercomputing, Swinburne University of Technology, Hawthorn, VIC 3122, Australia

²ARC Centre of Excellence for All Sky Astrophysics in 3 Dimensions (ASTRO 3D), Australia

³Centre for Extragalactic Astronomy, Department of Physics, Durham University, South Road, Durham DH1 3LE, UK

⁴Institute for Computational Cosmology, Department of Physics, Durham University, South Road, Durham DH1 3LE, UK

⁵Department of Astronomy, University of Texas, Austin, TX 78712, USA

⁶University of Maryland, College Park, MD 20742, USA

⁷Sub-department of Astrophysics, University of Oxford, Keble Road, Oxford, OX1 3RH, UK

⁸Center for Computational Astrophysics, Flatiron Institute, 162 Fifth Avenue, New York, NY 10010, USA

⁹Departamento de Astronomía, Universidad de Concepción, Barrio Universitario, Concepción 4070032, Chile

¹⁰Institute for Astronomy, School of Physics, Zhejiang University, 866 Yuhangtang Road, Hangzhou, 310027, China

¹¹Department of Astronomy & Astrophysics, University of California, San Diego, CA, USA

¹²Research School of Astronomy and Astrophysics, Australian National University, Canberra, ACT 2611, Australia

Accepted XXX. Received YYY; in original form ZZZ

ABSTRACT

We measure resolved (kiloparsec-scale) outflow properties in a sample of 10 starburst galaxies from the DUVET sample, using Keck/KCWI observations of H β and [OIII] λ 5007. We measure ~ 450 lines-of-sight that contain outflows, and use these to study scaling relationships of outflow velocity (v_{out}), mass-loading factor (η ; mass outflow rate per SFR) and mass flux ($\dot{\Sigma}_{\text{out}}$; mass outflow rate per area) with co-located SFR surface density (Σ_{SFR}) and stellar mass surface density (Σ_*). We find strong, positive correlations of $\dot{\Sigma}_{\text{out}} \propto \Sigma_{\text{SFR}}^{1.2}$ and $\dot{\Sigma}_{\text{out}} \propto \Sigma_*^{1.7}$. We also find shallow correlations between v_{out} and both Σ_{SFR} and Σ_* . Our resolved observations do not suggest a threshold in outflows with Σ_{SFR} , but rather we find that the local specific SFR ($\Sigma_{\text{SFR}}/\Sigma_*$) is a better predictor of where outflows are detected. We find that outflows are very common above $\Sigma_{\text{SFR}}/\Sigma_* \gtrsim 0.1 \text{ Gyr}^{-1}$ and rare below this value. We argue that our results are consistent with a picture in which outflows are driven by supernovae, and require more significant injected energy in higher mass surface density environments to overcome local gravity. The correlations we present here provide a statistically robust, direct comparison for simulations and higher redshift results from JWST.

Key words: galaxies: evolution – galaxies: starburst – galaxies: star formation – galaxies: ISM

1 INTRODUCTION

The evolution of galaxies is shaped by the baryon cycle. Cold gas is accreted onto galaxies, used as fuel in star formation which in turn enriches the gas, and is then ejected from the galaxy to enrich the surrounding environment (Somerville & Davé 2015). Star formation-driven outflows are a necessary component of this cycle, contributing to the enrichment of the circumgalactic medium (CGM) (Tumlinson et al. 2017; Cameron et al. 2021), and suppressing star formation through the removal of gas (Veilleux et al. 2005; Bolatto et al. 2013; Reichardt Chu et al. 2022b). Galaxy-wide outflows are required for simulations to reproduce basic galaxy properties including the galaxy mass function, typical galaxy sizes, and the Kennicutt-Schmidt Law (e.g. Springel & Hernquist 2003; Oppenheimer & Davé

2006; Hopkins et al. 2012, 2014). To constrain the implementation of galaxy-wide outflows in simulations, the simulations need to be compared to empirical measurements of outflow quantities. It is, therefore, necessary that we understand the observational properties of outflows and their driving mechanisms.

Star formation-driven outflows have been observed across cosmic time (e.g. Heckman et al. 2000; Chen et al. 2010; Rubin et al. 2010; Davies et al. 2019). Outflows are an observational tracer of the feedback process that regulates star formation, preventing runaway star formation in multiple ways. First, it is expected that the gravitational weight of the disk creates pressure in the interstellar medium (ISM) which is balanced by the energy and momentum injected into the ISM by young massive stars and supernovae. This injected energy and momentum creates turbulence, suppressing the star formation occurring within the galaxy disk (e.g. Ostriker et al. 2010; Faucher-Giguère et al. 2013; Hayward & Hopkins 2017; Krumholz et al. 2018;

* E-mail: breichardtchu@swin.edu.au

The evolution of the SFR and Σ_{SFR} of galaxies in cosmic morning ($4 < z < 10$)

A. Calabrò¹, L. Pentericci¹, P. Santini¹, A. Ferrara², M. Llerena¹, S. Mascia¹, L. Napolitano¹, L. Y. A. Yung³,
L. Bisigello^{4,5}, N. J. Cleri^{6,7}, A. Dekel⁸, M. Dickinson⁹, M. Franco¹⁰, M. Giavalisco¹¹, M. Hirschmann¹²,
B. W. Holwerda¹³, A. M. Koekemoer³, R. A. Lucas³, F. Pacucci^{14,15}, N. Pirzkal¹⁶, G. Roberts-Borsani¹⁷,
L. M. Seillé¹⁸, S. Tacchella^{19,20}, S. Wilkins^{21,22}, R. Amorín^{23,24}, P. Arrabal Haro⁹, M. B. Bagley¹⁰,
S. L. Finkelstein¹⁰, J. S. Kartaltepe²⁵, and C. Papovich^{7,26}

(Affiliations can be found after the references)

ABSTRACT

The galaxy integrated star-formation rate (SFR) surface density (Σ_{SFR}) has been proposed as a valuable diagnostic of the mass accumulation in galaxies as being more tightly related to the physics of star-formation and stellar feedback than other star-formation indicators. In this paper, we assemble a statistical sample of 230 galaxies observed with JWST in the GLASS and CEERS spectroscopic surveys to estimate Balmer line based dust attenuations and SFRs (i.e., from H α , H β , and H γ), and UV rest-frame effective radii. We study the evolution of galaxy SFR and Σ_{SFR} in the first 1.5 Billion years of our Universe, from redshift $z \sim 4$ to $z \sim 10$. We find that Σ_{SFR} is mildly increasing with redshift with a linear slope of 0.16 ± 0.06 . We explore the dependence of SFR and Σ_{SFR} on stellar mass, showing that a star-forming ‘Main-Sequence’ and a Σ_{SFR} ‘Main-Sequence’ are in place out to $z = 10$, with a similar slope compared to the same relations at lower redshifts, but with a higher normalization. We find that the specific SFR (sSFR) and Σ_{SFR} are correlated with the [O III] $\lambda 5007\text{\AA}$ /[O II] $\lambda 3727\text{\AA}$ ratio and with indirect estimates of the escape fraction of Lyman continuum photons, hence they likely play an important role in the evolution of ionization conditions at higher redshifts and in the escape of ionizing radiation. We also search for spectral outflow signatures in the H α and [O III] emission lines in a subset of galaxies observed at high resolution (R= 2700) by the GLASS survey, finding an outflow incidence of 2/11 (= 20%_{9%}^{32%}) at $z < 6$, but no evidence at $z > 6$ (0/6, < 26%). Finally, we find a positive correlation between A_V and Σ_{SFR} , and a flat trend as a function of sSFR, indicating that there is no evidence of a drop of A_V in extremely star-forming galaxies between $z \sim 4$ and ~ 10 . This might be at odds with a dust-clearing outflow scenario, which might instead take place at redshifts $z \geq 10$, as suggested by some theoretical models.

Key words. galaxies: evolution — galaxies: high-redshift — galaxies: ISM — galaxies: star-formation — galaxies: statistics

1. Introduction

The cosmic evolution of galaxy star formation rates (SFRs) is one of the fundamental predictions of astrophysical models and cosmological simulations, and one of the most studied processes observationally. Indeed, it provides essential insights into cosmic structure formation across all scales, the accretion of gas into these structures, the efficiency of conversion into stars, and ultimately the diffusion of baryonic material in the intergalactic medium (IGM) through stellar feedback (White & Rees 1978; White & Frenk 1991; Springel & Hernquist 2003; Shapley 2011; Hopkins et al. 2012; Behroozi et al. 2013; Madau & Dickinson 2014).

The SFR is intimately linked to other galaxy properties, the most important of which is stellar mass (M_*). A correlation between SFR and M_* , known as the ‘Main Sequence’ of star-formation (Noeske et al. 2007), has been determined across over 5 orders of magnitudes in M_* at all redshifts. Many studies also focus on the specific SFR (sSFR=SFR/ M_*), that is, the SFR normalized by the total stellar mass content, showing that it follows a rather smooth, monotonic increase by at least one order of magnitude from redshift 0 to the reionization epoch (Davé et al. 2011; Menci et al. 2014; Speagle et al. 2014; Santini et al. 2017).

In addition to the SFR and the sSFR, a quantity that is gaining increasing attention now that JWST can resolve galaxy sizes out to the EoR, is the surface density of star-formation (Σ_{SFR}). This quantity represents the SFR normalized by the surface area where it occurs, and encapsulates information about the spatial distribution of star formation (SF). It is usually defined by the expression $\Sigma_{\text{SFR}} = \text{SFR}/(2\pi \times r_e^2)$, where r_e is the half-light radius. As galaxies become increasingly more compact at higher redshifts, since the dependence on the size is quadratic, Σ_{SFR} increases more rapidly with redshift compared to the sSFR. In particular, it can rise by more than three orders of magnitudes in typical star-forming galaxies from $z \sim 0$ to $z \sim 6$ (Wuyts et al. 2011; Holwerda et al. 2015), reaching extreme conditions at the epoch of reionization ($\Sigma_{\text{SFR}} \gtrsim 10 M_\odot / \text{yr}/\text{kpc}^2$). Therefore, it is even more essential to characterize the peculiar conditions of SF in the first phases of galaxy assembly.

Being more intimately related to the physics of star-formation, such as to the gas mass surface density through the Kennicutt-Schmidt relation (Kennicutt 1989; Kennicutt et al. 2007), and to the effectiveness of stellar feedback, Σ_{SFR} is thought to regulate the redshift evolution of the sSFR and M_* (Lehnert et al. 2015). Moreover, for the same reason, Salim et al. (2023) introduced the term ‘ Σ_{SFR} Main Sequence’ to indicate the Σ_{SFR} vs M_* relation, and they claim that this is even more fundamental than the sSFR - M_* relation. Along this new

The X-ray enhancements of radio-loud quasars at high redshift: New results at $z = 4 - 7$

Zihao Zuo,¹ Shifu Zhu,^{1,2,4,5}★ W. N. Brandt,^{1,2,3} Gordon P. Garmire,⁶ F. Vito,⁷ Jianfeng Wu,⁸ and Yongquan Xue^{4,5}

¹Department of Astronomy & Astrophysics, The Pennsylvania State University, University Park, PA 16802, USA

²Institute for Gravitation and the Cosmos, The Pennsylvania State University, University Park, PA 16802, USA

³Department of Physics, 104 Davey Lab, The Pennsylvania State University, University Park, PA 16802, USA

⁴CAS Key Laboratory for Research in Galaxies and Cosmology, Department of Astronomy, University of Science and Technology of China, Hefei 230026, China

⁵School of Astronomy and Space Sciences, University of Science and Technology of China, Hefei 230026, China

⁶Huntingdon Institute for X-ray Astronomy, LLC, 10677 Franks Road, Huntingdon, PA 16652, USA

⁷INAF – Osservatorio di Astrofisica e Scienza dello Spazio di Bologna, Via Gobetti 93/3, I-40129 Bologna, Italy

⁸Department of Astronomy, Xiamen University, Xiamen, Fujian 361005, People's Republic of China

Accepted XXX. Received YYY; in original form ZZZ

ABSTRACT

Highly radio-loud quasars (HRLQs; $\log R > 2.5$) at $z \gtrsim 4$ show apparent enhanced X-ray emission compared to matched HRLQs at lower redshifts, perhaps due to a redshift-dependent fractional contribution to the X-ray luminosity from inverse-Compton scattering of cosmic microwave background photons (IC/CMB). Using new *Chandra* observations and archival X-ray data, we investigate this phenomenon with an optically flux-limited sample of 41 HRLQs at $z = 4-5.5$ all with sensitive X-ray coverage, the largest sample utilized to date by a wide margin. X-ray enhancements are assessed using X-ray-to-optical flux ratios and spectral energy distributions. We confirm the presence of X-ray enhancements at a $4.9-5.3\sigma$ significance level, finding that the median factor of enhancement is ≈ 1.8 at our sample median redshift of $z \approx 4.4$. Under a fractional IC/CMB model, the expected enhancement at lower redshifts is modest; e.g., $\approx 4\%$ at $z \approx 1.5$. We also investigate a sample of seven radio-loud quasars (RLQs; $\log R > 1$) at even higher redshifts of $z = 5.6-6.8$, using new and archival X-ray data. These RLQs also show evidence for X-ray enhancements by a median factor of ≈ 2.7 at a $3.7-4.9\sigma$ significance level. The X-ray spectral and other properties of these $z = 5.6-6.8$ RLQs, however, pose challenges for a straightforward fractional IC/CMB interpretation of their enhancements.

Key words: galaxies: high-redshift – quasars: general – X-rays: galaxies

1 INTRODUCTION

Quasars are powered by the accretion process happening in the vicinity of supermassive black holes (SMBHs) located in the central regions of host galaxies. Quasars at high redshifts are of particular interest since they provide insights into SMBH growth and galaxy formation in the early universe. The discovery of significant samples of rare high-redshift quasars was made possible by large-scale sky surveys such as the Sloan Digital Sky Survey (SDSS, York et al. 2000). Since Ly α emission is redshifted to the near-infrared (NIR) bands at $z \gtrsim 5.5$, wide-field NIR surveys like the UKIRT Infrared Deep Sky Survey and the VISTA Hemisphere Survey (e.g. Lawrence et al. 2007; McMahan et al. 2013) are also important. As of December 2022, there are 531 quasars with $z \geq 5.3$ in the literature (Fan et al. 2022). Based on the radio-loudness parameter

$R = f_{5\text{GHz}}/f_{4400\text{\AA}}$, where $f_{5\text{GHz}}$ and $f_{4400\text{\AA}}$ are the flux densities at rest-frame 5 GHz and 4400 Å (Kellermann et al. 1989), quasars can be divided into radio-quiet quasars (RQQs; $R \leq 10$) and radio-loud quasars (RLQs; $R > 10$). RLQs harbor strong relativistic jets (e.g. Padovani 2017). The fraction of RLQs remains $\sim 10\%$ up to $z \sim 6$ (Bañados et al. 2015). It is well known that the quasar number density peaks at $2 < z < 3$ (e.g. Dunlop & Peacock 1990; Croom et al. 2004; Brown et al. 2006; Yang et al. 2016) and then rapidly declines with increasing redshift. In contrast to the strong redshift dependence of the quasar number density, previous studies have shown that the UV/optical and NIR spectral properties of quasars do not show significant evolution up to $z \sim 6$ (e.g. Fan et al. 2004; Jiang et al. 2007; Shen et al. 2019). Current observations suggest that AGNs and SMBH feeding modes do not show significant evolution after the first billion years of the Universe.

Almost all quasars are bright in the X-ray regime. The X-ray emission from RQQs is proposed largely to be generated by the

★ E-mail: SFZAstro@gmail.com

Breakdown of Hawking Evaporation opens new Mass Window for Primordial Black Holes as Dark Matter Candidate

Valentin Thoss,^{1,2,3*} Andreas Burkert^{1,2,3} and Kazunori Kohri^{4,5,6}

¹Universitäts-Sternwarte, Ludwig-Maximilians-Universität München, Scheinerstr. 1, 81679 Munich, Germany

²Max-Planck Institute for Extraterrestrial Physics, Giessenbachstr. 1, 85748 Garching, Germany

³Excellence Cluster ORIGINS, Boltzmannstrasse 2, 85748 Garching, Germany

⁴Division of Science, National Astronomical Observatory of Japan (NAOJ), and SOKENDAI, 2-21-1 Osawa, Mitaka, Tokyo 181-8588, Japan

⁵Theory Center, IPNS, and QUP, KEK, 1-1 Oho, Tsukuba, Ibaraki 305-0801, Japan

⁶Kavli IPMU (WPI), University of Tokyo, Kashiwa, Chiba 277-8568, Japan

Accepted XXX. Received YYY; in original form ZZZ

ABSTRACT

The energy injection through Hawking evaporation has been used to put strong constraints on primordial black holes as a dark matter candidate at masses below 10^{17} g. However, Hawking’s semiclassical approximation breaks down at latest after half-decay. Beyond this point, the evaporation could be significantly suppressed as was shown in recent work. In this study, we review existing cosmological and astrophysical bounds on primordial black holes taking this effect into account. We show that the constraints disappear completely for a reasonable range of parameters, which opens a new window below 10^{10} g for light primordial black holes as a dark matter candidate.

Key words: dark matter – black hole physics – gamma-rays: general

1 INTRODUCTION

The hypothesis of black holes forming in the early universe has been discussed for more than 50 years (Zel’dovich & Novikov 1967; Hawking 1971; Carr & Hawking 1974), with Chapline (1975) first to suggest that primordial black holes (PBHs) could constitute the entire dark matter of the universe. Since the 1970s, people have studied the consequences of PBHs as a dark matter candidate from the Planck mass $M_{\text{PBH}} = M_{\text{pl}}$ up to the ‘incredulity limit’¹ beyond $M_{\text{PBH}} \sim 10^{10} M_{\odot}$. This has led to strong bounds which exclude PBHs of a single mass from constituting the entirety of the dark matter with the exception of a mass window in the asteroid range $M_{\text{PBH}} \in [10^{17}, 10^{22}]$ g (Carr et al. 2021, and references therein).

The lower limit is a result of constraints due to black hole evaporation at low masses. This process was first described by Hawking (1974) as he was studying the consequences of light PBHs. He showed that a black hole will emit a thermal spectrum of particles, with the temperature of the radiation scaling as $T \sim 1/M_{\text{PBH}}$. The described evaporation process is self-similar and ends with a final burst as $M \rightarrow 0$.

It was soon realized that the energy injection from low-mass PBHs is in conflict with observations of γ rays, the cosmic microwave background (CMB) and the abundance of light elements produced during big bang nucleosynthesis (BBN) unless these black holes constitute only a tiny fraction of the dark matter (Chapline 1975; Hawking 1975; Novikov et al. 1979; Carr et al. 2010, for a historical

overview). Furthermore, if the PBHs have a mass below $M \approx 5 \times 10^{14}$ g, they would have completely evaporated by now (see Auffinger (2023) for a review on constraints of evaporating PBHs).

However, it is possible to avoid some of the constraints that are a result of black hole evaporation. Pacheco et al. (2023) have studied ‘quasi-extremal’ PBHs and found that they can be a viable dark matter candidate. Friedlander et al. (2022) and Anchordoqui et al. (2022) have investigated PBHs in the context of large extra dimensions (Arkani-Hamed et al. 1998) and showed that this opens up new mass windows for light PBHs as dark matter candidate.

In this work, we focus on ‘ordinary’ 4D black holes. Dvali et al. (2020) have shown that Hawking’s semiclassical calculations break down at latest when the black hole has lost roughly half of its initial mass. Hawking’s result is only exact in the limit $M \rightarrow \infty, G \rightarrow 0, r_s = \text{const.}$, where G is the gravitational constant and $r_s = 2GM/c^2$ the Schwarzschild radius. It entirely neglects the backreaction of the emission on the black hole itself. However, this effect can no longer be ignored when the energy of the released quanta becomes comparable to that of the black hole. Dvali et al. (2020) summarize this as: ‘An old black hole that lost half of its mass is by no means equivalent to a young classical black hole of equal mass.’ The crucial insight by Dvali et al. (2020) is that this backreaction leads to a universal effect of so-called ‘memory burden’, first introduced by Dvali (2018). This can significantly suppress further evaporation.

As Dvali et al. (2020) have discussed, there are two possibilities for the fate of an evaporating black hole beyond half-decay. Either it continues to emit quanta with a strongly suppressed rate due to the memory burden or a new classical instability sets in. In the latter case, light PBHs cannot constitute the dark matter. However, if the

* E-mail: vthoss@usm.lmu.de

¹ This term was coined by B. Carr and refers to the limit that at least one black hole must exist in a given environment (e.g. galaxy, universe).

Galaxy cluster virial-shock sources in eROSITA catalogs

Gideon Ilani*, Kuan-Chou Hou, Gil Nadler, and Uri Keshet**

Physics Department, Ben-Gurion University of the Negev, POB 653, Be'er-Sheva 84105, Israel

February 29, 2024

ABSTRACT

Context. Virial shocks around galaxy clusters and groups are being mapped, tracing accretion onto large-scale structure.

Aims. Following the recent identification of discrete *ROSAT* and radio sources associated with the virial shocks of MCXC clusters and groups, we examine if the early *eROSITA-DE* data release (EDR) shows virial-shock X-ray sources within its 140 deg² field.

Methods. EDR catalog sources are stacked and radially binned around EDR catalog clusters and groups. The properties of the excess virial-shock sources are inferred statistically by comparing the virial-shock region to the field.

Results. An excess of X-ray sources is found narrowly localized at the $2.0 < r/R_{500} < 2.25$ normalized radii, just inside the anticipated virial shocks, of the resolved 532 clusters, for samples of both extended (3σ for 534 sources) or bright (3.5σ for 5820 sources; 4σ excluding the low cluster-mass quartile) sources. The excess sources are on average extended (~ 100 kpc), luminous ($L_X \approx 10^{43-44}$ erg s⁻¹), and hot (\sim keV), consistent with infalling gaseous halos crossing the virial shock. The results agree with the stacked *ROSAT*–MCXC signal, showing the higher L_X anticipated at EDR redshifts and a possible dependence upon host mass.

Conclusions. Localized virial-shock spikes in the distributions of discrete radio, X-ray, and probably also γ -ray sources are new powerful probes of accretion from the cosmic web, with strong constraints anticipated with future all-sky catalogs such as by *eROSITA*.

Key words. galaxy clusters

1. Introduction

In recent years, the long-awaited virial-shock (VS) signals around galaxy clusters and groups (for brevity, henceforth ‘clusters’) were finally detected in inverse-Compton (Keshet et al. 2017; Reiss et al. 2017; Reiss & Keshet 2018; Keshet & Reiss 2018), synchrotron (Keshet et al. 2017; Hou et al. 2023), and thermal SZ (Keshet et al. 2017; Hurier et al. 2019; Keshet et al. 2020; Pratt et al. 2021; Anbajagane et al. 2022) signatures, both in stacking analyses and in individual clusters. The stacked leptonic signals indicate highly localized emission at normalized $2.2 \lesssim \tau \equiv r/R_{500} \lesssim 2.5$ radii, where subscript 500 refers (henceforth) to the radius around a cluster enclosing 500 times the critical mass density of the Universe.

An unexpected signal was reported recently (Ilani et al. 2024, henceforth I24) in X-ray and radio catalog sources stacked around MCXC (Piffaretti et al. 2011) clusters, with a highly localized, $2.25 < \tau < 2.50$ excess precisely coincident with the previous VS leptonic signals. These sources were found to be on average extended, \sim keV hot, magnetized, and radially polarized, and so were tentatively identified as the shocked halos of infalling galaxies or galaxy aggregates, possibly including aging relativistic particles from previous galactic outflows (I24). However, these stacking analyses of leptonic emission or discrete sources relied on the same low-redshift MCXC clusters and their tabulated, X-ray-based, characteristic R_{500} values.

We examine if the early *eROSITA-DE* data release (EDR) catalogs (described in §2) are sufficient to show an excess of VS X-ray sources within their 140 deg² field, and, if so, to characterize the properties of these sources. EDR catalog sources are thus

stacked and radially binned around EDR catalog clusters (in §3). The properties of the excess sources are then inferred statistically (in §4), by comparing VS-region sources to their field counterparts. Finally, the results are analyzed and discussed (in §5) in comparison to the *ROSAT*–MCXC results.

We generally follow the I24 methods and notations. A Λ CDM model is adopted with an $H_0 = 70$ km s⁻¹ Mpc⁻¹ Hubble constant and an $\Omega_m = 0.3$ mass fraction.

2. Catalog samples

We combine the EDR¹ catalogs of X-ray sources (Brunner et al. 2022), clusters (Liu et al. 2022), and cluster X-ray properties (Bahar et al. 2022). Better results are expected with the first *eROSITA* allsky survey² (eRASS1) and future all-sky catalogs, as they become available³.

Figure 1 presents the EDR and MCXC cluster catalogs in the phase space of M_{500} mass vs. projected $\theta_{500} = R_{500}/d_A$ angle, where $d_A(z)$ is the angular diameter distance at redshift z . Thanks to the better resolution and sensitivity of *eROSITA*, EDR clusters, including massive ones, are available at higher redshifts and thus smaller θ_{500} than in MCXC. However, due to the smaller field of view, the EDR catalog lacks rare, highly extended or very massive clusters found in MCXC. We divide the 542 EDR clusters into four mass bins, each with about the same, 135 or 136 number of clusters. Due to the $\sim 1'$ resolution of the cluster catalog (Liu et al. 2022), we exclude the 10 clusters with $\theta_{500} < 1'$. The mass bins and θ_{500} cutoff are shown as lines in the figure.

¹ <https://erosita.mpe.mpg.de/edr/eROSITAObservations/Catalogue>

² https://erosita.mpe.mpg.de/dr1/AllSkySurveyData_dr1/Catalogue

³ The cluster catalog for the first data release (DR1) of the SRG/eROSITA all-sky survey (eRASS1) has become available only after this study was concluded.

* Posthumously. Gideon Ilani was killed in action on December 10, 2023. This paper is based in part on his Ph.D. research.

** e-mail: keshet.uri@gmail.com

The FLAMINGO simulation view of cluster progenitors observed in the epoch of reionization with JWST

Seunghwan Lim^{1,2*}, Sandro Tacchella^{1,2}, Joop Schaye³, Matthieu Schaller^{4,3}, Jakob M. Helton⁵, Roi Kugel³, Roberto Maiolino^{1,2}

¹*Kavli Institute for Cosmology, University of Cambridge, Madingley Road, Cambridge, CB3 0HA, UK*

²*Cavendish Laboratory, University of Cambridge, 19 JJ Thomson Avenue, Cambridge, CB3 0HE, UK*

³*Leiden Observatory, Leiden University, PO Box 9513, 2300 RA Leiden, the Netherlands*

⁴*Lorentz Institute for Theoretical Physics, Leiden University, PO box 9506, 2300 RA Leiden, the Netherlands*

⁵*Steward Observatory, University of Arizona, 933 N. Cherry Ave., Tucson, AZ 85721, USA*

29 February 2024

ABSTRACT

Motivated by the recent JWST discovery of galaxy overdensities during the Epoch of Reionization, we examine the physical properties of high- z protoclusters and their evolution using the FLAMINGO simulation suite. We investigate the impact of the apertures used to define protoclusters, because the heterogeneous apertures used in the literature have limited our understanding of the population. Our results are insensitive to the uncertainties of the subgrid models at a given resolution, whereas further investigation into the dependence on numerical resolution is needed. When considering galaxies more massive than $M_* \simeq 10^8 M_\odot$, the FLAMINGO simulations predict a dominant contribution from progenitors similar to those of the Coma cluster to the cosmic star-formation rate density during the reionization epoch. Our results indicate the onset of suppression of star formation in the protocluster environments as early as $z \simeq 5$. The galaxy number density profiles are similar to NFW at $z \lesssim 1$ while showing a steeper slope at earlier times before the formation of the core. Different from most previous simulations, the predicted star-formation history for individual protoclusters is in good agreement with observations. We demonstrate that, depending on the aperture, the integrated physical properties including the total (dark matter and baryonic) mass can be biased by a factor of 2 to 5 at $z = 5.5\text{--}7$, and by an order of magnitude at $z \lesssim 4$. This correction suffices to remove the $\simeq 3\sigma$ tensions with the number density of structures found in recent JWST observations.

Key words: methods: statistical – galaxies: formation – galaxies: evolution – galaxies: clusters: general – galaxies: high-redshift

1 INTRODUCTION



Galaxies and the extensive cosmic structures observable in the contemporary Universe are postulated to have originated from minute density fluctuations that occurred immediately following the inflationary epoch in the early Universe. Their hierarchical growth over cosmic epochs has been extensively documented (see Mo et al. 2010). The emergence of the inaugural galaxies and primal cosmic structures, originating within regions characterized by the highest density fluctuations, is believed to have played a pivotal role in the reionization and episodic star-formation events in the Universe (e.g., Furlanetto et al. 2006; Matthee et al. 2015; Ishigaki et al. 2016; Overzier 2016). Protoclusters, identified as overdensities of galaxies in the early Universe, have been demonstrated through both theoretical frameworks and observational data

to contribute significantly, to over 20 per cent of the cosmic star-formation activity until approximately the cosmic noon at redshift $z \simeq 2$ (e.g., Casey et al. 2015; Umehata et al. 2015; Chiang et al. 2017; Shi et al. 2020). Recently, Sun et al. (2024) estimated about 50 per cent of the total star formation has occurred in protocluster environments at $z \simeq 5$. This underscores the substantial significance of this population in comprehending the genesis of galaxies and their concurrent evolution within the broader context of large-scale cosmic environments.

Despite their significance, protocluster studies encounter numerous critical challenges that pose difficulties in achieving a thorough, unbiased analysis and a comprehensive understanding of the population (see Lim et al. 2021 for an extensive discussion). Firstly, protoclusters, as implied by their nomenclature, are commonly regarded as the high-redshift precursors of clusters observable at $z \simeq 0$ (e.g., Chiang et al. 2013; Overzier 2016; Alberts & Noble 2022). While the theo-

* E-mail: sl2207@cam.ac.uk

scida: scalable analysis for scientific big data

Chris Byrohl ¹ and Dylan Nelson ¹

¹*Heidelberg University, Institute for Theoretical Astronomy,
Albert-Ueberle-Str. 2, 69120 Heideberg, Germany*

15 Sep 2023

Summary

scida (<https://scida.io>) is a Python package for reading and analyzing large scientific data sets. Data access is provided through a hierarchical dictionary-like data structure after a simple `load()` function. Using the `dask` library for scalable, parallel and out-of-core computation ([Dask Development Team, 2016](#)), all computation requests from a user session are first collected in a task graph. Arbitrary custom analysis, as well as all available `dask` (array) operations, can be performed. The subsequent computation is executed only upon request, on a target resource (e.g. a HPC cluster, see Figure 1).

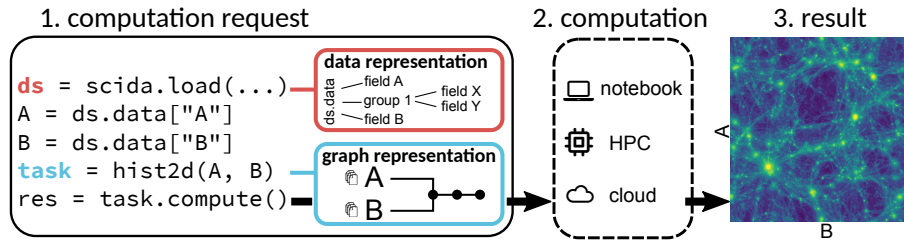


Figure 1: Schematic of the workflow. In a user session, a recipe (i.e. sequence of analysis operations) for desired data product can be built by consecutive chaining of operations, which are internally represented by `dask` task graphs. Calculation is triggered by the `compute()` command, evaluating the graph on a target resource. The result, much smaller than the original data, is sent back to the user session for further analysis/plotting.

Features

Scida begins by providing a clean, abstract, dictionary-like interface to the underlying data, regardless of its file format or structure on disk. Physical